Universitetet i Stavanger

FACULTY OF SCIENCE AND TECHNOLOGY

MASTER'S THESIS

Study program/ Specialization: Petroleum Engineering / Drilling and Well Technology	Spring semester, 2018 Open
Author: ***Erling Bendiksen Bjørndal***	………………………………………… (Author's signature)
Supervisor: ***Kjell Kåre Fjelde***	
Title of master's thesis: ***Reliability-Based Casing Design with Focus on an APB Collapse Scenario***	
Credits (ECTS): 30	
Keywords: • Reliability-Based Design • Working Stress Design • Casing design • Collapse	Number of pages: 99 + supplemental material/other: 29 Stavanger June 15th, 2018

Acknowledgement

This Master's thesis was carried out at the University of Stavanger during the spring semester of 2018. While working on this thesis I was introduced to the academic writing process of an independent scientific study. I would like to thank my supervisor, Professor Kjell Kåre Fjelde, for proposing this thesis topic. His friendly approach, guidance and encouragement during this process was of great motivational value.

Stavanger, June 2018

Erling Bendiksen Bjørndal

Abstract

In times of unstable oil price, optimization related to casing and tubing design becomes more important than ever. Reducing cost and at the same time ensuring reliable and safe drilling and completion installations becomes a challenge to the petroleum industry. Reliability-based casing and tubing design allows for optimization of design by quantifying a probability of failure.

The conventional method for casing and tubing design, working stress design, relies on the application of design factors that to a large degree is based on company specific guidelines. This method is deterministic and overly conservative. It also lacks the ability to quantify the reliability of the design. It does not take into account varying uncertainties in load and strength, or the variation in consequence of failure for different well or completion designs.

Quantitative Risk Analysis is a method used to quantify risk by predicting the failure probability, in combination with Monte Carlo Simulation, the method will account for uncertainty in multiple variables involved in load and strength estimation. Load and strength will be represented by probability distributions which will define the failure probability, one may allow for an acceptable failure probability in the design.

This study provides an overview of theory and methods that can be used for reliability-based casing and tubing design. In addition, an attempt is made to illustrate the implementation of Quantitative Risk Analysis by the use of Monte Carlo Simulation on a collapse mode tubing design. A case study is prepared, considering a collapse load on a production tubing caused by Annular Pressure Buildup in the A annulus.

The Reliability-based design approach is compared to that of the deterministic working stress design for the case study tubing string. The case study show that significantly lower required yield strength of the tubing string can be obtained when replacing working stress design by a reliability-based approach. Acceptable probabilities of failure can be selected based on the cost and consequence of an anticipated failure, thus a reliability-based design is more flexible as it can be tailored to specific well and field conditions. Two different probabilities were considered for the design. As the reliability-based approach predicts the failure probability, it gives a better view of the real risk involved in the design. The study shows that savings in yield strength or tubing grade depend on both the selected acceptable failure probability and on the type of reliability-based design being used.

Table of Contents

List of figures

List of tables

Symbols

A_p	Pipe cross sectional area $[inch^2]$
A_i	Inner cross-sectional area $[inch^2]$
A_o	Outer cross-sectional area $[inch^2]$
A_s	Steel cross-sectional area $[inch^2]$
D_i	Inner diameter [inch]
D_o	Outer diameter [inch]
D_{packer}	Depth of packer [m]
F_a	Axial force [Lbf]
$F_a{}'$	Buoyed weight or effective force [psi]
P_{Y_p}	Yield strength collapse pressure [psi]
P_E	Elastic collapse pressure [psi]
P_T	Transitional collapse pressure [psi]
$P_{b,load}$	Burst load pressure [Pa]
P_b	Burst pressure [psi]
$P_{c,load}$	Collapse load pressure [psi]
P_c	Collapse pressure [psi]
P_{ci}	Equivalent collapse pressure [psi]
P_f	Failure probability [%]
P_p	Plastic collapse pressure [psi]
P_t	Target probability [%]
T_{res}	Reservoir temperature
$T_{surface}$	Surface ambient temperature
T_{wh}	Wellhead temperature
Z_{shoe}	Depth of casing shoe, TVD [m]
f_M	Moody (Darcy-Weisbach) friction factor
f_f	Fanning friction factor
$p_{e\;ult}$	Tamano ultimate collapse strength [psi]
p_i	Inner pipe pressure [psi]
p_o	Outer pipe pressure [psi]
r_i	Inner radius [inch]

v_f	Fluid velocity [m/s]
w_{air}	Weight in air pr. unit length [Lbs/ft]
$\bar{x}$	Mean
γ_{oil}	Oil density [sg]
$\gamma_{packer\ fluid}$	Packer fluid density [sg]
μ_{oil}	Oil viscosity [Pa s]
σ'	Effective stress [psi]
σ_1	First principal stress [psi]
σ_2	Second principal stress [psi]
σ_3	Third principal stress [psi]
σ_{VME}	Von Mises triaxial stress (equivalent tensile stress) [psi]
σ_a	Axial principal stress [psi]
σ_a	Axial stress excluding bending forces [psi]
σ_{max}	Maximum principal stress [psi]
σ_{min}	Minimum principal stress [psi]
σ_{pore}	Pore pressure [psi]
σ_r	Radial principal stress [psi]
σ_{std}	Standard deviation
σ_{tot}	Total stress [psi]
σ_y	Lower yield stress [psi]
σ_{ya}	Axial stress equivalent grade [psi]
σ_{ycom}	Combined loading equivalent grade [psi]
σ_z	Axial stress [psi]
σ_θ	Tangential or hoop principal stress [psi]
$\Delta P_{friction}$	Frictional pressure loss [psi]
$\Delta\sigma_z$	Additional axial stress from pressure differential [psi]
c	Fluid compressibility [bar^{-1}]
DF	Design factor
E	Youngs modulus [psi]
LF	Load Factor
M	Median
OD	Outer diameter [inch]

RF	Resistance factor
s	Variance
SF	Safety factor
UF	Utilization factor
ΔF_a	Differential load due to temperature and pressure changes [psi]
Tol	Tolerance
a	Triangular and uniform distribution minimum value
b	Triangular and uniform distribution maximum value
c	Triangular distribution mode
ec	Eccentricity
ov	Ovality
rs	Residual stress
t	Pipe wall thickness [inch]
v	Youngs modulus
α	Coefficient of thermal expansion [K^{-1}]
α	Weibull scale parameter
β	Geometry factor
β	Weibull shape parameter
γ	Weibull location parameter
ε	Relative roughness
ε	Strain
μ	Mean
σ	Standard deviation
σ	Stress [psi]
τ	Shear stress [psi]
ϵ	Roughness [inch]

*Note that some symbols are used for multiple purposes

Abbreviations

API	American petroleum institute
APB	Annular pressure buildup
QRA	Quantitative risk analysis
PDF	Probability density function
RBD	Reliability-based design
WSD	Working stress design
TVD	True vertical depth
SRS	Simple random sample
CDF	Cumulative distribution function
LRFD	Load and resistance factor design
LSD	Limit State Design
WH	Wellhead
TOC	Top of cement
NCS	Norwegian continental shelf
USC	United Stated Customary units
SI	International System of Units
MCS	Monte Carlo Simulation
COV	Covariance

1 Introduction

The conventional design approach for tubular design in the petroleum industry has been the application of Working Stress Design. The lack of ability to predict failure probability of the particular design considered typically result in overdesign with unnecessary cost and material usage. The objective of this study is to compare the use of reliability-based design applied on casing and tubing to the conventional design methodology. We will demonstrate how quantitative risk analysis can be applied in practice to casing design and compare this approach to conventional working stress design. An approach will be made to first review both underlying theory and different design methodologies and then apply reliability-based design as well as working stress design on a case study, where a production tubing is subjected to collapse load caused by a annular pressure build up in the A annulus.

The API Bulletin 5C3 equations for tubular design will be used for collapse strength calculations. In the working stress design approach, only deterministic input parameters are used to predict a deterministic load and strength. Nominal parameters, that is minimum or conservative values are used for strength calculations. A load limit, representing the maximum allowable load is here given by dividing the strength by a design factor. While using the reliability-based approach however, Monte Carlo simulations will be used to sample input parameters for load and strength represented by probability distributions, this provides output distributions of load and strength. The failure probability is represented by the overlapping area of these output distributions. This approach might be referred to as Quantitative Risk Analysis.

By using sensitivity analysis on the collapse load and strength distributions, the effect of different input parameters on uncertainty in load and strength will be evaluated. Reducing the uncertainty in load and strength will also reduce the predicted collapse probability.

Lastly, we will investigate the results of the different approaches considered and find out if the implementation of a reliability-based design will reduce the required yield strength of the tubing. Two different types of reliability-based design will be considered. We will also look into the effect of choosing different acceptable probabilities of collapse for the tubing

This study will outline different approaches for reliability-based design and most importantly investigate the implications related to required yield strength. Put differently we will investigate if more of the tubular strength can be utilized in design when reliability-based design approach.

This thesis is divided into six chapters, these are outlined below.

1. The first chapter provides an introduction

2. The second chapter is an introduction to casing design with emphasis on the API 5C3 tubular design equations. It also introduces us to casing, tubing, well integrity, casing loads and load cases which the casing or tubing can be subjected to.

3. The third chapter introduces us to the conventional design methodologies of working stress design and limit state design.

4. The forth chapter presents reliability-based design methodologies, to do so it also reviews underlying theory of statistics and Monte Carlo simulations.

5. The fifth chapter presents a case study where different design methodologies are applied to a base case production tubing design, where the tubing is subjected to an annular pressure buildup load case. Assumptions of the case study are included.

6. The sixth chapter summarizes this study by discussion, conclusion and proposed further work on reliability-based casing and tubing design.

2 Casing Design

2.1 Casing

While drilling an open hole, formation material called cuttings are cut or crushed by the drillbit and transported up to the surface by mud circulation. Now the walls are supported only by the downhole pressure that is controlled by the mudweight. To prevent the hole from collapsing, casings need to be installed at certain intervals depending on casing strength, pore pressure, fracture pressure and geology. In addition, they must be set to avoid fracturing of the formation above as the mudweight must be increased due to increasing pore pressure when drilling the next sections. A casing is a steel tubular designed to withstand any forces and conditions of the well during its lifetime. A casing string is made up from many casing tubulars. The casing string is normally cemented in place above the setting depth at the casing shoe up to top of cement (TOC) or all the way up to the wellhead (WH). At the wellhead, the casing strings are supported and locked in the casing hanger. The first casing string is called the conductor, it is cemented up to the surface, it is not hung from a casing hanger but serves as the foundation for the wellhead and the other casing strings. As drilling commences each casing string become smaller in diameter to fit into the previous. When drilling is completed this arrangement resembles an extended telescope. After the conductor, the surface casing, intermediate casing and production casing are installed. Some tubulars called liners may extend from a production casing or intermediate casing. These are casing strings that does not extend to the wellhead but instead are hung off and supported from the previous casing by a liner hanger. A casing is characterized by an inner and outer diameter ID and OD, wall thickness t, weight pr. feet in air w_{air} and its yield strength or grade σ_y. Some important purposes of casing are to prevent the collapse of weak formations, act as flow conduit for well fluids, isolate formation fluids from the wellbore fluids preventing contamination, allow production from selective formations, support and protect installed tubing and downhole equipment [6]. A typical drilling program of the Norwegian continental shelf (NCS) is shown below with total vertical setting depths Z_{shoe}, casing grade and size.

Table 1 Typical drilling program on the NCS

Casing:	Hole size[inch]	Casing OD[inch]	Grade[ksi]	Z_{shoe} [mTVD]
Conductor	36"	30"	K55	50-100
Surface casing	26"	20"	L80	300-1200
Intermediate casing	17 ½"	13 3/8"	T95	1300-2000
Production casing	12 ¼"	9 5/8"	P110	2500-4500
Liner	8 ½"	7"	P110	Target depth

The actual casing string configuration and number of casing strings to be used to reach the target depend largely on the setting depths of the individual strings restrained by geological conditions such as plastic shale and mobile salt formations, and on pore and fracture pressure gradients [6]. The hydrostatic mudweight column must be such that the dynamic equivalent circulation pressure (ECD) while drilling is below the fracture pressure, and that the static pressure (while making connections) is above the pore pressure of the formation. Account must be taken for design factors, possibly riser and surge/swab margins, and kick handling criteria (kick tolerance). The mudweight used to drill a section is thereby limiting the setting depth of the corresponding casing string [5]. The median line principle is often used for mudweight, implying that the mudweight is kept around the average of the pore and fracture pressure gradients. However, for the top-hole sections, either seawater or a mud is used close to pore pressure. In this case, mud is returned at the seabed and it puts strict requirements on what fluids can be used. A schematic of the pore and pressure gradients showing casing setting depths are shown in the figure below.
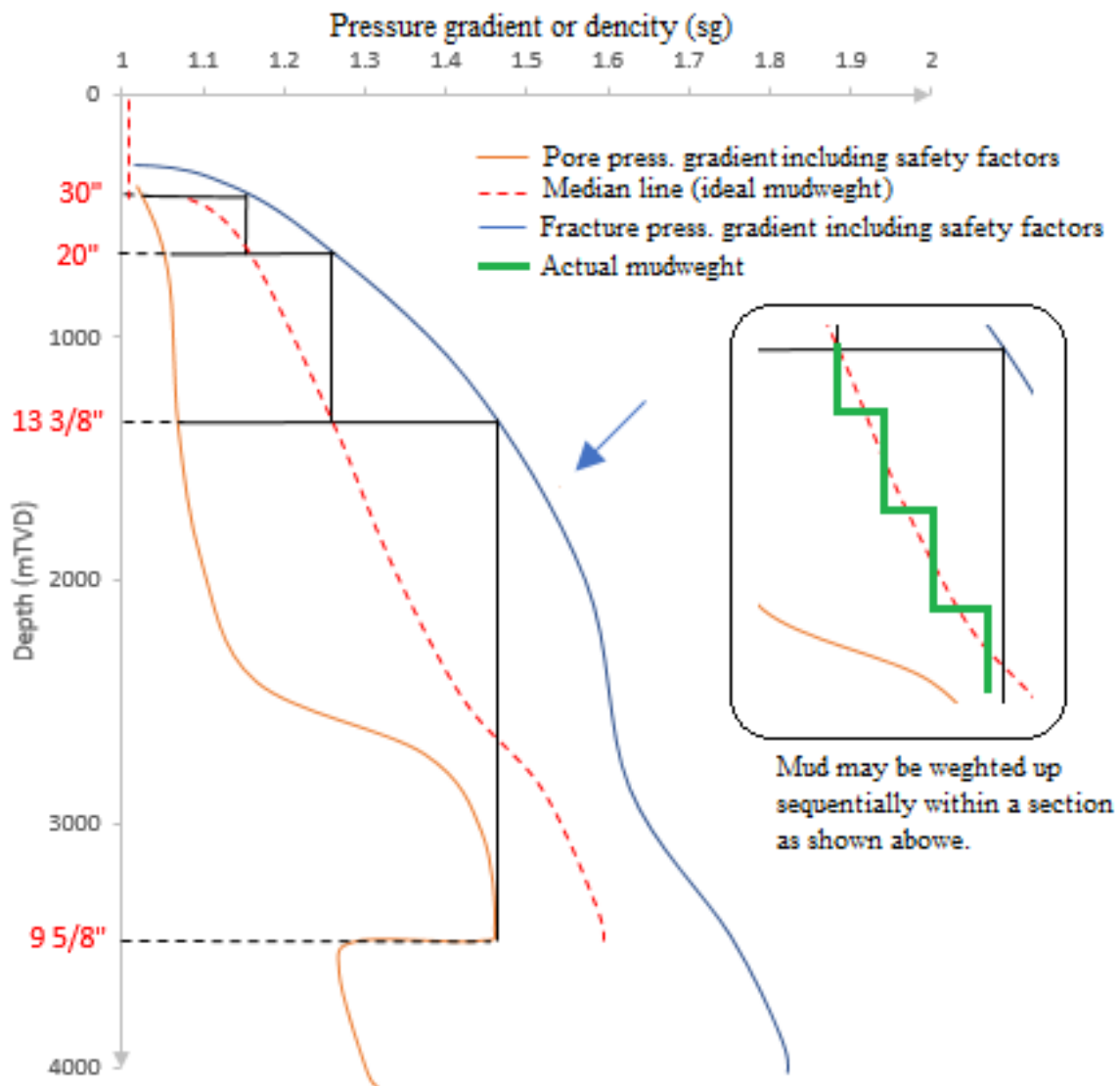
Figure 1 Casing setting depths using the median line principle for mudweight, modified from [5]

2.2 Tubing

When drilling and casing installation commences, a well completion process starts to prepare the well for production. A well completion almost always involves the installation of a production tubing to guide the production fluid to surface, protecting the casing from corrosion and erosion during production. The space between each casing or tubing string is called an annulus, starting from outside the production tubing with the A annulus, next comes the B annulus and so forth. The annular space between the casing and production tubing, the A annulus, is filled with a completion fluid to protect both tubulars. In some cases this annular space may be used as an additional production conduit when producing from multiple reservoir

zones [2]. The annular space described will be further discussed, considering annular pressure buildup (APB) as a collapse load on production tubing in later sections. Just like a casing string, a tubing is typically made up from steel tubulars needed to be designed for forces subjected to the tube and conditions during the lifetime of the well. The tubing string is hung in a tubing hanger in the wellhead or in a vertical Christmas-tree. Tubing is characterized by the same dimensions as the casing described in the previous section. *"The size of the production tubing string plays a vital role in conducting oil and gas to the surface at an economic rate"* [6]. By enlarging the diameter, the less restricted the flow will be due to friction and the cross-sectional area. In addition, tubing serviceability will be improved.

2.3   Well integrity and failure causation

Well integrity is defined by NORSOK D-010 as *the "application of technical, operational and organizational solutions to reduce risk of uncontrolled release of formation fluids and well fluids throughout the life cycle of a well"* [1]. *"This standard defines requirements and guidelines relating to well integrity in drilling and well activities"* [1]. We will therefore refer to NORSOK D-010 for well integrity and design purposes. The standard requires a two-barrier solution to prevent uncontrolled release of formation fluids. The figure below shows the primary and secondary barriers for an example subsea well with a vertical Christmas tree. The production tubing constitutes one of the barrier elements of the primary barrier. If the tubing collapses below the down hole safety valve (DHSV), the primary barrier is broken, and the containment cannot be regained by shutting the DHSV as shown in the figure. The well integrity then relies on the secondary barrier. The barrier elements are required to be identified for all well operations. These are also listed in the figure example with corresponding validation and monitoring of each element.

Well barrier elements	EAC table	Verification/monitoring
Primary well barrier		
In-situ formation	51	n/a after initial verification
Liner cement (top reservoir to production casing shoe)	22	n/a after initial verification
Casing (production liner)	2	n/a after initial verification
Liner hanger packer	7	n/a after initial verification
Casing (between production packer and liner hanger packer)	2	n/a after initial verification
Production packer	7	Continuous pressure monitoring of A-annulus
Completion string	25	Continuous pressure monitoring of A-annulus
DHSV / control line	8	Periodic leak testing. AC DHSV: xx bar/xx min.
Secondary well barrier		
In-situ formation	51	n/a after initial verification
Production casing cement (above production packer)	22	daily monitoring of the B-Annulus
Production casing (above production packer)	2	Continuous pressure monitoring of A-annulus
Production casing hanger with seal assembly	5	Continuous pressure monitoring of A-annulus
Tubing hanger (seals)	10	Continuous pressure monitoring of A-annulus
Wellhead (WH/tree connector)	5	Continuous pressure monitoring of A-annulus
Subsea tree	31	Periodic leak testing of valves AC: xx bar/xx min.

Figure 2 Production well with vertical Christmas tree, taken from [1]

The integrity of the primary and secondary barriers relies on all the barrier elements to function together. If one barrier element fails, the barrier itself fail. The tubing is the one element where failure occur most often. In fact, 29 out of 75 wells with well integrity problems resulted from tubing failure according to a survey presented in the PhD thesis *Contribution to well integrity and increased focus on well barriers from a life cycle aspect* [4]. The high frequency of production tubing problems sets focus on improving design methodology such as increasing implementation of quantitative risk analysis (QRA) for design of production tubing. A failed tubing can in many cases be repaired by patching it from the inside inserting a smaller tubing held in place by a packer on each end of the damaged length [7], otherwise a recompletion may be necessary.

Number of wells with well integrity problem
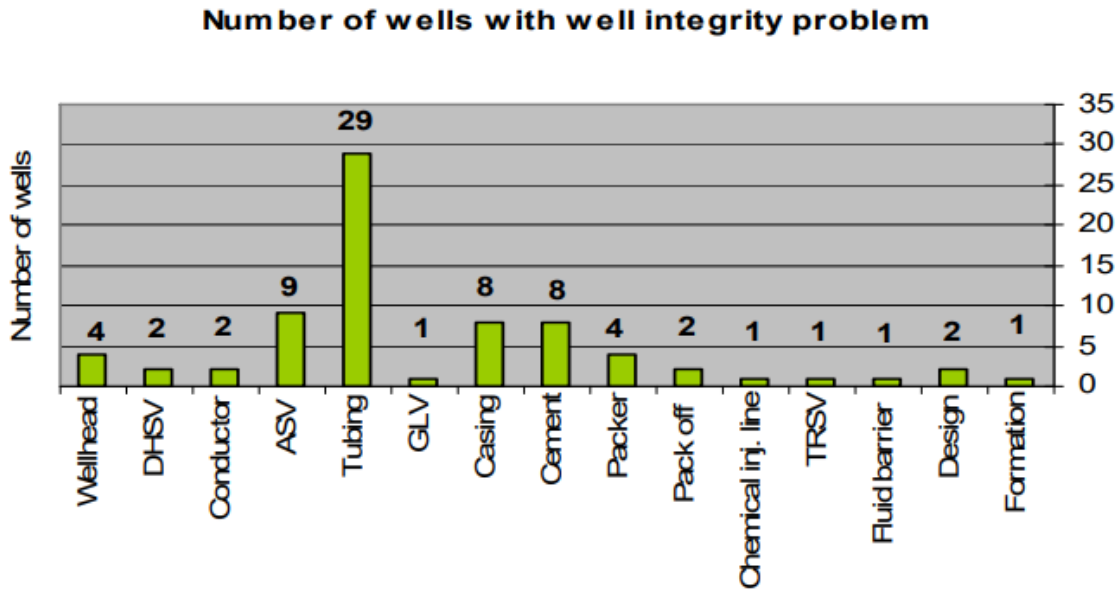
Figure 3 Causation of well integrity problems, taken from [4]

2.4 Casing design model using API 5C3 equations

Now that we have seen how casing strings and tubing can be configured in the well, we need to consider individual sections of casing strings to determine the strength required for the tubular. This largely depend on the expected internal and external pressure and on the axial load the casing is being subjected to during various load cases considered. The loads the casing is subjected to can be defined as axial, collapse and burst loads. The axial load is the resultant load on the casing in the axial direction. The collapse load is the differential pressure across the casing wall when the pressure is larger on the outside. The burst load is the differential load across the wall of the casing when the pressure is larger at the inside. The advantage of defining these loads, burst, collapse and axial, is that the failure mode of the casing, burst, collapse or axial is evident. Collapse, burst and axial strength is differently predicted as will be described in the next sub-sections.

The American Petroleum Institute (API) has developed formulas for casing and tubing design through the API standard *Bulletin on Formulas and Calculations for Casing, Tubing, Drill Pipe, and Line Pipe Properties* (API Bulletin 5C3). The tree main failure modes; axial, burst and collapse are represented here by strength models of the API standard. We will later look at how the API design model compares to other design models and principles and see how the strength and loads can be visualized by design plot schematics.

8

2.4.1 Axial

Axial failure mode is a result of the axial force acting on the string being the crucial factor leading to failure. Defining the axial load on the string as tension positive, meaning that the hanging weight of the string is positive increasing upwards as more weight is added with length. A positive axial load referred to as tension may lead to yield failure. Similarly, a negative load referred to as compression may lead to buckling. When no mechanical forces are applied to the casing string, the axial load is often regarded as the buoyed weight of the casing, from the shoe up to the point considered i.e. before it is cemented or weight being transferred otherwise. When the casing is subjected to additional load, this will add or subtract to the buoyed weight. Such may include overpull while running the casing or bump plug while cementing [8]. Bending forces due to dogleg, shock loads due to accelerated movement or drag forces while running casing may also contribute to the load case at different times [6]. The axial load can either be tensional or compressional. The buoyed weight or effective force is expressed as.

$$F_a' = (Z_{shoe} - Z)\, w_{air} + p_{i,shoe}\, A_i - p_{o,shoe}\, A_o \qquad (1)$$

After the casing cement is set and the casing is fixed at the top by the casing hanger, the casing cannot expand or contract, thus any changes in pressure or temperature will impact the tensional load on the casing as expressed below. The axial load caused by the buoyed weight of the casing will remain as the stretch in the string now is locked at both ends. These equations also apply for a tubing string locked at both ends by the production packer and tubing hanger. The differential load ΔF_a caused by temperature and pressure changes is added to the buoyed weight F_a' [8]. Here α is the coefficient of thermal expansion and v is the Poisson's ratio of the steel (typically around 0.3). The temperature and pressure change are taken as the average over an uncemented interval. *"For casing depths axially constrained by cement, changes in force are due to changes in temperature and pressure at that particular depth"* [8].

$$\Delta F_a = \alpha E A_p\, \Delta T + 2\,v\, (\Delta p_i A_i - \Delta p_o A_o) \qquad (2)$$

$$F_a = F_a' + \Delta F_a \qquad (3)$$

To compute the axial stress used in collapse calculation we need to divide the axial force by the cross-sectional area of the pipe steel wall A_s.

$$\sigma_z = \frac{F_a}{A_s} \qquad\qquad (4)$$

The axial strength of a casing is regarded as the lower yield stress of the casing, shown as the casing grade in ksi. For example, an API L-80 casing has a lower yield strength of 80ksi. Axial tensile load of the casing should not exceed the lower yield strength of the material during running, drilling or production operations because beyond the elastic limit the casing will permanently deform resulting in loss of strength [6]. For high temperatures, the yield strength need to be de-rated as high temperatures decrease the strength. *"Temperature-dependent yield is often defaulted to a reduction of* 0.03%/F *starting at 70F"* [2]. However temperature deration is specific to the manufacturer, and *"for shallower wells with a maximum temperature in the order of* $80 - 100°C$, *no correction is usually applied"* [5].

The casing string with couplings however must not be loaded axially beyond a load resulting in exceeding either the casing lower yield strength, the coupling fracture strength or the tensional force for joint pullout, which ever being the limiting factor. These considerations are beyond the scope of this study.

The lower yield strength can be used to approximate elastic limit, however for alloy steel, the yield strength is not obviously located so the yield point is approximated by using a 0.2% offset strain (permanent strain for yield stress) as the base of the corresponding unloading curve [9] as shown in the figure below. The figure shows the stress strain curve for carbon steel and alloy steel tensile test. Both materials are commonly used for casing. Engineering strain ε is defined as the material elongation divided by its original length. Below the plastic limit, the curve is straight with a slope called the modulus of elasticity, in this case it is the Young's modulus E which is a measure of resistance to axial elastic deformation of a material. As seen in the left figure, the lower yield strength and plastic limit are approximate. The upper yield strength occurs for carbon steel and allows for some plastic deformation. The ultimate tensile strength corresponds to the maximum load possible and the fracture strength to the load at which the test sample part.
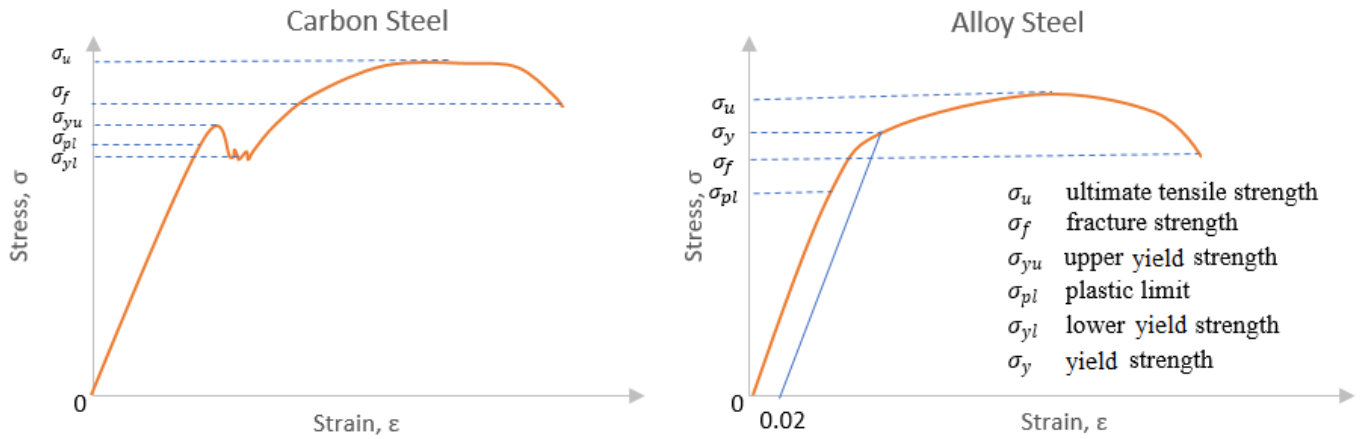
Figure 4 Stress-strain curves for steel and alloy steel

Alternatively to comparing axial stress to the yield strength of the material as described above, we can compare the axial load force F_a to the Pipe Body Yield Strength P_y as defined by the API5C3 [10]. The only difference between the two approaches is that the first compares axial stress and the latter compares axial force. In both cases, in the application of WSD, the same chosen design factor is applied to the strength. The pipe body yield strength is defined below. Note that the equation is just the steel cross section multiplied by the yield strength.

$$P_y = 0.7854(OD^2 - ID^2) \cdot \sigma_y \tag{5}$$

2.4.2   Burst

Burst failure mode implies that the string fails due to the inner pressure of the casing being higher than the pressure outside the casing. When the differential pressure over the pipe thickness exceeds the burst strength, the pipe will burst outward. The burst load is defined as the differential pressure over the pipe thickness.

$$P_{b,load} = P_i - P_o \tag{6}$$

The burst strength predicted as the internal yield pressure proposed by API 5C3 is an adaptation of the Barlow burst equation for thin walled pipe as shown in equation 7. The thin walled assumption is an assumption of a ratio $r_i/t < 10$. *"A casing string can be considered a thin walled vessel"*[5]. A tolerance of 0.875 is applied. Tolerance is defined as 1/DF, it is applied as a tolerance wall thickness correction to allow casing wear and corrosion [11]. This tolerance

however is not to be confused with the design factors used in casing design by WSD, as the tolerance is part of the burst pressure rating of the tubular. The ISO/TR 10400 standard states that the tolerance "*is the factor to account for the specified manufacturing tolerance of the pipe wall*"[12]. The WSD design factor is applied in addition to the API tolerance. API 5C3 also proposes burst equations for couplings to be used when they are limiting the design, however that is beyond the scope of this work.

$$P_b = 0.875 \left(\frac{2\sigma_y t}{D_o} \right) \tag{7}$$

2.4.3 Collapse

Collapse failure mode implies that the string fails due to the outer pressure of the casing being higher than the inner pressure. When the differential pressure over the pipe thickness is higher than the collapse strength, the pipe will collapse inward. The collapse load is defined as the differential pressure over the pipe wall thickness.

$$P_{c,load} = P_o - P_i \tag{8}$$

The collapse strength formulas proposed in the API 5C3 standard are empirical equations developed for four regions of collapse, i.e.: yield strength, plastic, transitional and elastic collapse. The appropriate collapse strength equation is selected based on the slenderness ratio of the pipe, that is the ratio of the outside diameter to the wall thickness of the pipe D_o/t. In the figure below the collapse strength or resistance is shown as a function of the slenderness ratio through the different regions of collapse modes. The bolder line shows the equation prevailing for each region for a 7", L-80 tubing. In general the most important parameters for collapse strength is the casing outer diameter D_o, wall thickness t, the material yield strength and Poisson's ratio v which is the negative ratio of lateral to axial strain [6]. The Poisson's ratio is not an input parameter in the empirical API equations. The collapse formulas for the collapse pressure P_c will now be presented for each region. The equations are available in the standards ISO/TR 10400; Chapter 8 [12], and the API5C3; Chapter 2 [10].
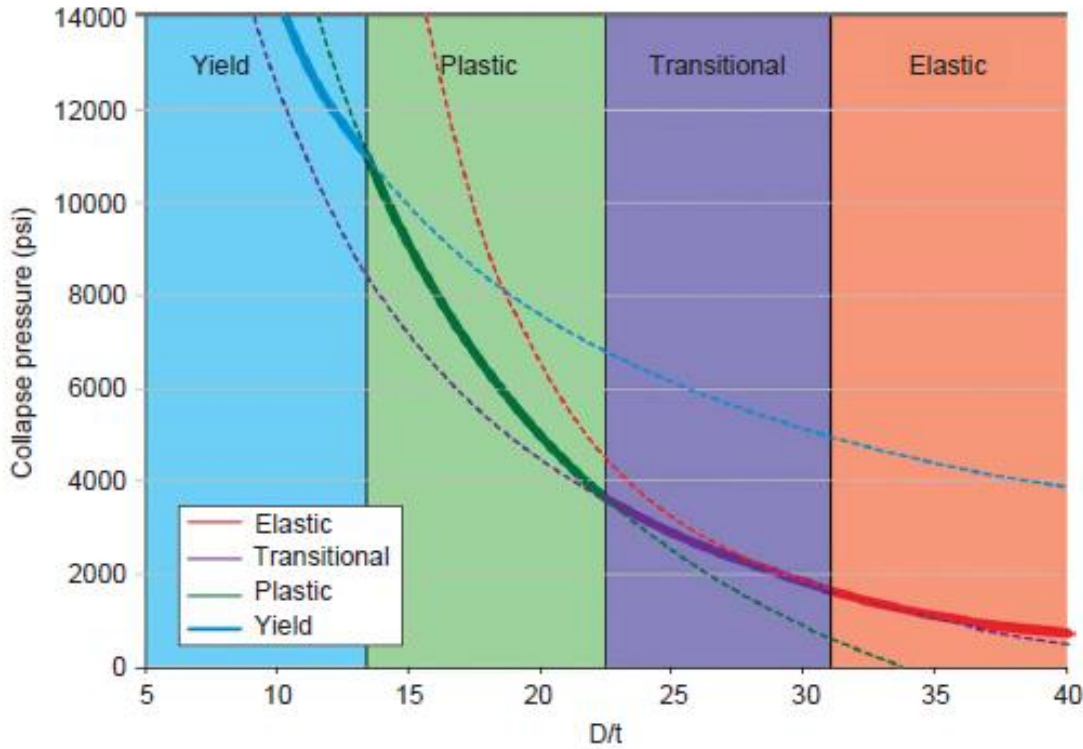
Figure 5 API Collapse Resistance and Collapse regions for an L-80 tubing [2]

The yield strength collapse pressure formula P_{Y_p} is valid within the yield strength region, that is for values of slenderness ratio up to the intersection with the plastic collapse formula. This intersection or upper limit of the yield strength collapse region can be determined by the following formula for $\left(\frac{D}{t}\right)_{yp}$.

$$\left(\frac{D}{t}\right)_{yp} = \frac{\sqrt{(A-2)^2 + 8\left(B + \frac{C}{\sigma_y}\right)} + (A-2)}{2\left(B + \frac{C}{\sigma_y}\right)} \tag{9}$$

The yield strength collapse pressure P_{Y_p} is given by the following formula.

$$P_{Y_p} = 2\sigma_y \left(\frac{(D_o/t) - 1}{(D_o/t)^2}\right) \tag{10}$$

$$A = 2.8762 + 0.10679 \times 10^{-5}\sigma_y + 0.2131 \times 10^{-10}\sigma_y^2 - 0.53132 \times 10^{-16}\sigma_y^3 \tag{11}$$

13

$$B = 0.026233 + 0.50609 \times 10^{-6}\sigma_y \tag{12}$$

$$C = -465.93 + 0.030867\sigma_y - 0.10483 \times 10^{-7}\sigma_y^2 + 0.36989 \times 10^{-13}\sigma_y^3 \tag{13}$$

The numbers involved in the equations for the constants above require the use of USC units. USC units stand for United States customary units (feet, Lb etc.) and is wildly used in the petroleum industry along with the use of SI units (m, kg etc.), which stand for the International System of Units.

2.4.3.1 Plastic collapse pressure

The Plastic collapse pressure formula P_p is valid within the plastic region, that is for values of slenderness ratio above the intersection with the yield strength collapse formula and below the intersection with the formula for transitional collapse pressure. The upper limit of the plastic region can be determined by the formula for $\left(\frac{D}{t}\right)_{PT}$ given below.

$$\left(\frac{D}{t}\right)_{PT} = \frac{\sigma_y(A - F)}{C + \sigma_y(B - G)} \tag{14}$$

$$G = F\frac{B}{A} \tag{15}$$

$$F = \frac{46.95 \times 10^6 \left(\dfrac{\frac{3B}{A}}{2 + \frac{B}{A}}\right)^3}{\sigma_y \left(\dfrac{2B/A}{2 + \left(\frac{B}{A}\right) - \left(\frac{B}{A}\right)}\right)\left(1 - \dfrac{3B/A}{2 + \left(\frac{B}{A}\right)}\right)^2} \tag{16}$$

The plastic collapse pressure is given by the following formula.

$$P_p = \sigma_y\left(\frac{A}{D/t} - B\right) - C \tag{17}$$

2.4.3.2 Transitional Collapse pressure

The transitional collapse pressure equation P_t is valid within the transitional region between the plastic and elastic region. The upper limit of this region, that is the intersection between the transitional and elastic collapse equation is given as $\left(\frac{D}{t}\right)_{TE}$ below.

$$\left(\frac{D}{t}\right)_{TE} = \frac{2 + B/A}{3B/A} \tag{18}$$

The transitional collapse pressure is given by the following formula.

$$P_T = \sigma_y \left(\frac{F}{D/t} - G\right) \tag{19}$$

2.4.3.3 Elastic Collapse Pressure

The elastic collapse pressure formula P_E is valid within the elastic collapse region, that is for values of slenderness ratio above the intersection $\left(\frac{D}{t}\right)_{TE}$ with the transitional collapse equation.

$$P_E = \frac{46.95 \times 10^6}{\left(\frac{D}{t}\right)\left(\left(\frac{D}{t}\right) - 1\right)^2} \tag{20}$$

2.4.3.4 Axial stress equivalent grade

The collapse model proposed by API 5C3 as presented above incorporates the material minimum yield stress of the casing σ_y. This works fine when the casing is only being subjected to the collapse load defined as the differential pressure across the pipe thickness, however when the pipe in addition is loaded under axial tension σ_z, the collapse strength is reduced without the model taking account [8]. To adjust for this effect, we replace the material minimum yield stress σ_y with the axial stress equivalent grade σ_{ya}, for use in the API collapse equations. This implies that the new yield stress σ_{ya} is used as if the pipe was not loaded axially in the first place. The API collapse model is not valid for axial stress equivalent grade less than 24000psi [10].

$$\sigma_{ya} = \left(\sqrt{1 - 0.75\left(\sigma_z/\sigma_y\right)^2} - 0.5\,\sigma_z/\sigma_y \right) \sigma_y \qquad (21)$$

2.4.3.5 Equivalent collapse pressure

The API collapse equations were developed empirically from experiments on casings, the equations give the collapse resistance when neglecting the internal pressure. The effect of internal pressure on collapse load is *"caused by the external pressure acting on a larger area than the internal pressure"* [2]. A correction in collapse strength for internal pressure acting on the inner circumference has been developed and is incorporated in the *ISO/TR 10400 Technical report* [12]. *"The API collapse rating is compared to the equivalent collapse pressure P_{ci}"* [8]. This means that P_{ci} is a correction of the collapse resistance or strength P_c which can be determined by the API collapse equations. *"The value P_c is the collapse resistance calculated neglecting internal pressure, but accounting for any axial load"* [12].

$$P_{ci} = P_c + \left(1 - 2\frac{t}{D}\right) P_i \qquad (22)$$

2.4.3.6 Combined loading equivalent grade

The combined loading equivalent grade σ_{ycom} was presented in the October 2015 Annex M. addendum to the *API Bulletin 5C3* and *ISO/TR 10400 Technical report*. The Combined loading equivalent grade replaces the Axial stress equivalent grade and Equivalent collapse pressure. *"The modifications are technically necessary to provide a more rigorous calculation for collapse by combining the effects of axial stress and internal pressure"* [13]. The equation is valid for $\sigma_a + p_i \geq 0$, where σ_a is the axial stress component not due to bending.

$$\sigma_{ycom} = \left(\sqrt{1 - 0.75\left((\sigma_a + P_i)/\sigma_y\right)^2} - 0.5\,(\sigma_a + P_i)/\sigma_y \right) \sigma_y \qquad (23)$$

2.5 Loads and Principal Stresses

During the well lifetime, casing and tubing strings installed in the well is subjected to different types of loading. Collapse, burst, and axial loads will result from different load cases as we will investigate in section 2.7. The burst and collapse load are combination loads that are useful for design purposes. These loads rely on the inner and outer pressure and can be the same for different combinations of inner and outer pressure that the string is subjected to. They are compared to the estimated burst and collapse strength as discussed previously. Another way of evaluating the stress state of a tubular is by the three principal stresses that act perpendicular to each other, stating a tree dimensional stress state.

In *Petroleum Rock Mechanics,* Aadnøy describes the principal stresses as such; *"If we rotate our coordinate system to an orientation where all shear stresses disappear, the normal stresses are then defined as principal"* [14]. A casing string is subjected to the principal stresses, radial stress σ_r, tangential stress σ_θ and axial stress σ_z, all which are perpendicular to one each other. The principal stresses can also be named after their value largest to smallest $\sigma_1, \sigma_2, \sigma_3$. The axial stress is the resultant load along the axial direction of the string whilst the radial and tangential stress works across the casing wall in the perpendicular cross section. The tangential stress works in the tangential direction of a point in the casing wall whilst the radial stress works in the radial direction. Because casing and tubing strings can be regarded as thin wall cylinders, only the thin walled simplification of the principal stresses acting on a cylinder subjected to a differential pressure ΔP are shown here [15]. These stresses are derived from the Lame equations [5].

$$\sigma_r = -\Delta P \tag{24}$$

$$\sigma_\theta = \frac{\Delta P \, r_i}{t} \tag{25}$$

$$\sigma_a = \frac{F_a}{A_s} + \Delta\sigma_z \tag{26}$$

$$\Delta\sigma_z = \frac{\Delta P \, r_i}{2 \, t} \tag{27}$$

$$\Delta P = P_i - P_o \tag{28}$$

For a closed cylinder, an additional axial stress is $\Delta\sigma_z$ is generated from the differential pressure, however if the cylinder is open ended with differential pressure no additional axial stress is generated [16]. A cylinder is thin walled when the thickness is less than or equal to one tenth of the inner radius r_i . As seen from these equations, the principal stresses can be evaluated at a point along a pipe, but they are not variable across the wall thickness, this is a result of the thin wall simplification. For the thick wall cylinder principal stresses, radial and tangential stress vary across the wall thickness t, that is they are dependent on a variable radius r, as shown in the figure below [11]. This figure shows a collapse mode, both the radial stress, axial stress and tangential or hoop stress is negative as the pressure on the outside is greater than that on the inside of the casing. This is because of the tensional positive convention, the radial, hoop and axial stress is compressional in this case. Note that the axial stress σ_a discussed here is that generated by the collapse mode, not including the buoyed weight or other axial forces F_a. When additional axial forces come in addition, such as the buoyed weight of a string, the axial principal stress could become positive.
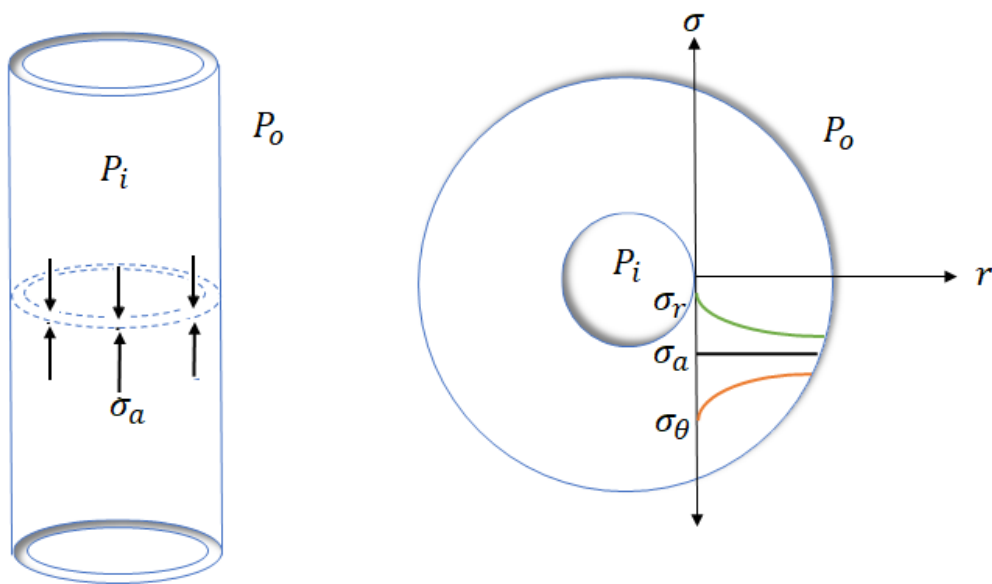
Figure 6 Thick wall principal stresses acting on a casing string cross section in collapse mode

2.6   Comparing design principles by design plots

As mentioned earlier, there are several other models for calculating collapse and burst strength aside from the empirical API models discussed until now. We will mention some of these methods in this section. First, for the analytical methods we need to define tree different failure criteria, that can be used to derive equations for analytical collapse equations. Failure criteria is a way of defining the stress state at which yielding of the material occurs, meaning that it is equated to the yield strength. The different failure criteria for a thin walled cylinder depend on the principal stresses defined in section 2.5. for a thin walled cylinder. If any combinations of principal stresses in the failure criteria surpasses the yield strength, then failure occurs. The criteria are the Maximum principal stress failure criteria, the Tresca failure criteria and the Von Mises failure criteria. The ranging of their absolute values of the principal stresses is important for the failure criteria's. Note that the sign convention of the principal stresses is such that tension is positive, regardless of the sign from the equations. For example, in the previous figure, radial stress is negative as it poses a compression force on the pipe wall, the tangential stress is negative as it is compressional in a collapse mode. The sign convention does not affect the failure criteria's as it uses absolute values for the principal stresses.

The Maximum principal stress failure criteria uses the maximum principal stress theory. It defines the stress state at which failure occur as the maximum principal stress. Meaning that the highest absolute value of the tree principal stresses at the specific load case is used. For example, if the tangential stress is the largest principal stress $\sigma_{max} = \sigma_1 = \sigma_r = -\Delta P$, such as is the case for a collapse mode, then this is equated to the yield stress, and the collapse will occur when the tangential stress reaches the yield strength of the material. The maximum principal stress is therefore defined as following [11].

$$\sigma_y = |\sigma_{max}| = |\sigma_1| \tag{29}$$

The Tresca failure criteria uses the Maximum shear stress theory, meaning that the material is assumed to yield at the maximum shear strength of the material. It accounts for the maximum and minimum principal stress. The yields stress is equated to the maximum minus the minimum principal stress. For a collapse mode for example, this becomes the tangential minus the radial stress. The Tresca failure criteria is given as following [11].

$$\sigma_y = |\sigma_{max}| - |\sigma_{min}| = |\sigma_1| - |\sigma_3| \tag{30}$$

19

The Von Mises failure criteria uses the maximum distortional energy theory and account for all the tree principal stresses. The material is assumed to yield at the load principal stress combination that gives the highest distortional energy. The yields stress is equated to the Von Mises equation that incorporates all the principal stresses as well as a possible shear stress τ [11]. It is important to note that the effective axial stress σ_z in the Von Mises equation includes any bending stresses and thermal induced stresses [11].

$$\sigma_y = \sigma_{VME} = \sqrt{\frac{1}{2}[(\sigma_\theta - \sigma_r)^2 + (\sigma_r - \sigma_z)^2 + (\sigma_z - \sigma_\theta)^2] + 3\tau^2} \qquad (31)$$

It is possible to plot these design principles in a two-principle stress plane, that is the plane at which the third principal stress is zero. Such a plot corresponds to either a burst or collapse mode. In the figure shown, the Maximum principal, the Tresca and the Von Mises principle stress theory is applied to a pipe body is presented.
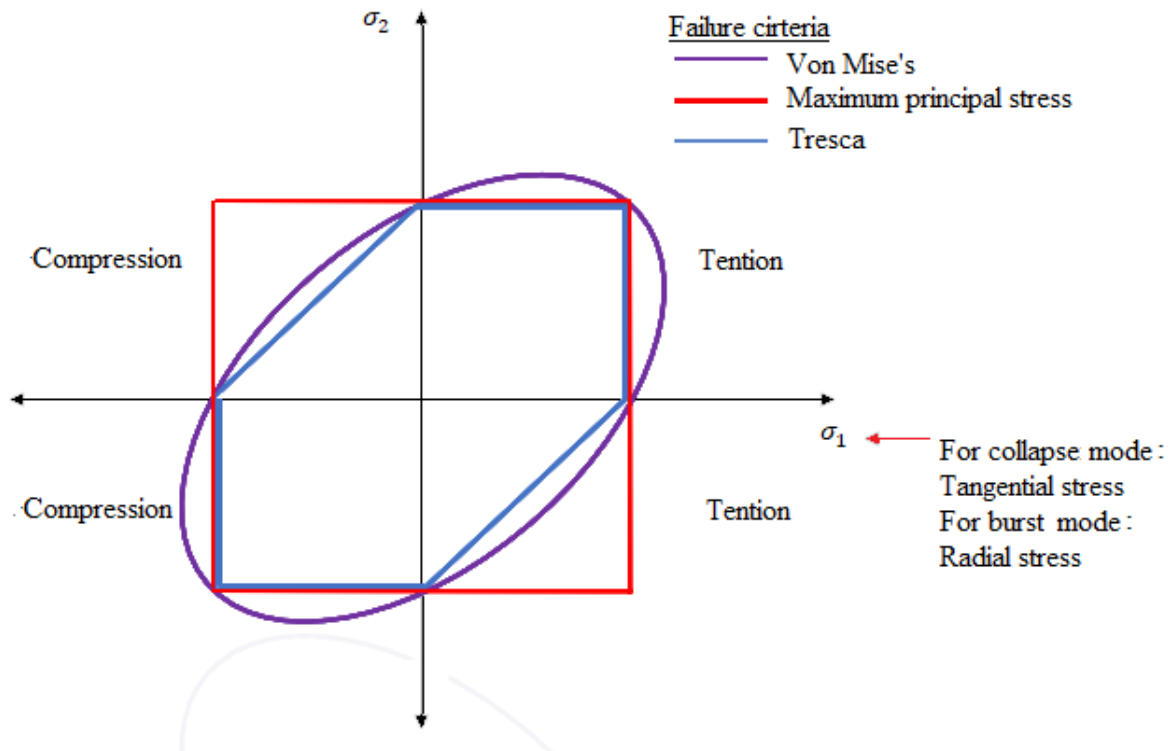

Figure 7 Two principal stress plot showing different design criteria

If the load, when plotted in the above figure, is within the constraints of one of the design criteria envelopes, then the load is acceptable for that criteria. If it is outside the envelope, then it is not an acceptable load. A design factor can be applied to each criteria by dividing the yield strength by the design factor, this reduces the envelope area, i.e. it becomes more conservative.

For each of the tree failure criteria, equations for burst and collapse pressure can be derived. This is done by first substituting the principal stresses in the criteria chosen by the equations for these stresses (for example the ones presented for thin walled cylinder in chapter 2.5, or for the thick-walled ones that we have not presented here). When this is done, the resulting equation is solved with respect to the differential pressure across the wall thickness that now represent the strength. Note that the difference when doing this for burst and collapse strength is that the principal stresses are ranged differently from highest to lowest in magnitude for burst and collapse mode.

As an example, we can get an expression for triaxial collapse strength for a thin walled cylinder if we insert the tree principal stress equations into the Von Mises equation (failure criteria) and solve for the differential pressure $P_c = \Delta P$, this derivation is not done here.

If we want a biaxial collapse equation for a thin walled cylinder, we insert the maximum and minimum principal stress equations in the Tresca failure criteria and solve for the same differential pressure $P_c = \Delta P$, this derivation is not done here.

Similarly, to get a uniaxial collapse equation for a thin walled cylinder, we insert the maximum principal stress equation in the maximum principal stress failure criteria and solve for the differential pressure $P_c = \Delta P$, this derivation is not done here.

The Barlow equation for burst as shown in section 2.4.2 can be derived by inserting principal stresses for thin walled cylinder into the Tresca failure criteria for a burst mode. Note that for a burst mode, the radial stress is negative as it is compressional on the tubing wall from the inside, and the tangential stress is positive as it is tensional. We get that $\sigma_y = \sigma_1 - \sigma_3 = \sigma_\theta - \sigma_r$, by inserting the principal stresses, we get $\sigma_y = (\frac{\Delta P \, r_i}{t}) - (-\Delta P)$. By applying a tolerance, Tol, this result in a biaxial burst equation for thin walled cylinder, the Barlow equation.

$$P_b = \Delta P = Tol \frac{2 \, \sigma_y \, t}{OD}$$

By using the Von Mises equation and inserting the equations for the principal stresses for thick walled cylinder, the following burst and collapse equations can be derived, given the geometry factor β. These can also be used for thin walled cylinders as the thin wall principal stresses is a

simplification. The below equations for burst and collapse are derived from the principal stresses and thereby from the Lame equations, these are found from [5].

The following equation is for collapse, it expresses the maximum outer pressure p_o, given a known inner pressure load p_i, here σ_a is the axial principal stress.

$$p_o = \frac{p_i(1\beta - 1) - \sigma_a + \sqrt{4\sigma_y^2 - 3(p_i + \sigma_a)^2}}{2(\beta^2 - \beta + 1)} \tag{32}$$

The following equation is for burst, it expresses the maximum inner pressure p_i, given a known outer pressure load p_o, here σ_a is the axial principal stress.

$$p_i = \frac{\beta p_o(2\beta - 1) + \sigma_a(\beta - 2) + \sqrt{4\sigma_y^2(\beta^2 + \beta + 1) - 3\beta^2(p_o + \sigma_a)^2}}{2(\beta^2 - \beta + 1)} \tag{33}$$

The geometry factor β is given in the below equation.

$$\beta = \frac{2r_o^2}{r_o^2 - r_i^2} = \frac{(d_o/t)^2}{2(d_o/t - 1)} \tag{34}$$

It is possible to plot different design criteria and models in a design plot, where tubing differential pressure is plotted against the axial stress. The NORSOK D-010 standard require both the API 5C3 model and the Von Mises design criteria as well as pipe end capacities to be fulfilled for tubular design. This standard also defines an allowable utilization area as the common performance envelope defined by the intersection between the design principles [1]. This is the allowable area for a load scenario to take place for the design considered, meaning that the load needs to be within the API model and the Von Mises envelope, and above the connection limitation at the same time. However, in the case study, we will only apply the API design criteria for simplicity. The triaxial Von Mises design criteria as well as the API model for collapse described above are shown together in the below design limit plot for comparison. Here connections are shown to limit the design because it poses a bottleneck for the axial compression strength as mentioned earlier. The envelopes include design factors (see parenthesis in the plot). The load is compared with the common performance envelope, with included bending forces it exceeds the connection limitation in axial compression and is therefore not acceptable for this design.
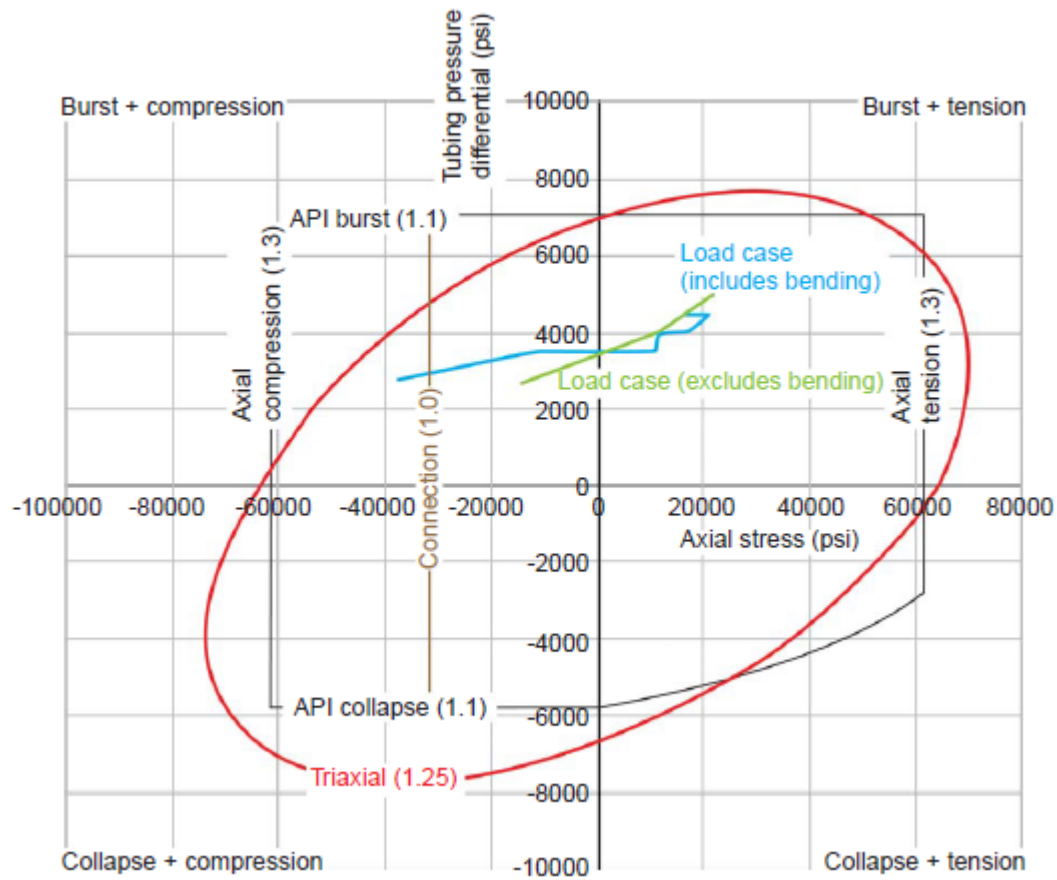
Figure 8 Design plot showing different design criteria for collapse and burst, taken from [2]

Another empirical model for collapse that can be used instead of the API equations is the Tamano equations for ultimate collapse strength $p_{e\ ult}$. The Tamano equations is considered the most accurate prediction of ultimate collapse strength for use in reliability-based design. In the paper *On the Development of Reliability-Based Design Rules for casing collapse* [17], different empirical collapse models, amongst them the API model, was plotted against actual collapse strength. It was established that "*the Tamano equations gives the best combination of a near-unity mean and low COV*", giving the best fit to actual collapse strength. The Tamano equations are presented below, taken from [17].

$$p_{e\ ult} = \frac{(p_e - p_y)}{2} - \sqrt{\frac{(p_e - p_y)^2}{4} + p_e \cdot p_y \cdot H} \tag{35}$$

23

$$p_e = \frac{2 \cdot E}{(1 - v^2)} \frac{1}{\frac{D_o}{t}\left(\frac{D_o}{t} - 1\right)^2} \tag{36}$$

$$p_y = 2\, f_y \left(\frac{D_o}{t} - 1\right)\left(\frac{t}{D_o}\right)^2 \left(1 + \frac{1.47}{\left(\frac{D_o}{t}\right) - 1}\right) \tag{37}$$

$$H = 0.0808\, ov + 0.00114\, ec - 0.1412\, rs \tag{38}$$

Here ov, ec, and rs stand for ovality, eccentricity and residual stress respectively.

2.7   Collapse Load Cases

In this section, we will look at different load cases that a casing or in some cases tubing can be subjected to during the installation, completion and production process. A casing string is made up from several casing tubulars, usually designed in such a manner that it has a higher yield strength at the bottom of the well and at the top. This is because the axial stress is greater at the top, and at the bottom where the differential pressure loads are greater, increasing downward due to different fluid weight inside and outside the casing. Other load considerations such as mobile salt may lead to other individual sections of the casing being designed with greater yield strength. Referring to the definition of collapse load, see section 2.3.3, the critical information for all load cases is the expected internal and external pressure of the tubular considered, either casing or tubing. In the following sections the annular pressure buildup (APB) and sustained casing pressure (SCP) load cases will be described in greater detail. Examples of some other load cases will be described in the proceeding sections as to set the concept in perspective. It is important to note that different load cases may be combined, and that the actual causation of the loads may be unknown.

2.7.1   Collapse due to Annular Pressure Buildup

Annular pressure buildup (APB) refers to the concepts of increasing pressure in the annulus between casing strings (B and C annulus) and in the A annulus between production tubing and production casing or liner. These pressure changes are critical for subsea wells where there can be no access to bleed-off the pressure from the wellhead for the B and C annuluses. In the case of APB, we need to design casings and tubing to withstand the increased burst and collapse loads respectively. The increased pressure from APB comes in addition to hydrostatic load

The term APB is used when an increased pressure in the A annulus is due to annular temperature increase caused by heat transfer from warmer production fluids in the production tubing. This will typically take place at production startup. Over time the heat will transfer to the B and C annulus as well. If the annulus is sealed and cannot be bled off at the top as is the case for most subsea wells, the increased temperature will lead to a thermal expansion of the annular fluid and a corresponding annular pressure buildup since the fluid will not be allowed to expand by the sealed geometry. A sealed annulus results when the production packer closes the A annulus or when a smaller casing is cemented with TOC above a larger casing shoe. The last is often done to isolate formation zones. Normally the A annulus can be bled off at the wellhead as is required by the NORSOK D-010 standard [1]

The simplest approach to APB estimation is obtained by regarding the production tubing and casings of the well to be closed rigid containers with no leak paths. In this case, the annular volume is constant. Presented below is the simple equations proposed by Moe and Erpelding [18] and Aadnøy [5] as means to *"provide a reasonable upper limit for the anticipated pressure rise"* [18], knowing that the model is likely to overestimate the APB as the annular volume is fixed. Although the fluid will not expand in a rigid container, the approach is to calculate an imaginary free volume increase by the coefficient of thermal expansion α and later compress the fluid back to its real volume by the fluid compressibility c, giving the final annular pressure increase ΔP.

$$V = V_o(1 + \alpha\Delta T) \tag{39}$$

$$\Delta P = (V - V_o)/V_o\, c \tag{40}$$

$$\Delta P = \alpha\Delta T/c \tag{41}$$

The temperature change ΔT in the annulus may be approximated by the difference between the average of the linear geothermal and production tubing temperature profiles along the annulus. Here we assume that the annular temperature will approach the well stream temperature. Put differently, it is the average of the temperature change at the wellhead and at the bottom of the annulus due to production heating up the annular fluid. The temperature change at bottom will be negligible when the annulus reaches close to the reservoir such as for the A annulus. For the A annulus, the annular temperature will be close to that of the well stream in the production tubing, but this approximation will get worse as we move away from the center of the well.

The concept is illustrated below together with equations to calculate average annular temperature change. Here the temperature T1 and T3 is the formation and well flow temperature at the wellhead respectively. T2 is the formation temperature at the bottom of the annulus and T4 is the fluid temperature at the bottom of the annulus. In the example the external temperature at the wellhead is taken as four degrees Celsius, increasing downward by a geothermal gradient of 0.03 °C /m. The reservoir temperature is taken as 120 degrees Celsius, and the well flow temperature is approximated to decrease linearly to a wellhead temperature of 60 °C. The temperature profile has in fact an asymptotic behavior as it approaches the reservoir temperature, but the linear approximation impact on the APB is assumed to be negligible for the A annulus.

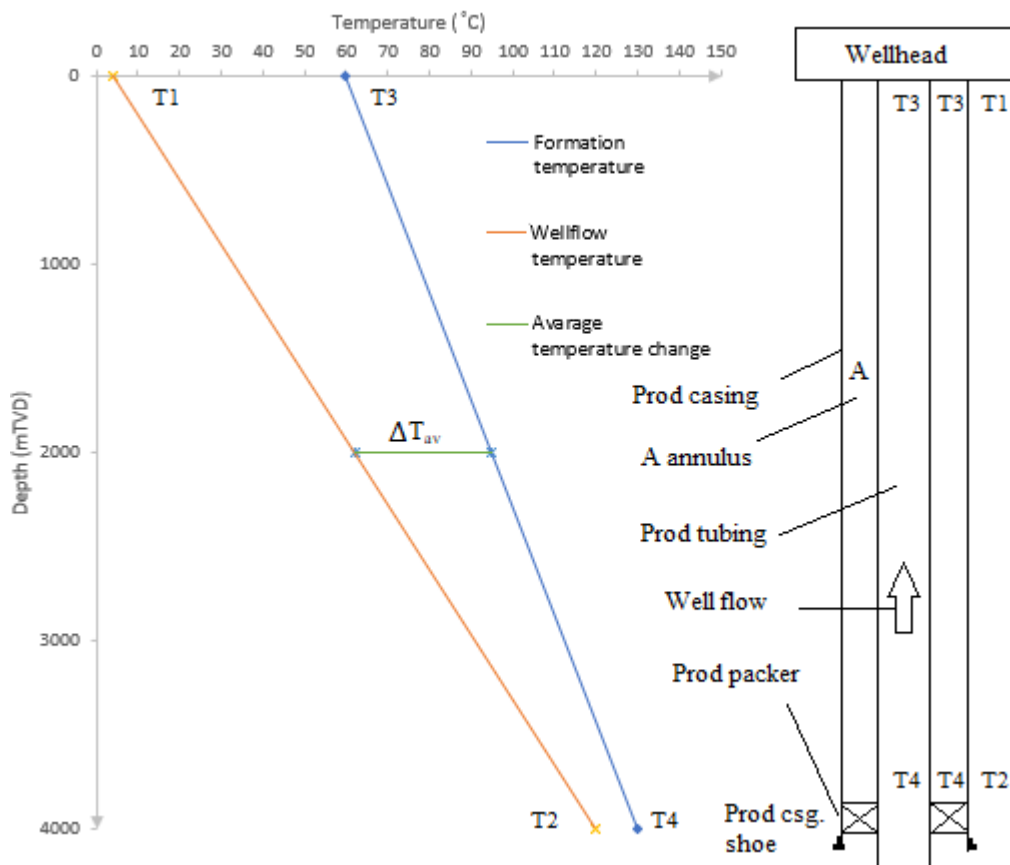$$\Delta T = \frac{T3 + T4}{2} - \frac{T1 + T2}{2} \tag{42}$$

Figure 9 Formation and well flow temperature profile with average annular temperature change

26

For a planned well, the temperature at the wellhead T3 is not a known parameter, it must be predicted to compute the temperature increase in the A annulus. As it moves towards the surface through the production tubing, the produced fluid from the reservoir will lose heat to the external environment. That is to the tubing, annular fluids in the annular spaces, casings, casing cement and the formation beyond. For an accurate prediction, the well should be discretized by depth as the external environment changes with depth. The number of casing strings and annular spaces decrease towards the reservoir. The ambient formation temperature also changes, although this may have a linear relation given by the geothermal gradient. As noted earlier the real temperature profile in the tubing is not entirely linear because the differential temperature across the wall increase towards the wellhead, increasing the driving force for heat transfer across the wall. At the bottom sections the ambient temperature is close to the reservoir temperature, so little heat is exchanged as the temperature difference across the wall is the driving force for heat exchange. The annular temperature is assumed to converge to a steady state as the well flow temperature profile, meaning that it will approach the well flow temperature over time. The temperature profile along the tubing can be simplified by a linear profile as shown in the figure above.

To calculate the wellhead temperature, a heat exchange equation must be applied to the well flow from the reservoir to the wellhead. A simple steady state model for the well flow temperature profile can be developed by equating two expressions for heat loss Q. Equation 40 expresses the specific heat capacity c_p. Equation 41 is a way of expressing Furrier's law $q = -kA\frac{dT}{dX}$, incorporating the overall heat transfer coefficient, the overall U value. The production tubing can be discretized by dividing it into N control volumes and calculating the temperature over each control volume as shown in the equations below. Starting at the reservoir with T_{out} as the reservoir temperature, we calculate the well flow temperature $T_{wf\ (n)}$ in the first control volume. We substitute T_{out} as the well flow temperature from the previous control volume for each step n.

$$T_{wf\ (n)} = T_{wf\ (n-1)} - \Delta T_{cv\ (n)} \tag{43}$$

$$Q = c_p\ \dot{m}\ \Delta T_{cv} \tag{44}$$

$$Q = U_{overall}\ A_{pipe}(T_{out} - T_{ambient}) \tag{45}$$

Because we know two expressions for heat loss Q, we equate them and the temperature change for each control volume becomes ΔT_{cv}.

$$\Delta T_{cv} = \frac{U_{overall} A_{pipe}(T_{out} - T_{ambient})}{\dot{m} c_p} \qquad (46)$$

$$A_{pipe} = \pi \, OD \, L_n \qquad (47)$$

Here A_{pipe} is the outer area of the pipe from the current control volume towards the wellhead, the area decreasing for each step as the next control volume is closer to the wellhead. $T_{ambient}$ is the ambient formation temperature at the considered depth of the control volume, $\dot{m}$ is the mass flowrate and c_p is the specific heat capacity of the production fluid. The overall U value $U_{overall}$ is calculated from the different material conductivities k, heat transfer coefficients of fluids, h_f in the tubing and h_c for (convection and conduction) and h_c for radiation in the annulus with corresponding radiuses as follows [19].

$$\frac{1}{U_{overall}} = \frac{1}{h_f} + \frac{r_o \ln\left(\frac{r_o}{r_i}\right)_{tube}}{k_{tube}} + \frac{1}{h_c + h_f} + \frac{r_o \ln\left(\frac{r_o}{r_i}\right)_{prod\ csg}}{k_{prod\ csg}} + \cdots + \frac{r_o \ln\left(\frac{r_o}{r_i}\right)_{cement}}{k_{cement}} \qquad (48)$$

The U value must be updated as the casing arrangement changes along the wellbore. Some relevant example material thermal properties are listed below.

Table 2 Wellbore thermal material properties

	Specific heat capacity k $[W/m°C]$	Thermal Conductivity C_P $[J/(kg\ °C)]$
Prod. Tubing	500	50
Casing	500	50
Packer fluid	2435	0.72
Cement	2000	0.7
Formation	800	2.25

*These thermal material properties are taken from [20]

In reality, due to the elasticity of the casing strings and the formation, the annular volume is not fixed, therefore *"the equilibrium pressure produced by thermal expansion must be calculated to balance fluid volume change with annular volume change"* [21]. Another difficulty with these calculations is that the volume changes in each annulus is dependent upon that in the others. When considering multiple casing strings, the pressure and volume changes must be determined by numerical iterations. A numerical model for APB for a well with multiple casing strings was presented in the 2014 ENCIT paper *Annular pressure build-up in oil wells* [22], based on methods on annular volume variation proposed by Halal and Michell [23]. In fact these show that *"annular heatup pressures are always overpredicted (by as much as 30%) by fully rigid single-string analysis"* [23]. This is the case for the simple approach previously presented.

Let's consider the case of APB in the A annulus between the production tubing and production casing. The production casing is fixed at both ends, that is by cement at the casing shoe up to TOC and at the wellhead by the casing hanger. Similarly, the production tubing is fixed by the production packer and tubing hanger. Thereby no axial expansion of the tubulars is possible, and the annulus is closed by the production packer and at the tubing hanger. The annular volume will change according to changes in the annular cross section due to deformation of the adjacent tubulars, in this case ballooning of the production casing and reverse ballooning of the production tubing. As noted before this volume change will balance the expansion of the annular fluid and limit the pressure buildup. However, for illustrational purposes we will use the simpler fully rigid single-string approach for collapse load calculations in the APB case study. The maximum differential pressure in the A annulus is that of the packer depth, the lowest point in the enclosed A annulus. This is a result of different fluid gradients on each side of the tubing. For collapse we therefore compare load and strength at packer depth.

The pressure in the A annulus can be predicted by adding the APB, ΔP to the hydrostatic pressure in the A annulus. The A annulus is filled with a packer fluid with density ρ_{pf}. In addition, the hydrostatic sea water column D_{sw} above a subsea well must be added, the sea water gradient can be taken as γ_{sw}=1.03 sg.

$$P_{annulus} = g * \left(D\rho_f + D_{sw}\rho_{sw}\right) + \Delta P \qquad (49)$$

The pressure in the production tubing must be considered as the minimum anticipated pressure there, meaning we consider worst case tubing pressure for collapse load. For a producing well, the pressure in the tubing is the hydrostatic column of the production fluid at depth D, plus the

29

choke pressure and frictional pressure drop along the producing tubing. For a worst-case scenario, we consider a fully open choke with no choke pressure.

$$P_{tubing} = \rho_f D g + \Delta P_{fric} + \Delta P_{choke} \tag{50}$$

The frictional pressure-drop $\Delta P_{friction}$ along the tubing can be predicted by the pressure drop equation below, the Darcy-Weisbachs formula [24]. The Moody friction factor can be found from the Moody chart [25] (see appendix A2). By dividing the moody friction factor by four we get the fanning friction factor f_f. Knowing the roughness ϵ of the pipe, the velocity of the produced fluid and its viscosity μ_f and density ρ_f, we can find the friction factor by calculating relative roughness ε of the pipe and the Reynold number Re of the well flow. Here L is the length of the tubing.

$$\Delta P_{friction} = 4 f_f \left(\frac{L}{ID}\right) \rho_f \frac{v_f^2}{2} \tag{51}$$

$$\varepsilon = \epsilon / ID \tag{52}$$

$$Re = \frac{\rho_f v_f \, ID}{\mu_f} \tag{53}$$

The collapse load on the pipe is now the differential load over the wall thickness, that is the annular pressure minus the tubular pressure.

$$P_{c,load} = P_{annulus} - P_{tubing} \tag{54}$$

2.7.2   Collapse due to Sustained casing pressure

The term Sustained casing pressure SCP is like APB in that pressure builds up between casing strings. However, in contrast to APB the pressure increase is not caused by temperature increase, but instead from gas migration. SCP is often caused by gas from strata below the previous casing shoe that migrates upwards into the annular space where pressure builds up as gas rise, similarly to a gas kick. It may also arise in the A annulus caused by a leaking tubing or production packer. If the smaller casing is cemented to above the previous casing shoe, it may occur when pressure at the shoe exceeds the fracture pressure of the cement. This leads to the pressure building up again if the pressure is bled of from the wellhead and so on, hence a sustained pressure. *"The*

pressure is the minimum of the fracture pressure at the shoe and the reservoir pressure plus the mud gradient" [21]. In the case of a subsea well with no access to the B annulus outside the production casing, the resulting external pressure may be used as a design criteria for casing collapse often using a completion fluid gradient in the A annulus [21].

2.7.3 Collapse due to partial and full evacuation

When a production tubing or A annulus is partially of fully evacuated, the hydrostatic pressure in the tubing or annulus is reduced or eliminated respectively. As the hydrostatic pressure is reduced, a pressure differential will occur. There are many means of which a partial or full evacuation can result, some are presented here.

Partial evacuation is typically a result during drilling from drop in mud level due to losses to formation when encountering lost-circulation zones. In this case, the previously set casing is subjected to a collapse load that increase as the internal pressure decrease when mud level drops. The mudweight should be designed such that the permissible collapse strength is not exceeded by the increased collapse load for an anticipated maximum drop in mud level [21].

Full evacuation may be a result during production of a gas-lift well, the collapse load being subjected on the production casing. In this case the A annulus inside the production casing is assumed to be fully filled with injection gas above the production packer. In an incident where the injection pressure is lost, the external pressure drops to that of a fully evacuated annulus. The collapse load on the casing is then increased as internal pressure decrease. Another situation in which full evacuation can be assumed is while drilling with air or foam, resulting in a greatly reduced internal pressure inside the casing during drilling [21].

2.7.4 Collapse due to mobile formation such as salt and shale intervals

Some types of formations such as salt and shale have a plastic behavior and can move inn on the casing and may cause it to collapse. The external load on the casing is than taken as the overburden pressure when uniformly distributed [21], as opposed to the pore pressure normally considered. The overburden pressure or the lithostatic confining pressure consist of the weight of the combined rock and fluid column above the considered depth. In soil mechanics, total stress σ_{tot} is defined as the effective stress σ' and the pore pressure P_{pore} combined, in our case the total stress is regarded as the overburden confining pressure and the effective stress as the weight of the overburden rock.

$$\sigma_{tot} = \sigma' + P_{pore} \tag{55}$$

Salt mobility is a rock property, the lateral movement depend on the overburden and buoyancy forces such as in salt diapirs [26]. If the section of casing considered is cemented in place, *"the effect of the cement is essentially to change a potentially non-uniform loading condition into one of uniform loading"* [27], non-uniform loading may result in casing deformation, but at elevated temperatures the salt encapsulate the casing at a higher rate, resulting in a uniform loading [27]. Shale formations differ from salt formations in that their mobility *"only occur if overpressured fluids are present"* [26], thereby limited to depth specific overpressured zones.

2.7.5   Collapse due to cement load

When a section of casing is cemented in place, the cement is a liquid slurry and thus add to the hydrostatic load column outside the casing string. The cement is pumped down the casing and is normally displaced by a kill weight mud that remain inside the casing as the cement sets. This to prevent the collapse load across the casing wall to exceed the load limit due to the high weight of the cement slurry. The load case largely depends upon the weight of the cement slurry and the displacement fluid. After the cement is set, the cement no longer poses a hydrostatic load. The external load is replaced by the pore pressure of the formation beyond the cement or the hydrostatic mud column above TOC. The cement is than typically bumped or pressure tested before it is drilled out as drilling commences. The casing needs to be designed to withstand the collapse load posed by the unset cement scenario if the collapse load is greater than any other after the cement is set.

3 Conventional Casing Design Methodology

Reliability-based design is still relatively new in the petroleum industry, although being used for a longer time in other engineering disciplines such as civil engineering. Before explaining the concept of reliability-based design, the conventional methods will be presented for a basis of concept as well as a means of comparing methods. Some of the methods such as Working Stress Design (WSD) is completely deterministic, another method Load and Resistance Factor Design (LRFD) is reliability-based but is still calculated similarly to the traditional WSD procedure. Later we will also see how different methods can be combined. In the case study, we will be combining a deterministic approach for collapse load and collapse strength represented by a probability distribution.

3.1 Working Stress Design

Working stress design (WSD) is the traditional and still dominating design methodology for casing and tubing design in the petroleum industry. This technique uses a deterministic approach for calculating load and strength, where the load is restricted by a design factor from the strength. *"Design factor is the minimum allowable safety factor, which is expressed as the ratio between the rated strength of the material over the estimated maximum load"* [1]. An allowable load thereby always has a safety factor higher or equal to the design factor, that can be calculated by dividing the strength by the load applied. The method can be applied to all kinds of design and is not restricted to load vs. strength applications, although it has its name from the simple application of stress design.

$$\sigma_{load} \leq \frac{1}{DF} \sigma_{strength} \tag{56}$$

$$SF = \frac{\sigma_{strength}}{\sigma_{load}} \tag{57}$$

$$DF = \frac{\sigma_{strength}}{\sigma_{load\ limit}} \tag{58}$$

As an example, we can use collapse load and strength for an L-80 casing with a collapse resistance or strength of 8500 psi. Let's say we use a design factor DF=1.1. This means that the maximum allowable collapse load or the limit state is $\frac{1}{DF}P_c = P_{c,load\ limit} = 7727psi$.
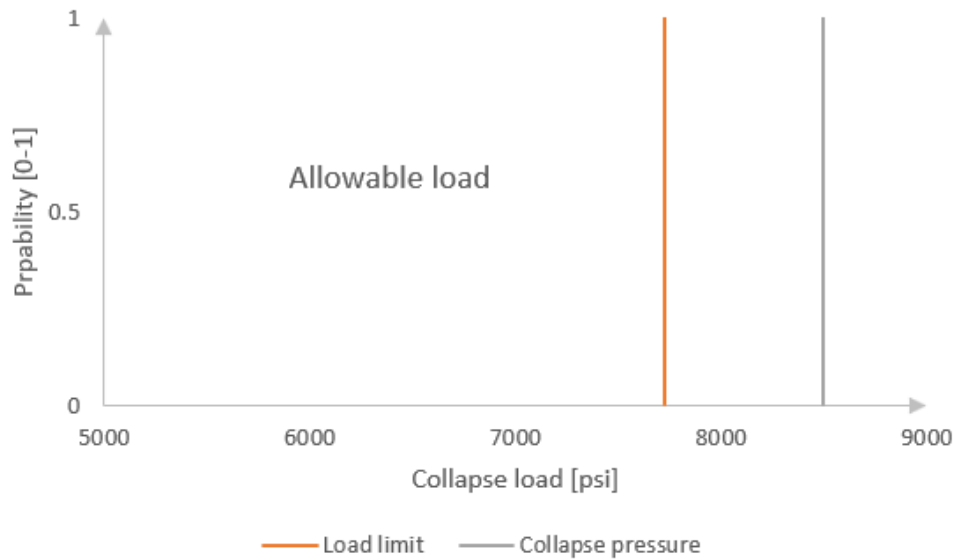
Figure 10 Example of WSD showing Collapse Pressure and Load Limit

The design factors may be proposed by standards such as NORSOK D10 but is more often chosen based on experience or the company's own regulations [28]. The design factors can be tailored to worst case load scenarios previously described. The table below shows design factors proposed by the NORSOK D-10 [1] and Shell Level One casing design criteria of 2000 [29] together with a typical range of design factors used [8].

Table 3 Design Factors

	Burst	Collapse	Axial	Triaxial
Typical range	1.0-1.25	1.0-1.1	1.3-1.9	1.25
NORSOK*	1.1	1.1	1.25	1.25
Shell Level One	1.25	1	1.3	1.25

"Based on wall thickness manufacturing tolerance of minus 12.5%" [1]

3.2   Limit State Design

In WSD we apply a design factor to make sure we don't reach the working stress, that is the strength considered such as the collapse strength. Sometimes the strength of a structure, the working stress, is not the limit we want to consider by applying the design factor. When unfavorable effects take place before the strength is reached, such as buckling or deflection of a drill string, we want to set a lower load as limit state to replace the working stress [8]. Limit states applied may be classified as ultimate limit states where a catastrophic failure takes place, and the serviceability limit states where the structure is no longer considered usable or safe to operate. *"In practice, a dual-design methodology of working stress design for normal loads and limit states design for infrequent survival-type loads may be applied"* [8]. The equations become slightly modified as shown below, as compared to WSD.

$$\sigma_{load} < \frac{1}{DF}\sigma_{limit\ state} \tag{59}$$

$$SF = \frac{\sigma_{limit\ state}}{\sigma_{load}} \tag{60}$$

$$DF = \frac{\sigma_{limit\ state}}{\sigma_{design\ load}} \tag{61}$$

4 Reliability-Based Design

In reliability-based design we recognize that both load and strength must be viewed as probability distributions and the chance for failure will be expressed as a percentage depending on the overlap of these distributions. The questions will then be if the chance of failure will be acceptable. This will vary depending on whether we consider catastrophic events (that should be avoided) or less serious events that may limit the functionality of the installation. In a casing and tubing design perspective this relates to if we can consider the event to be a repair event or a blowout/ultimate failure event. If the failure or damage is repairable, or otherwise manageable, the acceptable failure probability may be set lower as compared to where the event will lead to blowout or ultimate failure [30].

The load and strength distribution are a product of the variability of all the input data that are used in the models for predicting the load and strength. For instance, random variation in geometric properties like inner diameter and thickness will have impact on the strength calculations. For the load, one can also consider how often it occurs (frequency) and what value one put on this will also depend on the criticality of the event. If we consider a Tsunami event, it is not natural to consider the probability of occurrence when estimating how large waves that can occur. We must assume that it happens even if it statistically occurs only very seldom. One must bear in mind that the model themselves will have errors associated with them.

A reliability-based approach accepts uncertainty in estimations and attempts to take the variability into account to give more realistic estimates of what can happen.

Reliability-based design (RBD) opposed to the conventional design methodologies provide a more scientific design basis that based on relevant historic and experimental data can predict the uncertainty of the strength or load considered. Reliability is the complement of probability of failure, that is the probability of durability within an expected time frame. If the probability of failure within this time frame is 10%, then the reliability is 90%.

The methodology presented here is based on Monte Carlo simulations applied on input parameters provided by statistical distributions. Before describing RBD, some basic statistics and the Monte Carlo simulation procedure need to be reviewed.

4.1 Statistical distributions

4.1.1 Distributions and sampling procedure

To start to describe statistical distributions we can present some of the statistical definitions by introducing the Simple random sample SRS, this is one way of sampling a population on which the statistic is built upon. *"A simple random sample (SRS) of size n consists of n individuals from the population chosen in such a way that every set of n individuals has an equal chance to be the sample actually selected"* [31]. This sample is thus a subset of the larger population. Both the SRS and the larger population contains individuals with a measured or counted quantity. The sample variable X is a random variable representing the quantity considered for the statistical analysis and can be plotted as a sample distribution representing the larger population, the larger the sample size the more accurate this representation will be. As an example, the population can be tubing pipes of a specific type and grade, the sample can be a SRS of *n* pipes from the population and the sample variable can be the wall thickness of the sampled pipes X.
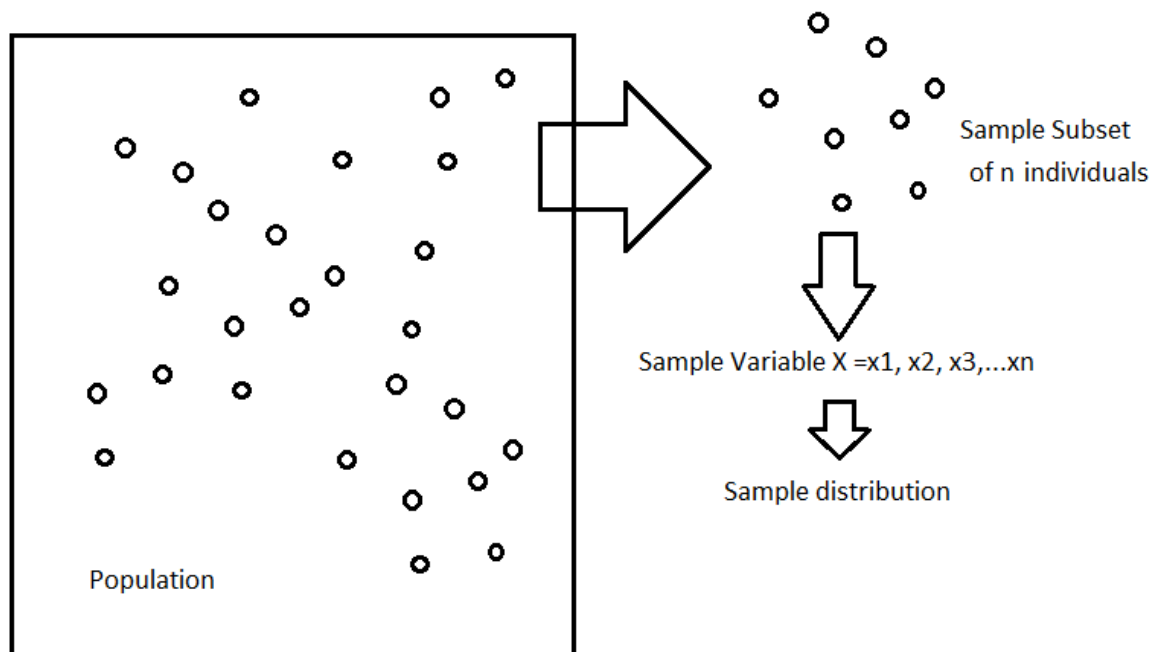
Figure 11 Random sampling process schematics

A sample such as the SRS described above consist of a set of *n* individuals and the corresponding *n* measurements or counts which constitute the sample variable. The sample variable has a mean $\bar{x}$, standard deviation σ_{std}, variance s and median M as shown in the equations below. The variance is the standard deviation squared and the median is the middle value of values listed in

increasing order of quantity. It is slightly differently defined depending upon the sample size n being an odd or even number [32].

$$\bar{x} = \frac{\sum_{i=1}^{n} x_i}{n} \tag{62}$$

$$\sigma_{std} = \sqrt{\frac{1}{n-1} \sum_{i=1}^{n} (x_i - \bar{x})^2} \tag{63}$$

$$s = \frac{1}{n-1} \sum_{i=1}^{n} (x_i - \bar{x})^2 \tag{64}$$

$$M_{odd} = x_{(n+1)/2} \tag{65}$$

$$M_{even} = \frac{x_{n/2} + x_{(n+1)/2}}{2} \tag{66}$$

As an example of mean and standard deviation, the table below show parameters for a 7", L80, 32Ibs/ft tubing represented by mean and standard deviation. The mean and standard deviation can be obtained from experimental datasets listed in ISO/TR 10400 [12].

Table 4 Mean and standard deviation of tubing string parameters

API L80, 7", 32Ibs/ft	Mean μ	Standard deviation σ
Yield strength σ_y $[psi]$	89520	17611
Outer diameter OD $[inch]$	7.0406	0.24892
Wall thickness t $[inch]$	0.45563	0.074031

"A random variable is a variable whose value is a numerical outcome of a random process" [31], such as the SRS of a population. The word random variable is used interchangeably with stochastic variable. We can consider two types of random variables, continuous variables are those that arise from a range of the real numbers R and discrete variables are those that take *"possible values that can be given in an ordered list"* [31], meaning that it takes permissible incremental values from ranges of real numbers R. Statistical distributions can be made by

randomly sampling a variable, either continuous or discrete, and then plotting the results, producing either a continuous or discrete (random/stochastic) distribution. As an example, take the distributions resulting from many tosses of two dices added together and those from the measured wall thicknesses of randomly selected pipes. The dice toss results will be a discrete distribution as the result from one toss is restricted to the range (1-12), whilst the wall thickness distribution will be continuous as the wall thickness can take any positive real number in the sampled range. As number of dice tosses are increased, the more symmetrical the triangular dice toss distribution will be, and as the number of pipes measured increase the wall thickness distribution will converge to a normal distribution. In the figure below, the resulting distribution of a simulation of 1000 dice toss with two dice and the normal distribution for wall thickness is shown, using the mean and standard deviation listed in the table above.
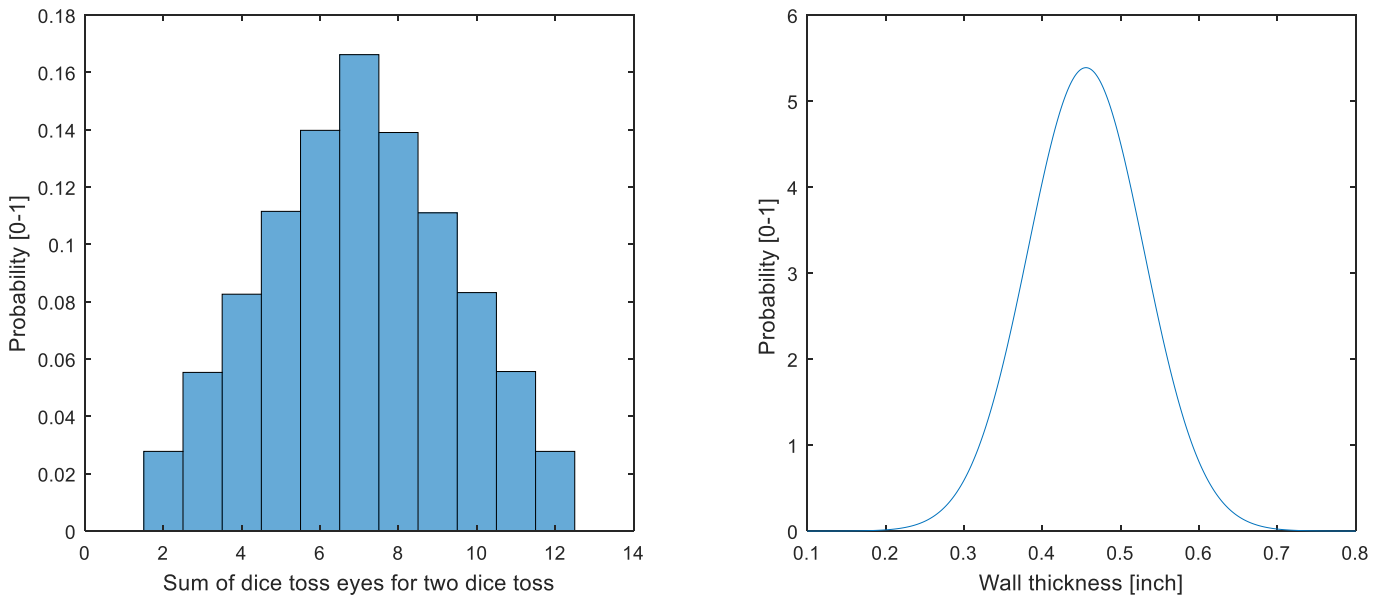
Figure 12 Two dice toss and wall thickness demonstrating discrete and continuous distributions

One important difference between a discrete and a continuous distribution is that the probability of obtaining a given value of the variable is the corresponding normalized column height for the discrete distribution, whilst it for a continuous distribution is always zero because each variable value is spaced by an infinitely small increment and thus the integral defining the probability is zero. This is somewhat misleading, we need to consider the probability of a variable occurring

39

within a defined range to get around the problem, introducing the concept of probability density function PDF and cumulative density function CDF and percentiles.

A PDF is a continuous distribution where the area under the entire graph or the integral is always equal to one, the integral over a defined range of the variable is the probability of the variable taking a value within that range.

A CDF is a continuous function that is the integral distribution of a corresponding PDF such that it at any given variable value gives the probability of the variable taking a value less than or equal to that value, thus a cumulative distribution.

Percentiles are variable values that is defined by the probability of the variable taking any value less than that value. Sometimes they are defined opposite as probability above that value, we will use the first definition. Some common percentiles used are P10, P50 and P90. The percentile P50 is always the median. As an example, there is a 10 percent probability of the variable taking a value less than P10. These are properties of the PDF. We may also use the difference between the P90 and P10 as a measure of spread or variability of the data. Eighty percent of the instances will be in the range obtained. We may call this a confidence interval of eighty percent.

The table and figure below show the PDF and corresponding CDF of a normal distribution with mean, median and P50 equal to ten and a standard deviation of three. Some distribution types commonly used to approximate random sampled data will now be presented. These may take the form of either discrete or continuous as described above.

Table 5 Common percentiles

Percentile	Probability below percentile	Probability above percentile
P10	10%	90%
P50 / Median	50%	50%
P90	90%	10%
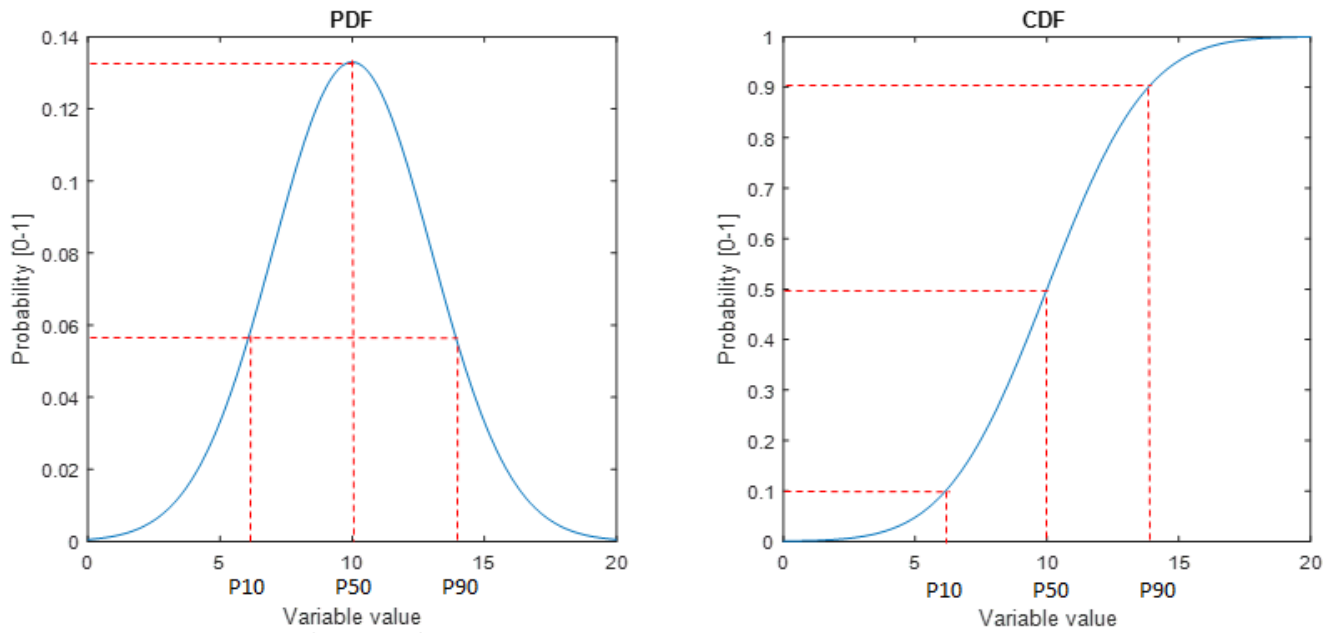
Figure 13 The PDF of a normal distribution $N(10,3)$ and its corresponding CDF showing common percentiles

4.1.2   Normal distribution

A normal distribution $N(\mu, \sigma)$ is a bell-shaped symmetrical function and is defined by its mean and its standard deviation. The wall thickness distribution in the previous section shows a typical example of a continuous normal distribution with mean μ and standard deviation σ as described above. Conversely the dice toss distribution will approach a discrete normal distribution when the number of dice per toss is increased [33]. When only throwing one dice at a time, the result is a random variable, so when throwing many dices at a time the result is the sum of random variables. A resulting normal distribution, when throwing many dice together n times is therefore in accordance with the Central Limit Theorem, that will be defined in section 4.2. A rule of thumb for a normal distribution is the (68-95-99.7) rule that says that the percentiles P68, P95 and P99.7 is one, two and three standard deviations away from the mean of the distribution respectively. The normal distribution has the function as shown below [32].

$$N(\mu, \sigma) = \frac{1}{\sigma\sqrt{2\pi}} \exp\left[\frac{-1(x - \mu)^2}{2\sigma^2}\right] \tag{67}$$

4.1.3 Triangle distribution

A triangle distribution $T(a, b, c)$ is defined by the minimum a, mode c and a maximum b variable value. The mode of a distribution is the variable value of the peak of the distribution, this is the most likely value. In the two dice toss figure above, the more simulations we do, the more symmetrical the stochastic distribution will be, it will be converging to a triangular stochastic distribution [33], this is only true when we use two dice. A continuous triangular distribution is often used to approximate these types of stochastic distributions only using the defining parameters. Below an arbitrary triangular distribution shown as discrete (left) and as continuous (right) to approximate the discrete distribution by using the defining parameters. The triangle distribution mean and variance is defined below [3].

$$\mu = \frac{a + b + c}{3} \tag{68}$$

$$\sigma^2 = \frac{\mu^2}{2} - \frac{ab + bc + ac}{6} \tag{69}$$
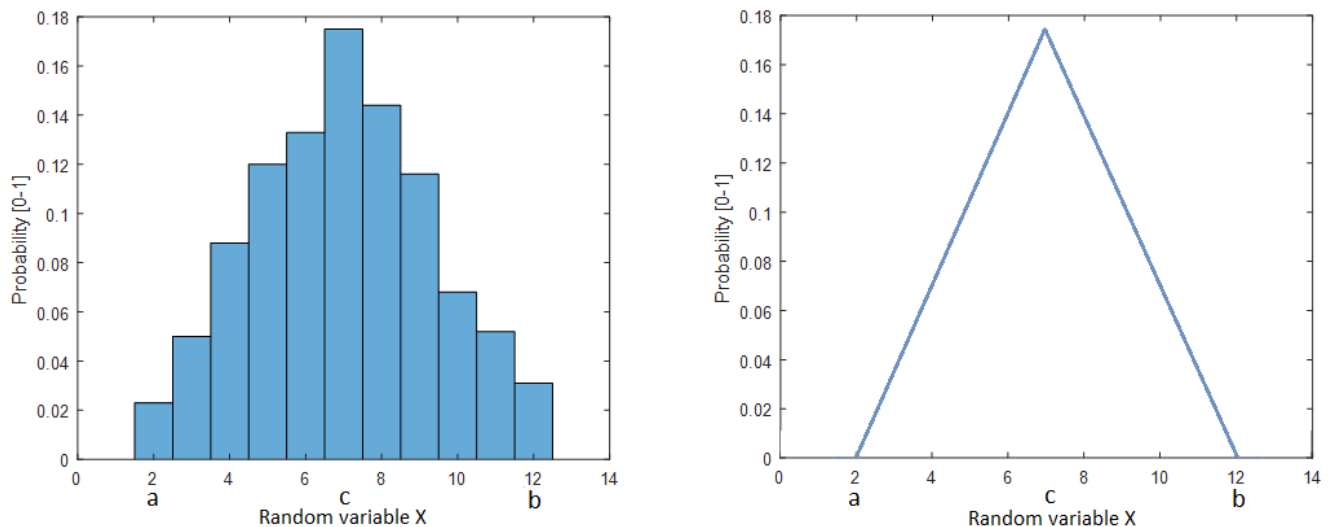
Figure 14 Discrete vs. continuous triangle distribution

4.1.4 Uniform distribution

A uniform distribution $U(a, b)$ is similarly to the triangle distribution defined by the minimum a and maximum b variable value. It does not require a mode value as it is rectangularly shaped. A continuous triangular distribution is often used to approximate stochastic distributions when these approaches a rectangular uniform shape. An example of a stochastic discrete distribution

42

is the one obtained from throwing one dice n times and plotting the result with number of eyes as the variable value. Below is an example of several single dice tosses resulting in a discrete uniform distribution (left), a continuous uniform distribution (right) may be used to approximate the discrete distribution. This approximation will become more accurate as number of dice tosses increase. The height of the continuous distribution can for example be determined by the average column height from the discrete distribution. The mean μ and variance σ^2 of the uniform distribution is defined below [3].

$$\mu = \frac{a + b}{2} \tag{70}$$

$$\sigma^2 = \frac{(a - b)^2}{12} \tag{71}$$
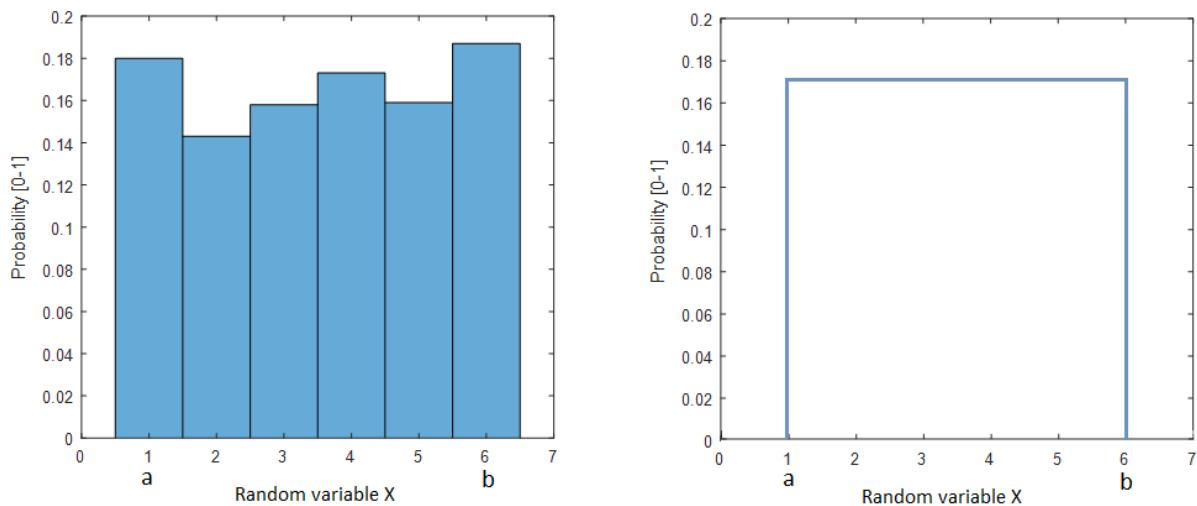
Figure 15 Uniform distribution, discrete (left) and continuous (right)

4.1.5   Weibull distribution

The Weibull distribution is a continuous distribution function that is controlled by tree parameters, these are the scale parameter α, the shape parameter β and the location parameter γ. These parameters can be used to fit the distribution to existing data from an appropriate discrete distribution. The distribution is often used to model time to failure of a component and

similar time variable distributions. The variable of the function is t. Examples of the PDF, $f(t)$ and the CDF, $R(t)$ for the Weibull distribution is shown below.
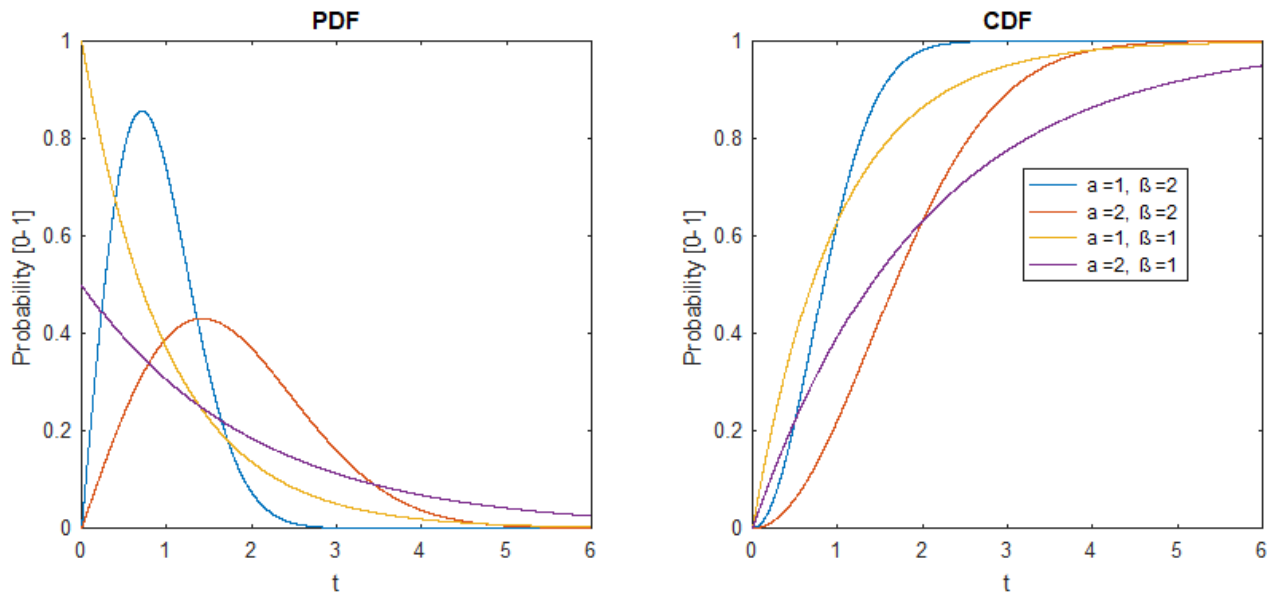
Figure 16 PDF and CDF of Weibull distribution for varying parameter α and β, in these cases γ is zero

$$f(t) = \frac{\beta}{\alpha}\left(\frac{t-\gamma}{\alpha}\right)^{\beta-1} e^{-\left(\frac{t-\gamma}{\alpha}\right)^{\beta-1}} \qquad (72)$$

$$R(t) = e^{-\left(\frac{t-\gamma}{\alpha}\right)^{\beta}} \qquad (73)$$

The location parameter γ is also known as the defect initiation time parameter because the distribution often is used with the variable t as time, this may not always be the case. If γ=0 this means that the possibility of failure starts at t=0, by setting a value for γ the onset of possible failure is delayed by γ thereby shifting the distribution. The scale parameter α increases the spread of the distribution whilst the shape parameter β effect the shape of the distribution. The equations are taken from [34].

4.2 The Central Limit Theorem

In the previous sections we have presented some elementary statistics, random variables, sampling and distribution types. The simple random sample was introduced where a population of individuals were sampled to create a stochastic distribution, and we have seen how these can be approximated by continuous distributions. We may sample statistically independent variables or even independent distributions, as we will do in the case study by Monte Carlo Simulation. *"Two random variables X and Y are independent if knowing that any event involving X alone*

44

did or did not occur tells us nothing about the occurrence of any event involving Y alone" [31]. When one variable can explain or cause change to another, these are referred to as the explanatory and response variable respectively.

The Central Limit Theorem says that the sum of n statistically independent random variables with mean μ and standard deviation σ will approach a normal distribution with mean μ and standard deviation $\sigma\sqrt{n}$ when n approaches infinity. The same holds true for the sum of n independent stochastic distributions. If we replace sum by multiplication the distribution approaches a log-normal distribution [35]. The theorem is important in the Monte Carlo Simulation process which we will be using to model casing collapse strength and load by sampling independent distributions for different input parameters. That will be the topic of the next section.

4.3   Monte Carlo Simulations

4.3.1   Monte Carlo Simulation procedure

In the previous section, we presented the Central Limit Theorem, it serves as a basis for the Monte Carlo Simulation (MCS) procedure. MCS is a method used in various disciplines to compute an output distribution of the desired variable based on known input distributions, preserving the uncertainty in the data. In his book *Making Good Decisions,* Bratvold puts it neatly *"The role of MCS is strictly the propagation of uncertainty from variables we can assess to variables used to make the decisions"* [3]. Of course, the output distribution is the distribution we need for making decisions about the design. In casing design, it could be the choice of casing string type and grade, and their appropriate configuration, number of casing strings and setting depths. The MCS procedure can be divided into five steps as described by Williamson et.al. [35].

1. Defining the model
2. Gathering data
3. Defining input distributions
4. Sampling input distributions
5. Interpreting and using the results

Step 1. Defining the model; This is merely the choice of mathematical model such as using the API equations for collapse strength calculation. All the input parameters will be represented by input distributions chosen.

Step 2. Gathering data; The process of gathering input data is crucial for later calculations, often the best source of data are historical data from similar wells or form experiments. In our case the strength is going to be predicted by MCS with experimental data for tubing parameters that can be provided by the ISO/TR 10400 standard.

Step 3. Defining input parameters; Each input parameter need to be represented by a distribution. We chose the type of distribution that fits the data best and the corresponding distribution parameters. Typical distributions as described before such as Uniform, Triangular, Normal and Weibull may be used.

Step 4. Sampling input distributions; Sampling distributions *X, Y,* etc. is an iterative proses that is carried out until the resulting distribution converges to a finite output distribution *Z.* Each time, the input distributions are sampled by the means of random sampling, the appropriate model calculations are carried out using the sampled distributions as input, the result x_i, y_i etc. are than stored. The process is repeated until the resulting distribution of stored quantities converges to an output distribution. The MCS procedure is illustrated below [3]. If the model consists of only summation and subtraction, The Central Limit Theorem ensures that the output distribution approaches a normal distribution when the number of *n* iterations approaches infinity and consist of *n* independent random samples from each input distribution. This is true regardless of the choice of input distribution types. Multiplication and division involved in the model will result in a log-normal output distribution [35].

Step 5. Interpreting and using the results; After the output distribution is computed, the result can be used to make decisions on how the design can meet the requirements of the predicted strength distribution provided by MCS.
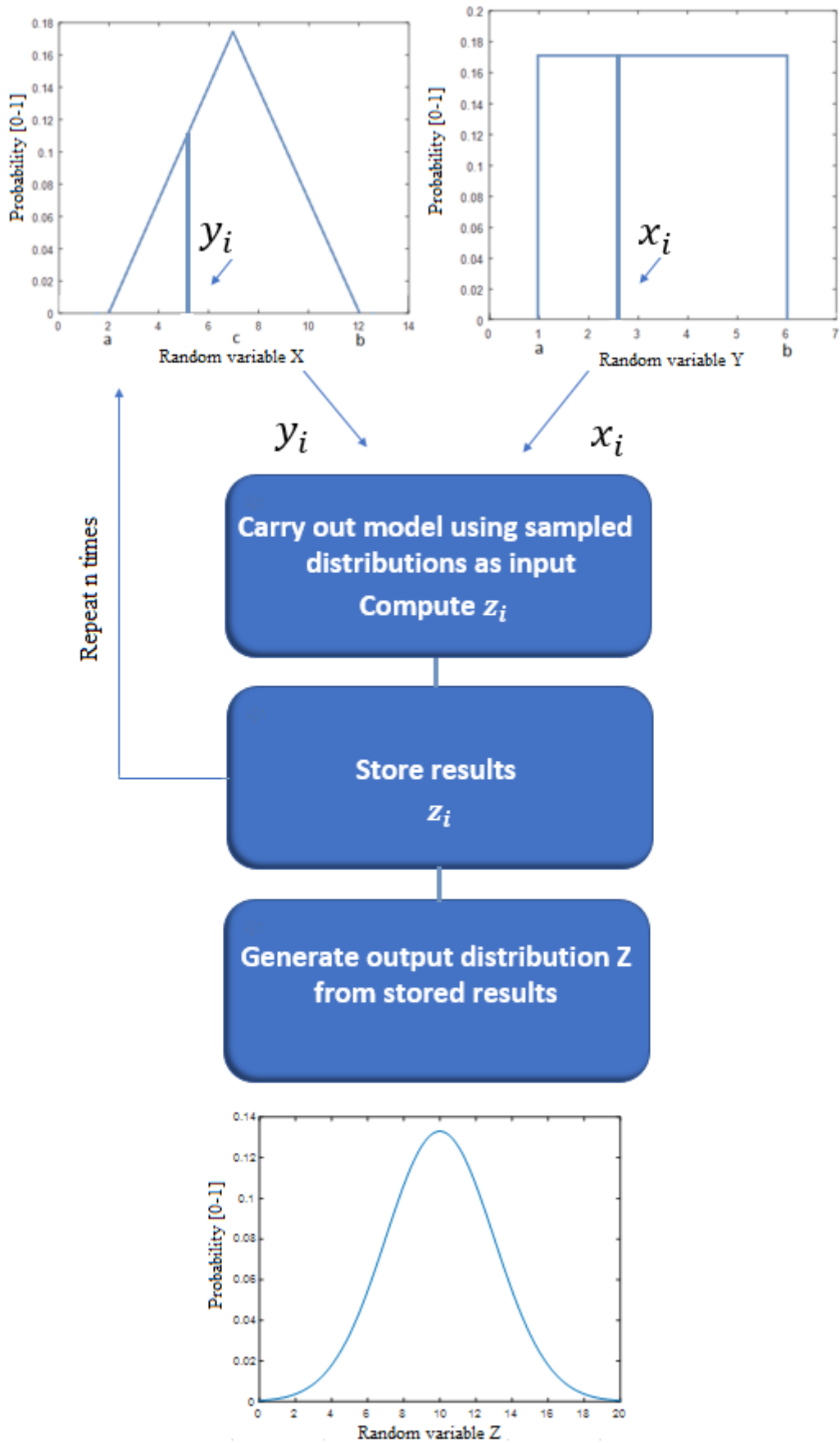
Figure 17 Monte Carlo Simulation procedure, modified from [3]

4.3.2   Input distribution for Monte Carlo Simulation in Casing Design

For our purpose, the MCS procedure will be utilized to compute an output distribution representing the collapse strength of a casing string. The input distributions will represent the input of the API collapse equation presented earlier. To gather data for casing strings we will as mentioned be using the *Drilling Data Handbook [36],* in combination with the ISO/TR 10400 standard. The uncertainty of the data gathered can then be used to construct an appropriate input distribution. For example, if we consider an L-80 tubing we know that the nominal yield strength is 80ksi, that is the minimum value for this parameter. We may choose a triangular distribution to represent the yield strength. For an API tubing the *Drilling Data Handbook* provides minimum and maximum yield strength for the API L80 tubing, it is minimum 80ksi and maximum 95ksi [36]. For a symmetric distribution we may chose the midpoint as the mean and mode of the distribution, $c = (95 + 80)/2 = 87.5$ksi. The flanks of the triangle will represent the uncertainty with a minimum and maximum value *a* and *b*. However, because the ISO standard provides mean and standard deviation from experimental casing/tubing data, these parameters will be represented by normal distributions. Triangular distributions will be used for the input parameters for collapse load, that is the wellhead temperature and uncertainty in the APB model.
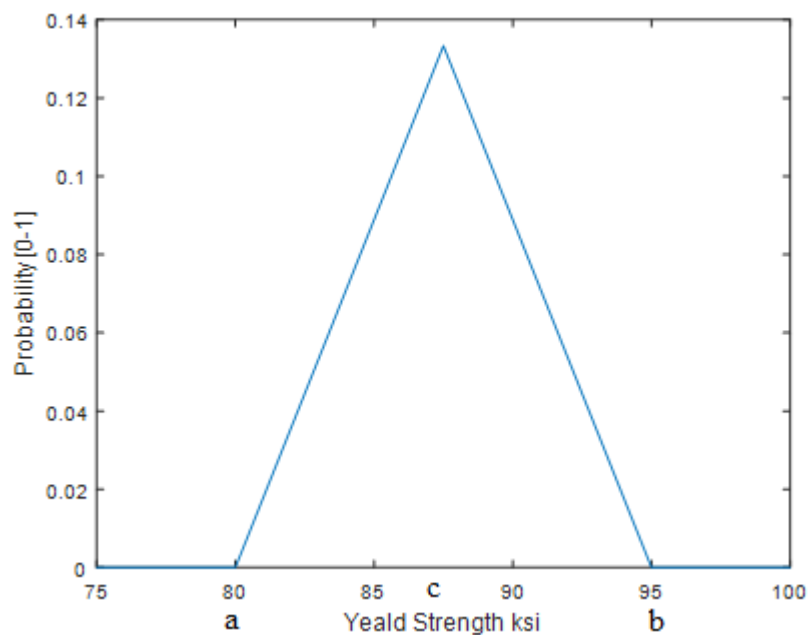
Figure 18 Triangular input distribution representing yield strength of an L-80 tubing string

4.4 Types of reliability-based design

4.4.1 Basic Reliability-based design

The basic approach of Reliability-based design which is the method to be applied for the temperature driven APB case study will be described in this section. Similarly, to the WDS we consider a load and a strength or resistance. These can be any type of load, in our case collapse load stress. However, this time the load and stress are not deterministic, instead it is represented by statistical distributions obtained from Monte Carlo simulations based on input distributions as described in the previous sections. In this way *"all of the uncertainty, frequency of occurrence, and variability in all the characteristic variables that define load and strength are considered explicitly"* [8]. In a fully reliability-based design, both the load and resistance are represented in this way. The two distributions for the load and resistance may intersect and the area of intersection will represent the probability of failure when both distributions are PDF's, meaning each of the distribution integrals are equal to one. An acceptable probability of failure, the target probability, can be set and will determine if the selected casing or tubing have the sufficient strength.

Companies use different guidelines to determine the target probability based on the cost and consequence of a failure related to a specific load case. An example of such a guideline is presented in the following table. "*These guidelines were developed using acceptable probability of failure data collected from other design practices*".

Table 6 Guidelines for target probability P_t [0-1] based on cost and consequence of failure, modified from [37]

	High Cost	Medium Cost	Low Cost
High Consequence	10^{-8}	$10^{-6.5}$	10^{-5}
Low Consequence	10^{-5}	$10^{-3.5}$	10^{-2}

To quantify the probability of failure we use Quantitative Risk Analysis (QRA) as described by Aadnøy et.al. in the book *Advanced Drilling and Well Technology* [8] and shown below. We will use Monte Carlo Simulation as our method for performing QRA. By naming the load and resistance distributions by $Q(x)$ and $R(x)$ respectively, a limit state function $g(x)$ can be defined by subtracting the load from the resistance. The probability of design failure than becomes P_f

and the corresponding design reliability P_r. Here b is the intersection of the *g(x)* function with the x-axis.

$$g(x) = R(x) - Q(x) \tag{74}$$

$$P_f = P[g(x) < 0] = \int_0^b (-g(x))dx \tag{75}$$

$$P_r = 1 - P_f \tag{76}$$

For illustrational purposes, an arbitrary casing string has been considered for QRA applied for casing collapse design as shown in the figure below. On the left the collapse load *Q(x)* and strength *R(x)*. On the right the function *g(x)* is plotted as its negative. Its integral $\int_0^b (-g(x))dx$ describes the probability of failure. Hence the CDF of *-g(x)* is also plotted giving the probability of failure P_f.
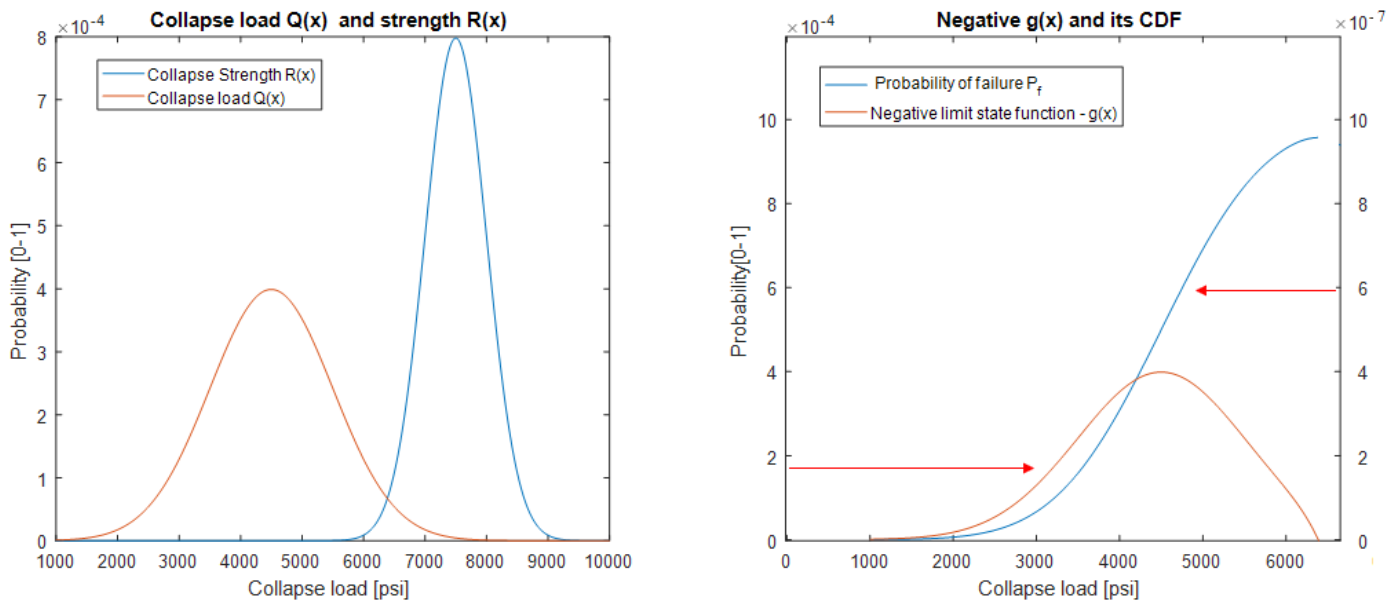
Figure 19 QRA applied for collapse design of an arbitrary casing string

4.4.2   Load and Resistance Factor Design

Load and Resistance Factor Design (LRFD) is a design methodology that dates back to 1930's civil engineering developments, but was first considered for tubular design in the late 1980's [28]. It is a reliability-based design method that resembles WSD and limit state design in the way that it is carried out.

The LRFD concept is double sided. We apply a load factor LF and a resistance RF to the deterministically predicted load and strength respectively. These factors are pre-calibrated to the uncertainties in load and strength, and some generic target probabilities, taking account for uncertainty in both load and strength. It is more appropriate as the uncertainty in load and strength is different [8]. The pre-calibrated factors ensure that we don't have to conduct a full basic approach reliability-based design. The factors are chosen based on the target probability selected for the design as discussed in the previous section. In this case the equations become as shown below. The figure below illustrates the concept.
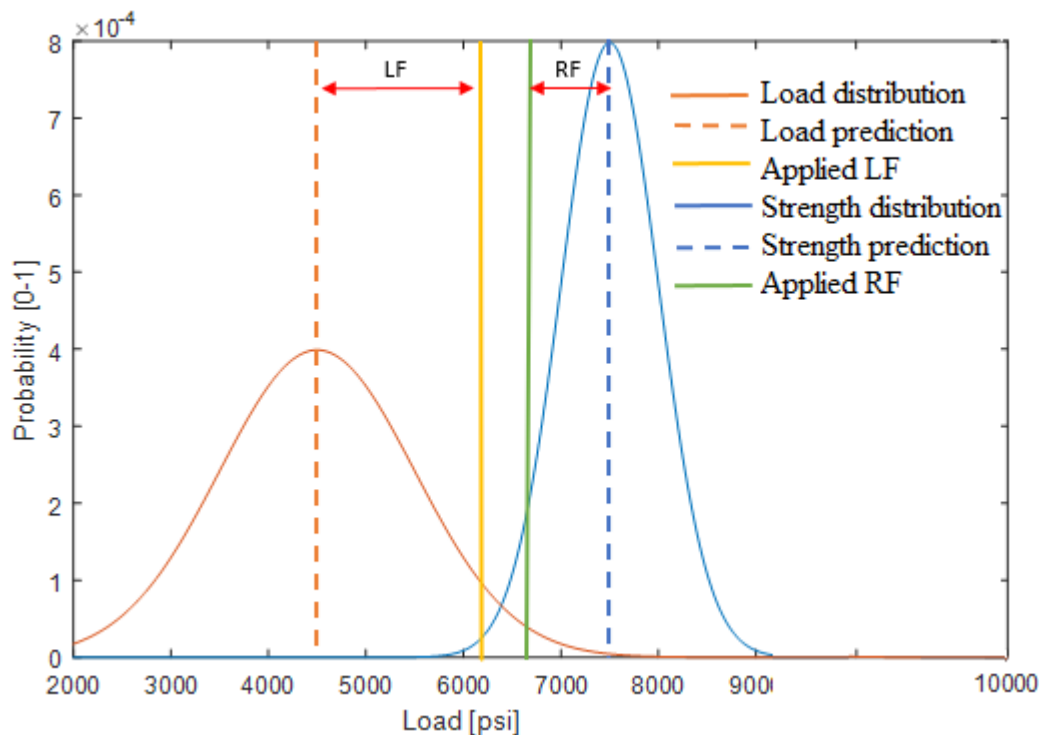
Figure 20 LRFD applied for collapse design of an arbitrary casing string using LF and RF

51

$$\sigma_{load} * LF < \sigma_{strength} * RF \tag{77}$$

$$LF = \frac{\sigma_{load\ limit}}{\sigma_{load}} \tag{78}$$

$$RF = \frac{\sigma_{strength\ limit}}{\sigma_{strength}} \tag{79}$$

A Utilization factor used to evaluate the design is defined in the OTC paper *Load and Resistance Factor Design Case Histories* [37]. *"The acceptability of LRFD designs is described by the term Utilization Factor (UF). This term is defined as the factored load divided by the factored resistance. The UF describes the percentage of the available strength utilized, for the given probability of failure"* [37]. If the UF is higher than one, the factored load exceeds the factored resistance, so that the design is not acceptable.

$$UF = \frac{\sigma_{load} * LF}{\sigma_{strength} * RF} \tag{80}$$

Taking account for an acceptable target probability, the utilization factor will depend on what kind of value one has accepted for failure in the specific load case. It will vary depending on what kind of load scenario one considers, but also which casing or tubing that is considered. Target probabilities are chosen for different load cases, choosing the appropriate load cases such as for example gas kick, running and cementing or lost returns, when drilling. For all load cases that are considered for the design, the UF must be below one.

An example is shown in the table below presenting probability of failure for scenarios considered for two different casing strings. From the table it is evident that although the acceptable probability of failure is set the same for a load case for the two different casing strings, the UF differ among them. Note that the design is acceptable up to a utilization factor of one. The UF is higher for the intermediate casing compared to that of the production casing for both load cases, meaning that a higher percentage of the available strength is utilized for that particular design. This mean that the intermediate string has a higher probability of failure as compared to the production casing, although both of them being below the acceptable failure probability that is the same for both of them in this case. All load cases evaluated for the design in the below table are acceptable as none of the utilization factors are above one.

Table 7 Example of probability of failure and Utilization Factor, modified from [37]

Load cases	Acceptable probability P_t [0-1]		Utilization factor UF	
Casing string	13 3/8" N-80 Interm. csg.	9 5/8" L-80 Prod. csg.	13 3/8" N-80 Interm. csg.	9 5/8" L-80 Prod. csg.
Running and Cementing	$10^{-3.5}$	$10^{-3.5}$	0.62	0.47
Lost returns	$10^{-3.5}$	$10^{-3.5}$	0.54	0.17
Kick	N/A	$10^{-6.5}$	N/A	0.6
Tubing leak	N/A	$10^{-6.5}$	N/A	0.82
Accidental evacuation	N/A	$10^{-3.5}$	N/A	0.75

4.5 Combining different design methodologies

In Chapter 3, the conventional design methodologies were presented, as was the reliability-based methods in this chapter. Sometimes one methodology may not be appropriate to describe both the load and strength considered. The choice of method depends on the amount of data, historical or experimental, that is available for example for Monte Carlo simulation, and on the uncertainty of the strength or load themselves. For example, the collapse strength of a casing is easy to predict using RBD, as the input parameters with experimental data may provide their uncertainties. However, the load applied to the casing may be calculated based on an appropriate load scenario, but the uncertainty in the load and the choice of load scenario is not so easily predicted. The design method for the load may more appropriately be deterministic based on a worst-case load scenario. Therefore, different ways of combining design methodology as applied to strength and load will be presented here. In a paper prepared by Suryanarayana and Lewis [38], a level four and five reliability-based design is defined. The lower levels relate to deterministic design.

The RBD Level Four is a combination of a deterministic approach determining the load and a reliability-based approach to determine the resistance represented by a probability distribution. Only the uncertainty in resistance is considered, and thus the probability of failure is for a

specific deterministic load applied [38]. For example, the load can be predicted deterministically by using conservative values as done in WSD, to be compared to a strength distribution provided by MCS. Of course, it is also possible to reverse the definition such that the load is represented by a probability distribution while the resistance by a deterministic approach.

The RBD Level Five is a fully reliability-based design where both load and resistance are represented by probability distributions [38]. The uncertainty of the predicted load and resistance is therefore considered, and the corresponding probability of failure takes both their uncertainties into consideration. Both probability distributions can be provided by MCS. The two approaches of RBD Level 4 and 5 are illustrated in the figure below.
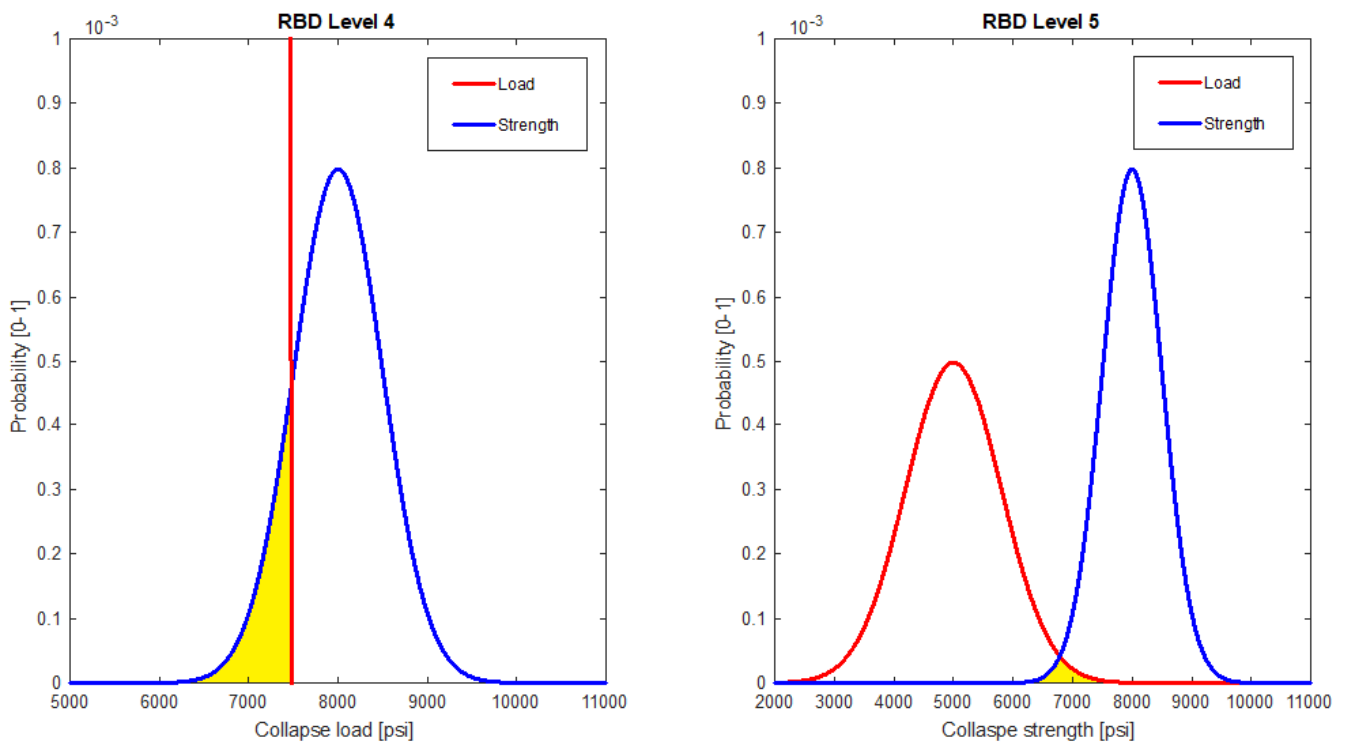
Figure 21 RBD Level 4 and 5 demonstrate failure probability by distribution overlap, modified from [38]

A third possible design approach combination is to combine the two RBD-methodologies LRFD with the Basic reliability-based design approach. Such that one represents the load and the other the resistance or vice versa. The LRFD is easily carried out by an engineer compared to the complex basic approach by using utilization factors [37].

One could for instance calculate the load by using LRFD and use this as single value input in an RBD Level four approach where the strength is calculated probabilistically. This would be more

flexible taking care of that different load scenarios have different uncertainties with respect to magnitude, probability of occurrence and consequences for further operability. It can possibly also take into account which type of well and hole section that is considered. If many load scenarios have to be considered, this might also ease the complexity of the computing process.

Therefore, it could be used for load calculations that will be carried out many times depending on the circumstances to save time and resources. It could be used for the collapse load that will vary with depth and from one well to another. On the other side the calculation of the strength of the casing will only need to be carried out one time for each casing string considered, and here the more complex basic reliability approach could be utilized.

As mentioned earlier, a rule of thumb could be *"In practice, a dual-design methodology of working stress design for normal loads and limit states design for infrequent survival-type loads may be applied"* [8].

4.6   Developments in reliability-based casing design

The application of reliability-based design for casing design is an unconventional and a fairly new approach in the petroleum industry. The traditional working stress design has been the main approach, although in other industries reliability-based design has been around for many decades. Although it took long time for the application of the methodology to be picked up by the industry, early work has been made on statistical tubular collapse design by Clinedinst, W.O. in 1939 [39] and in 1977 [40]. However, in 1991 the BP Exploration commissioned a study to implement quantitative risk analysis in their casing design practice [30]. Still in 1993, A.J Adams et.al. states that "*the oil industry has, to date, designed casing using deterministic methods alone*" [30]. With the increased computational power and computer competence being available at the average engineering office from the 80's and 90's and onward, simulations such as Monte Carlo simulations requiring many sampling iterations became more realistic and affordable to implement. In later years the ISO/TR 10400 standard recommends procedures and statistics for implementation of QRA in tubular design. We will now shortly present the litterateur and standards that has been used as references in this study, related to reliability-based design specifically applied to casing design.

4.6.1   Standards

ISO/TR 10400 Technical Report; *Petroleum and natural gas industries Equations and calculations for the properties of casing, tubing, drill pipe and line pipe used as casing or tubing.*

This standard presents the same equations for tubular design as is presented in the API standard *API Bulletin 5C3 Bulletin on Formulas and Calculations for Casing, Tubing, Drill pipe and Line Pipe Properties*. Additionally, the *ISO/TR 10400* presents datasets of casing strings and methods that can be used in applying these equations to reliability-based design by quantitative risk analysis. The experimental casing datasets contain mean and COV of casing parameters that are used in the calculation process, such that normal input distributions for sampling procedures in MCS can be made.

4.6.2   Literature review on reliability-based casing design

Casing System Risk Analysis Using Structural Reliability. This 1993 paper was prepared by Adams, A.J. et.al. This paper has emphasis on directing attention towards the benefits of reliability-based design as compared to conventional working stress design. It describes a method for reliability-based design using quantitative risk analysis and proposes target probabilities to be used for blowout and repair events. Additionally, this method was used to develop risk-calibrated design factors for both exploration and development wells [30].

Load and Resistance Factor Design Case Histories. This 1995 paper was prepared by Brand, P.R. et.al. The paper presents case histories of casing design with different casing configurations in the well. Working Stress Design and Load and Resistance Factor Design methods are outlined. The main objective was to compare WSD to LRFD by applying both on the same casing configurations. The study finds that some of the casing strings considered became acceptable using the LRFD approach for the specified target probability, although not accepted by the WSD method. Guidelines for selecting target probabilities based on anticipated cost and consequence of failure was proposed.

On the Development of Reliability-Based Design Rules for Casing Collapse. This 1998 paper was prepared by Adams, A.J. et.al. It made an effort to compare different models for tubular collapse applied to reliability-based casing design. The most important findings of this research were that the Tamano equations for ultimate collapse strength was found to be the best for this application based on having the smallest COV and near unity mean when compared to actual collapse strength. In this study, the API Bulletin 5C3 equations was found to have an "*unacceptable wide variation in predicted collapse probability*" [17].

A model for Well Reliability Analysis throughout the Life of a Well Using Barrier Engineering and Performance. This 2015 paper was prepared by Das, B. and Samuel, R. The paper presents a well reliability model to evaluate the integrity of casing as one of the secondary well barrier

elements. By combining models for strength, wear considerations, use of simulations and statistics, a dynamic reliability model for the well barriers was presented, that is to evaluate the well barrier reliability over time. [34].

A Reliability-Based Approach for Survival Design in Deepwater and High pressure/High Temperature Wells. This 2016 paper was prepared by Suryanaranana, P.V. and Lewis, D.B. The paper emphasizes to distinguish between survival and operating/service load design. The paper focus on discussing the procedure of conducting Working Stress Design and Reliability-Based Design. Two levels of reliability-based design are presented, that being level 4 and level 5. The paper proposes ranges of target reliabilities to be used for reliability-based tubular survival design. One range for high and one for low consequence of failure. It is expressed that especially deep water and HPHT wells will have great advantage from the reliability-based approach [38].

5 Case Study

5.1 Introduction to case study

In this case study, a production tubing as previously described will be considered for a collapse scenario caused by Annular Pressure Buildup (APB) in the A annulus. The APB is caused by production startup, heating up the adjacent annulus. We only consider the closest annulus to the production tubing, the A annulus. We will assume the average temperature in the annulus will approach the average well flow temperature along the production tubing. In Chapter 2.7 we looked at a simplified approach for modeling annular pressure buildup. We also looked at the API equations for collapse strength in Chapter 2.4. These two models will here be used for QRA of APB in the A annulus, predicting the APB and probability of collapse of a production tubing for the given base case.

5.2 Base Case

The base case consists of a vertical HPHT oil producing land well, drilled to a reservoir at 5000mTVD. The ambient surface temperature is $15°C$, and a geothermal gradient of $0.03°C/m$ is used. This gives a normal reservoir temperature of $165\,°C$. To estimate the wellhead temperature requires complex heat loss calculations. It requires a full well geometry and thermal parameters to be known as described in chapter 2.5. We assume the wellhead temperature has already been predicted to a worst case of $90°C$. It can be represented by a triangular distribution T_{wh}= [70,80,90].

A nominal 7inch, API L-80, 32Ib/ft production tubing will first be considered for the collapse scenario. The yield strength will later be adjusted to find the appropriate tubing grade. For simplicity, the depth of the production packer is also considered at the reservoir depth of 5000mTVD, although this is typically set slightly higher, leaving part of the tubing as the tail pipe. The well is producing a 0.7sg oil with a viscosity of $0.001 Pa \cdot s$. The A annulus is filled with a 1.2sg completion fluid to balance the external pressure of the production casing, being the formation pressure along the casing or the hydrostatic pressure in the B annulus depending on the depth considered. The density of the completion fluid help to prevent collapse of the

production casing by balancing the formation pressure. We consider a fully open choke giving zero choke pressure and a production rate of $1600 \ m^3/day$.

The frictional pressure drop along the tubing will be calculated from the production rate assuming a fully incompressible production fluid. This mean that the flowrate is constant along the production tubing. Since the inner tubing diameter and density is constant, the velocity is also constant.

$$v_{in} = v_{out} = \frac{Q}{A_i} = \frac{1600 \ / \ 86400}{\frac{\pi}{4}(\ 6.094 \cdot 0.0254)^2} = 0.9841 m/s$$

We calculate the Reynold number

$$Re = \frac{\rho v D_i}{\mu} = \frac{700 \cdot 0.98411 \cdot 6.094 \cdot 0.0254}{0.001} = 106630$$

The flow is turbulent. Assuming a tubing roughness of 0.0006inch [2], this gives a relative roughness of $R = \frac{\varepsilon}{ID} = \frac{0.0006}{6.094} = 9.8458 \cdot 10^{-5}$. The Moody friction factor f_M is now read from the Moody diagram, see Appendix A2. It gives a Fanning friction factor of:

$$f_f = \frac{f_M}{4} = \frac{0.0178}{4} = 0.00445.$$

The frictional pressure drop along the production tubing is then given as:

$$\Delta P_{friction} = 4 f_f \left(\frac{L}{ID} \right) \rho_f \frac{v_f^2}{2} = 4 \cdot 0.0445 \frac{5000}{6.049 \cdot 0.0254} 700 \frac{0.9841^2}{2} = 194900 Pa = 1.9490 bar$$

To summarize the base case, relevant field parameters and parameters for the production tubing are shown in the tables below, also showing various API grades. In addition, an illustration of the temperature profile and tubing is shown below.

Table 8 API Production tubing data

API Grade	$\sigma_y \ [psi]$	$OD \ [inch]$	$ID[inch]$	$t \ [inch]$	$w[lbs/ft]$
L-80	80000	7	6.094	0.453	32
C-90	90000	7	6.094	0.453	32
T-95	95000	7	6.094	0.453	32
P-110	110000	7	6.094	0.453	32

*Tubing data are taken from Drilling Data Handbook [36]

Table 9 Base case field parameters

$D_{packer}[m]$	$T_{surface}[°C]$	$T_{res}[°C]$	$T_{wh}[°C]$	γ_{oil}	$\gamma_{packer\ fluid}$	μ_{oil}	$\Delta P_{friction}[bar]$
5000	15	165	90	0.7	1.2	0.001	1.9490
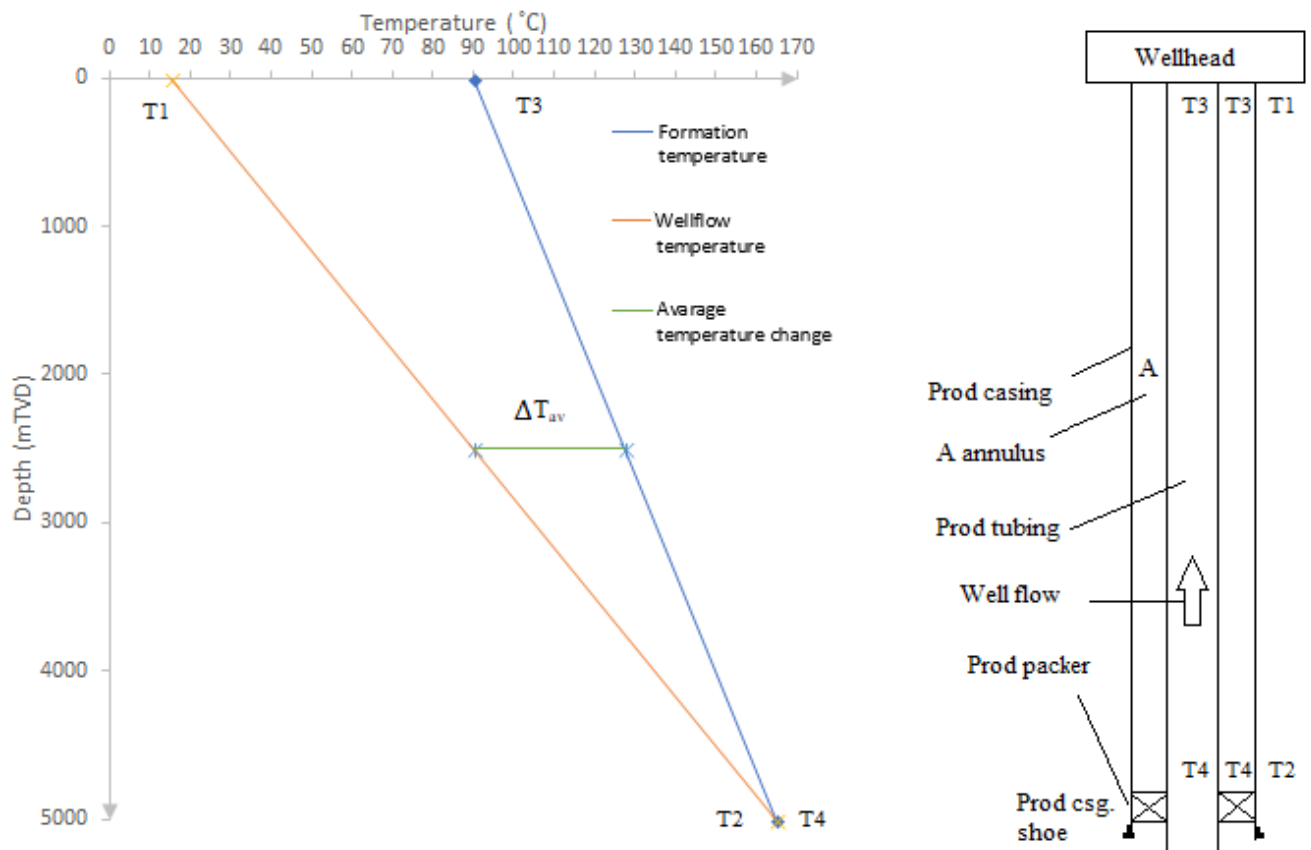
Figure 22 Base case temperature profile and tubing

5.3 Working Stress Design

For Working stress design, we use nominal parameters when calculating strength. The nominal parameters can be viewed as "safe" or "minimum" parameter sizes. For example, the nominal yield strength of a casing is given by its name, an API L-80 casing has a nominal yield strength of 80ksi. Because the WSD gives a deterministic approach, we use these minimum or safe parameters given by the manufacturer. We will use the nominal parameters from the *Drilling Data Handbook* given in table 6. The collapse load is calculated using fixed field parameters.

5.3.1 API Collapse resistance calculation compared to Drilling Data Handbook rating

We will calculate the API collapse resistance of the production tubing to illustrate the calculation process, first without taking axial load or inner pressure correction into consideration. We can then compare the result to the collapse resistance given in the *Drilling Data Handbook* [36]. We calculate the slenderness ratio OD/t to choose the collapse equation for the collapse region. $\frac{OD}{t} = \frac{7}{0.453} = 15.45$. We then need to calculate the model constants and the yield-plastic model intersection $\left(\frac{D}{t}\right)_{yp}$. If OD/t is smaller than $\left(\frac{D}{t}\right)_{yp}$ then the yield region is prevailing.

$$A = 2.8762 + 0.10679 \times 10^{-5}\sigma_{Yp} + 0.2131 \times 10^{-10}\sigma_{Yp}^2 - 0.53132 \times 10^{-16}\sigma_{Yp}^3 = 3.0708$$

$$B = 0.026233 + 0.50609 \times 10^{-6}\sigma_{Yp} = 0.0667$$

$$C = -465.93 + 0.030867\sigma_{Yp} - 0.10483 \times 10^{-7}\sigma_{Yp}^2 + 0.36989 \times 10^{-13}\sigma_{Yp}^3 = 1955.3$$

$$F = \frac{46.95 \times 10^6 \left(\frac{\frac{3B}{A}}{2+\frac{B}{A}}\right)^3}{\sigma_y\left(\frac{2B/A}{2+\left(\frac{B}{A}\right)-\left(\frac{B}{A}\right)}\right)\left(1-\frac{3B/A}{2+\left(\frac{B}{A}\right)}\right)^2} = 1.9975$$

$$G = F\frac{B}{A} = 0.0434$$

$$\left(\frac{D}{t}\right)_{yp} = \frac{\sqrt{(A-2)^2+8\left(B+\frac{C}{\sigma_y}\right)}+(A-2)}{2\left(B+\frac{C}{\sigma_y}\right)} = 9.4152 < 15.45$$

The region is not the yield region so the next model intersection $\left(\frac{D}{t}\right)_{PT}$ between the plastic and transitional region is checked. The plastic model is valid from $\left(\frac{D}{t}\right)_{yp}$ to $\left(\frac{D}{t}\right)_{PT}$.

$$\left(\frac{D}{t}\right)_{PT} = \frac{\sigma_y(A-F)}{C+\sigma_y(B-G)} = 22.4730 > 15.45$$

This mean that the prevailing region is the plastic region, we don't need to check the other intersections. However, if this was not the case, the approach to proceed is carried out in the same matter, until we reach the elastic region. We now use the plastic collapse equation for strength calculation.

$$P_p = \sigma_y\left(\frac{A}{D/t} - B\right) - C = 8605 \text{ psi}$$

The plastic collapse equation predicts the collapse resistance to be 8605psi. In the Drilling Data handbook, the collapse resistance for the tubular is given as 59.3MPa=$8.60 \cdot 10^3$ psi. The

handbook is consistent with our calculations. This also confirms that nominal parameters should be used. Similar calculations were carried out for the API L80, C90, T95 and P110 grades, only varying the yield strength. The results are listed below.

Table 10 Calculated API collapse resistance compared to Drilling Data Handbook collapse resistance

Grade	API Collapse resistance [psi]	DDH Collapse resistance [psi]
API-L80	8605	8599
API-C90	9377	9367
API-T95	9745	9744
API-P110	10782	10774

5.3.2 WSD Collapse load calculation

The axial load and inner pressure at the depth considered must be known before calculating the collapse strength of the tubing for the base case application. The axial load and inner pressure is used to calculate the Combined loading equivalent grade. As mentioned earlier, the location where the collapse load is largest is at the production packer, due to different fluid gradients in the annulus and tubing.

We first calculate the outer pressure. This is the hydrostatic pressure of the completion fluid plus the APB at packer depth. We need to calculate the APB in the A annulus first.

The temperature increase in the A annulus, midway to the packer is given as below. Here it is assumed that the packer is set close to the reservoir, such that the annular and production temperature is the same as the reservoir temperature at the depth of the packer.

$$\Delta T = \frac{T3+T4}{2} - \frac{T1+T2}{2} = \frac{90+165}{2} - \frac{15+165}{2} = 37.5°C$$

The APB, ΔP at the depth of the production packer is then calculated as follows.

$$\Delta P = \frac{\alpha \Delta T}{c} = \frac{3 \cdot 10^{-4} \cdot 37.5}{3 \cdot 10^{-5}} = 375 bar$$

The annular pressure at the production packer can now be computed.

$$P_{annulus} = g \, D \, \rho_f + \Delta P = 0.0981 \cdot 5000m \cdot 1.2sg + 375 = 963.6bar = 13976psi$$

The corresponding tubular pressure now becomes the sum of the hydrostatic column of production fluid and the previously calculated frictional pressure drop, the choke is considered fully open.

$$P_{tubing} = \rho_f Dg + \Delta P_{fric} + \Delta P_{choke} = 0.7 \cdot 5000 \cdot 0.0981 + 1.9490 + 0 = 345.296 bar = 5008 psi$$

Comparing the APB in the A annulus to the frictional pressure drop along the tubing calculated previously and to the annular pressure at the packer, we see that the frictional pressure drop of *1.96bar* for this particular production rate is small as compared to both the annular pressure buildup and the tubular hydrostatic pressure, it could possibly be neglected. The collapse load can now finally be computed.

$$P_{c,load} = P_{annulus} - P_{tubing} = 618.3 bar = 8968 psi$$

By applying the design factor DF=1.1 for collapse, proposed by NORSOK D-010, we may calculate the minimum collapse strength required for this load case. In the next section we will calculate the collapse strength of different tubing grades. We need to work backwards from the available tubing grades to find the weakest grade that surpasses the minimum required collapse strength.

$$P_{c.min} = P_{c,load} \cdot DF = 8865 psi$$

5.3.3 WSD Collapse strength calculation

To calculate the collapse strength for the case study application, the yield strength of the tubing must be de-rated for the high temperature conditions at the packer. The temperature at the packer is $165°C = 329F$. The deration factor can be calculated as described in section 2.4.

$$(329F - 70F) \cdot 0.03\%/F = 7.77\%$$

The temperature de-rated yield strength becomes

$$\sigma_{yT} = 80000 \cdot \left(1 - \frac{7.77}{100}\right) = 73784 psi$$

The axial load and inner pressure also must be considered when calculating collapse strength. We use the Combined loading equivalent grade σ_{ycom} as yield strength in the collapse equations, for deration of the collapse resistance due to axial stress and correcting for inner pressure. Here we de-rate the already temperature de-rated yield strength. The axial stress at the depth of the packer is considered zero as the end of the production tubing is considered at the depth of the packer.

In some applications the buoyed weight of a tailpipe and possibly axial forces caused by reverse ballooning of the tubing, due to the collapse load, may be considered when determining axial force σ_z. Reverse ballooning will lead to elongation of the pipe, but as the packer holds the pipe in place the effect will be compression, increasing the collapse strength. For our application we will assume the tubing can move freely through an expansion joint made up from a polish bore receptacle (PBR) and seal assembly.

When considering the buoyed hanging weight of a tailpipe, the axial force at the depth of the production packer becomes as given below.

$$F_a' = (Z_{tube\ end} - Z_{packer})\, w_{air} + p_{i,pipe\ end}\, A_i - p_{o,pipe\ end}\, A_o \tag{81}$$

Below the packer, the production fluid holds the same pressure inside and outside the tubing. The equation for axial stress becomes as shown below, here A_s is the steel cross section of the tubing.

$$\sigma_z = \frac{F_a'}{A_s} = \frac{(Z_{tube\ end} - Z_{packer})\, w_{air} - p_{pipe\ end}\, A_s}{A_s} \tag{82}$$

As both the hanging weight and ballooning effects are not considered, no further deration is needed. The yield strength stays the same as $\sigma_z = 0$, still we need to account for the inner pressure.

$$\sigma_{ycom} = \left(\sqrt{1 - 0.75\left((\sigma_z + P_i)/\sigma_y\right)^2} - 0.5\,(\sigma_z + P_i)/\sigma_{yT} \right)\sigma_{yT} = \ 7195 psi$$

We now have the parameters we need to calculate the collapse strength. The slenderness ratio OD/t=15.45 is the same as in the collapse rating example in section 5.3.1. The collapse region is needed to be determined, now using the de-rated yield strength in a similar manner as before. The region is determined to be plastic, so we use the plastic collapse equation. σ_{Yp} in the collapse equation now correspond to the de-rated yield strength.

$A = 2.8762 + 0.10679 \times 10^{-5}\sigma_{Yp} + 0.2131 \times 10^{-10}\sigma_{Yp}^2 - 0.53132 \times 10^{-16}\sigma_{Yp}^3 = 3.0435$

$B = 0.026233 + 0.50609 \times 10^{-6}\sigma_{Yp} = 0.0626$

$C = -465.93 + 0.030867\sigma_{Yp} - 0.10483 \times 10^{-7}\sigma_{Yp}^2 + 0.36989 \times 10^{-13}\sigma_{Yp}^3 = 1.7143$

$P_p = \sigma_y \left(\frac{A}{D/t} - B \right) - C = 7949$ psi

The temperature derations of the yield strength obviously reduced the collapse strength considerably as compared to the first example.

By applying the design factor DF=1.1 recommended for collapse by *NORSOK D-010*, the load limit of the L80 tubing can be calculated as shown below. This is the maximum load acceptable for this particular design.

$$\sigma_{load\ limit} = \frac{1}{SF}\sigma_{strength} = \frac{1}{1.1}7949 = 7227psi$$

5.3.4 WSD Results and weak point assurance

The WDS schematics shown below was developed using MATLAB for the entire WSD calculation process described. The collapse load is well above the load limit previously calculated. The schematics of the WSD for the L80 tubing is shown in the below figure.
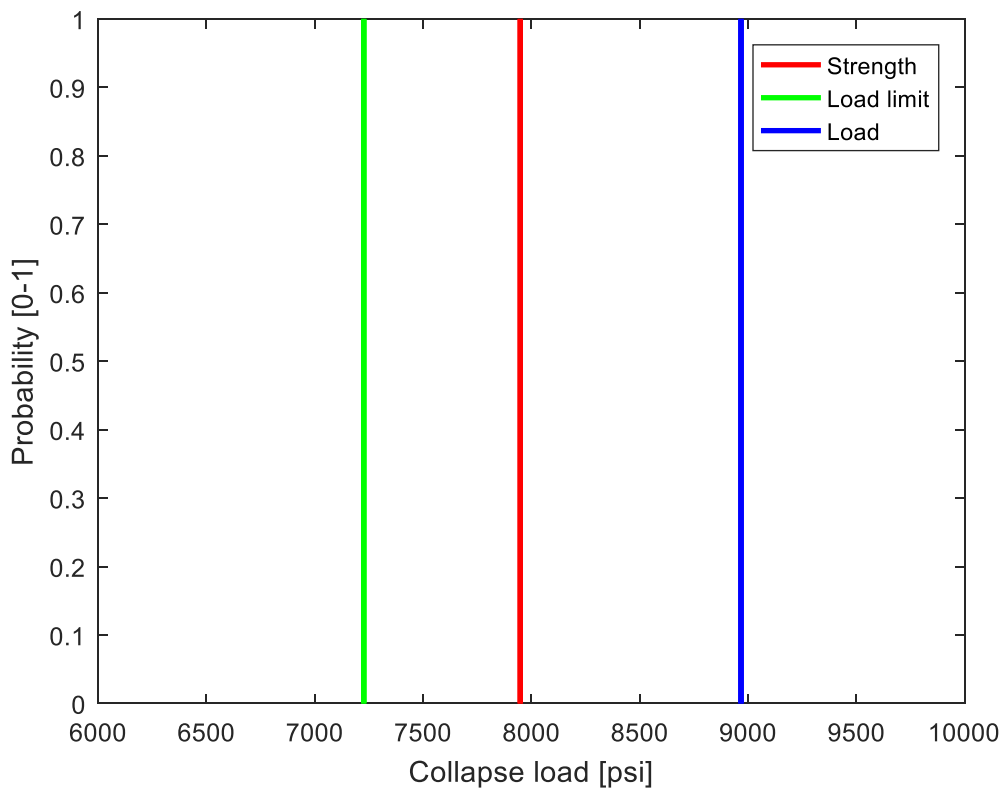
Figure 23 WSD of collapse scenario on L-80 production string

Because the collapse load is exceeding the load limit of the WSD, we will increase the yield strength of the production string until the load is below the load limit such that the WSD fulfills the NORSOK design factor. In the following figure the WDS schematics for 7inch T95 and P110 production strings are shown. The P110 tubing grade is the first whose collapse load limit

65

and strength is above the imposed load. As this is the case, the P110 grade is preferred by WSD. The corresponding table shows the strength and load limit as well as the imposed load of the considered production strings.
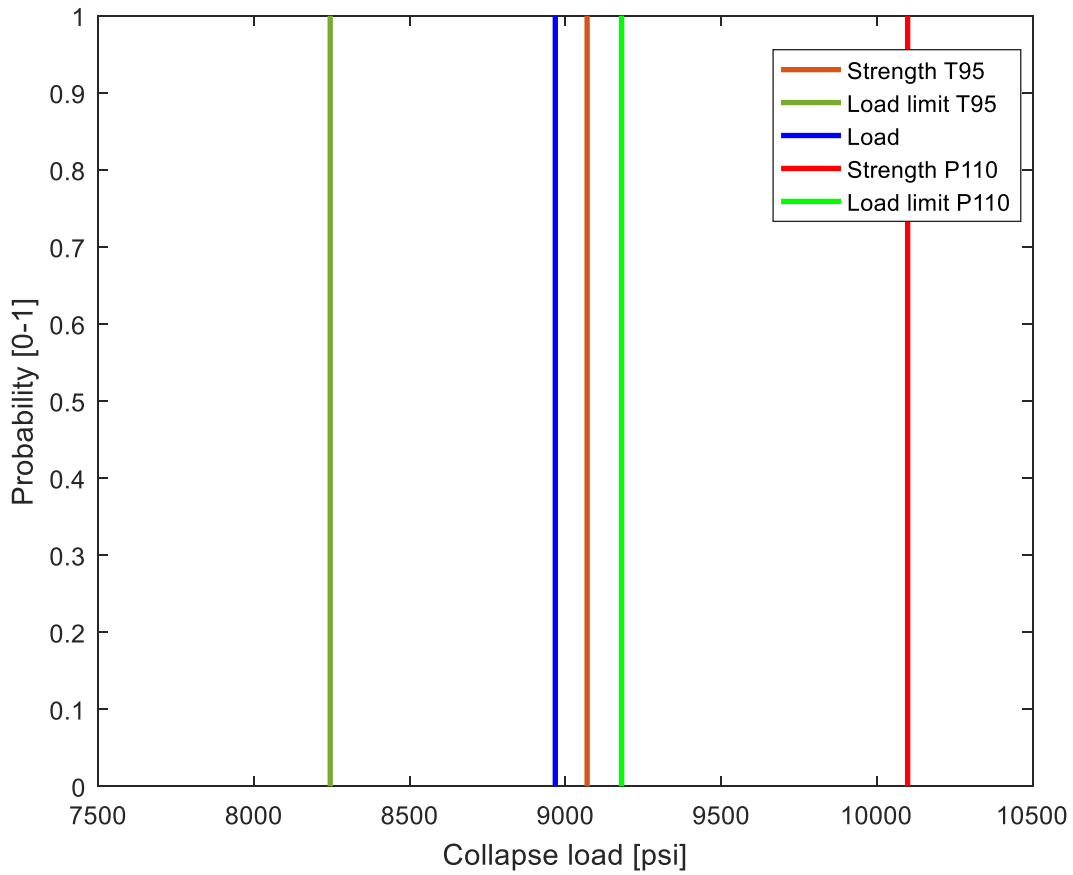
Figure 24 WSD schematics showing collapse mode of T95 and P110 production tubing

Table 11 Production tubing load, load limit and strength

Grade	Load [psi]	Load Limit [psi]	Strength [psi]
L80	8968	7227	7949
C90	8968	7915	8707
T95	8968	8245	9070
P110	8968	9181	10099

The figure below shows the pressure profile inside and outside the production tubing and the differential pressure across the tubing wall, that is the collapse load. The initial tubing and annular pressure before the APB takes place is zero at the top because there is no hydrostatic or frictional pressure left at the top. The annular pressure buildup is constant along the annulus. After the APB takes place, the annular pressure starts at the APB at the top and increases downward by the hydrostatic pressure. The load then becomes the annular pressure after APB minus the tubing pressure at each depth considered.
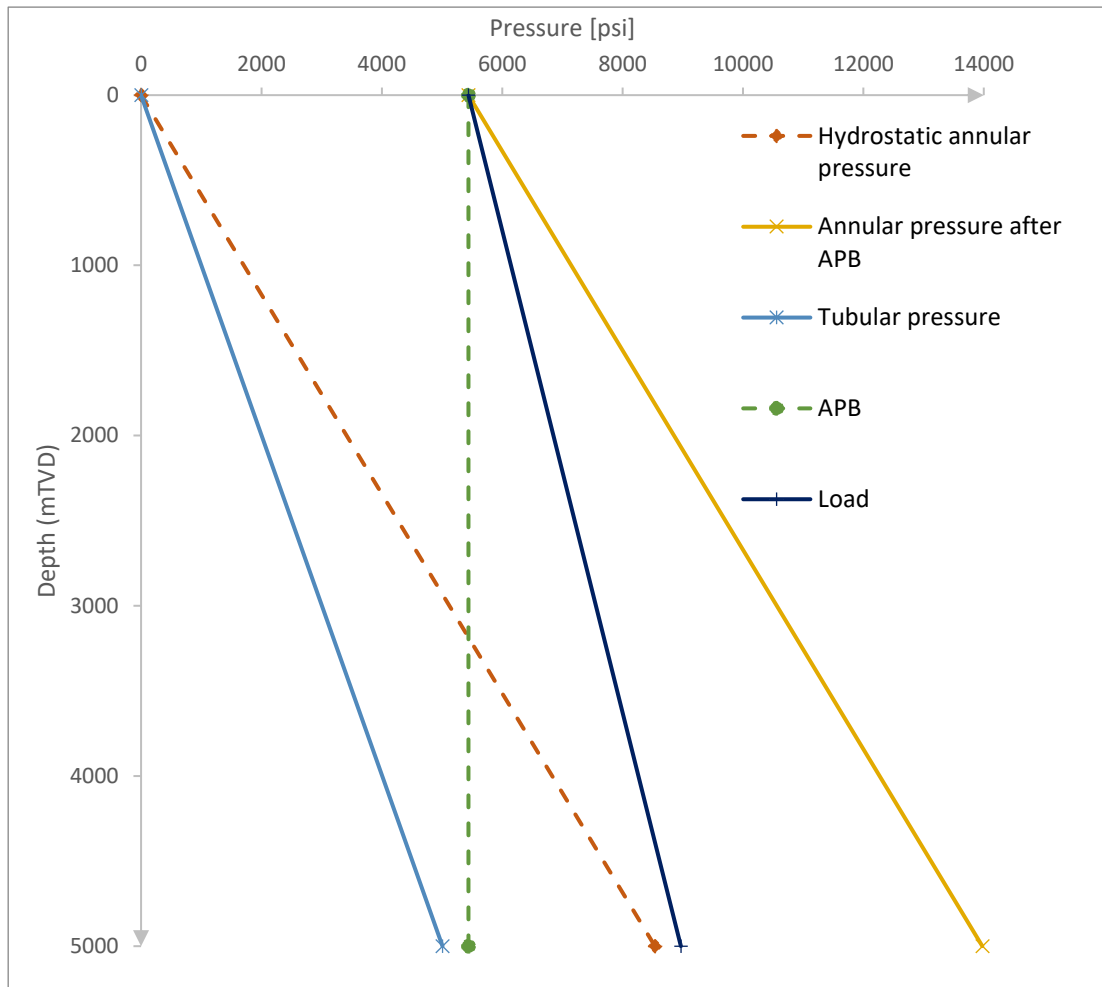
Figure 25 Pressure profile along production tubing

Assuming we use the same tubing grade for the whole tubing string length, we may for assurance check that the weakest point is at the production packer as anticipated. NORSOK D-010 require the weakest point(s) along the string to be identified [1]. It is evident from the figure above that the load is greatest at the production packer. Due to axial stress at the tubing hanger, due to the hanging buoyed weight of the string, the yield strength of the string is reduced at the top. At the same time the temperature deration of the yield strength is lower here than at the higher temperature at the packer. We will do the calculation of the load strength scenario at the tubing hanger only for the P110 tubing to assure that the tubing will collapse first at the packer. It is important to note that in the case of the weak point being at the top, the

upper string section can be replaced by a stronger grade such as Q125. Since the differential pressure is greatest at the bottom, and the axial stress deration is most severe at the top, the middle sections may use a weaker grade as discussed for casing in section 2.1. However, for simplicity we will consider a single grade string in this case study, only assuring the weak point is at the packer.

The load at the top is just the external annular pressure buildup as the hydrostatic pressure is zero on both sides of the tubing wall.

$$\sigma_{load} = 375 \ bar = 5438.92 psi$$

The de-rated yield strength of the P110 tubing for wellhead temperature is calculated. The wellhead temperature is considered $90°C = 194 \ F$

$$(194F - 70F) \cdot 0.03\%/F = 3.72\%$$

$$\sigma_{yT} = 110000 \cdot \left(1 - \frac{3.72}{100}\right) = 105908 psi$$

The yield strength for combined loading becomes as calculated below. The steel cross section given as $A_s = A_o - A_i$, and the inner tubing pressure is zero at the top.

$$\sigma_z = \frac{F_a'}{A_s} = \frac{(Z_{tube \ end} - Z_{packer}) \ w_{air} + p_{i,pipe \ end} A_i - p_{o,pipe \ end} A_o}{A_s}$$

$$\sigma_z = \frac{\left(\frac{5000m}{0.3048}\right) 32 Ib/ft + 5008 \cdot 29.167 - 13976 \cdot 38.485}{9.317} = 14289.6 \ psi$$

$$\sigma_{ycom} = \left(\sqrt{1 - 0.75\big((\sigma_z + P_i)/\sigma_{yT}\big)^2} - 0.5 \ (\sigma_z + P_i)/\sigma_{yT}\right)\sigma_{yT} = 98037.7 psi$$

The plastic collapse equation now gives a collapse strength at the tubing hanger.

$$A = 2.8762 + 0.10679 \times 10^{-5}\sigma_{Yp} + 0.2131 \times 10^{-10}\sigma_{Yp}^2 - 0.53132 \times 10^{-16}\sigma_{Yp}^3 = 3.1356$$

$$B = 0.026233 + 0.50609 \times 10^{-6}\sigma_{Yp} = 0.0758$$

$$C = -465.93 + 0.030867\sigma_{Yp} - 0.10483 \times 10^{-7}\sigma_{Yp}^2 + 0.36989 \times 10^{-13}\sigma_{Yp}^3 = 2495.3$$

$$P_p = \sigma_{ycom}\left(\frac{A}{D/t} - B\right) - C = 9963.6 < 10099 \ psi.$$

The tubing collapse strength is in fact slightly less at the top compared to at the bottom, previously calculated to 10099psi. The weak point of the string is at the production packer, due to the difference between load and load limit being greater at the top than at the bottom, as shown in the table below. We can continue using the P110 grade, although there is a good possibility of reducing yield strength in sections stepwise towards the top when installing the tubing string.

Table 12 Collapse load and strength compared at production packer and tubing hanger

	Collapse Load [psi]	Collapse strength [psi]	Load limit [psi]	Load limit - Load [psi]
At tubing hanger	5439	9964	9058.18	3619.18
At prod. packer	8968	10099	9180.91	918.09
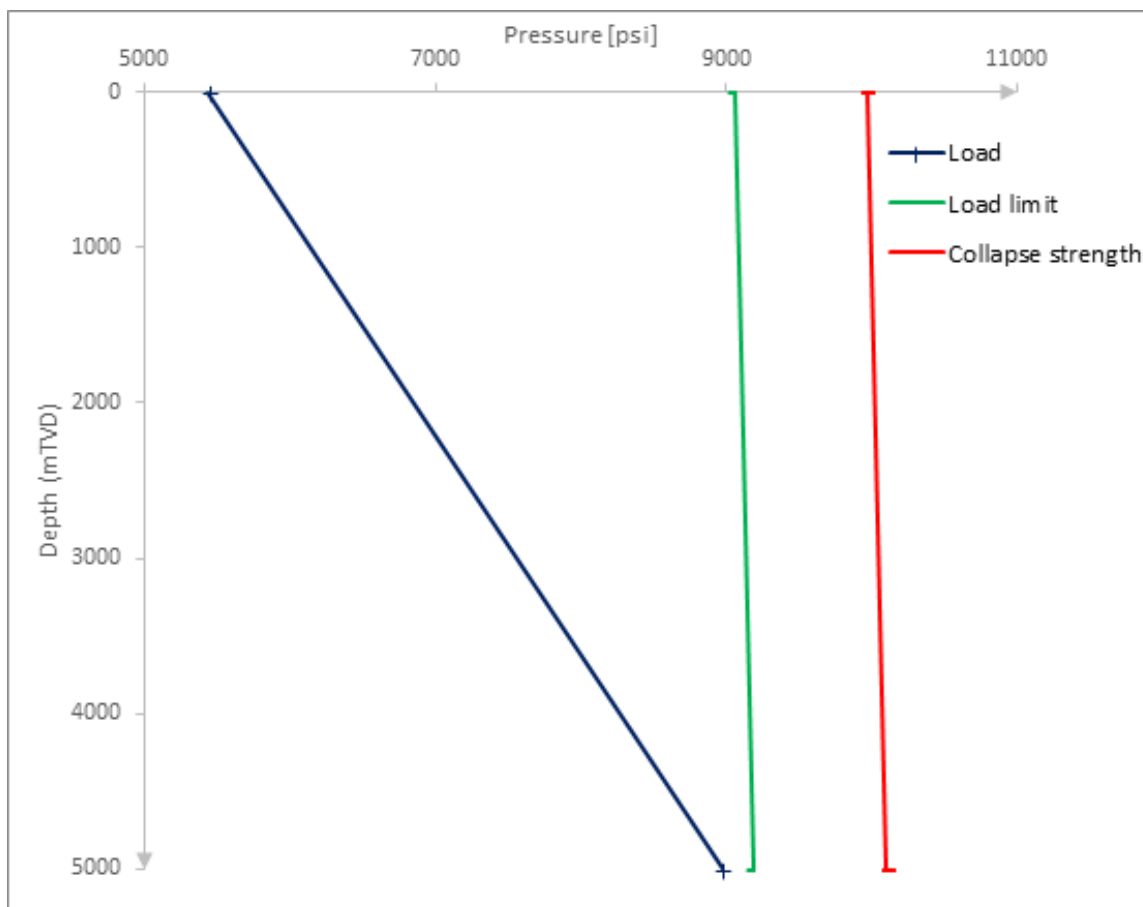
Figure 26 Load, strength and load limit profiles for the P110 tubing string

5.4 Quantitative Risk Analysis by Monte Carlo Simulation

The same case study example used in the WSD calculations in the previous section will now be used for Quantitative Risk Analysis by using Monte Carlo Simulation for both collapse load and strength. The calculations procedure is the same as demonstrated in the WSD, apart from the application of the Monte Carlo Simulation procedure. The MCS and sampling procedure is described in section 4.3.1. The procedure will be implemented in MATLAB simulation using N number of samples from the input distribution as shown in Appendix A1. For implementation of QRA, we don't use nominal parameters as input parameters. An output distribution (such as for collapse load or strength) instead relies on input parameter distributions. These input distributions describe the probability of the input parameter taking any value, thus the parameter must be described by a most likely value (the mode of the distribution) with corresponding uncertainties. The most likely value, that is the mode of the distribution, is taken as the mean of the parameter (for symmetric distributions), this is found by multiplying a bias by the nominal parameter, as the mean is a larger number than the nominal minimum value. In the case of a triangular distribution, the distribution is defined by the minimum, mode and maximum values [a, c, b]. The normal distribution is similarly described by its mean μ (mode of the distribution for normal distributions) and by its standard deviation σ describing its spread.

The collapse load will rely on input parameters such as the depth of the production packer, the geothermal gradient, the wellhead temperature, the density of the production fluid and packer fluid etc. We will consider some parameters such as depth and densities as relatively certain and assign triangular distributions for the parameters that is more questionable such as the wellhead temperature. Although the wellhead temperature is assumed to have been predicted by considering heat exchange of control volumes along the production tubing, these calculations rely on assumptions such as ambient temperature at the cement-formation interface. APB calculations also involves uncertainties due to the assumption of a fully rigid casing and tubing arrangement. The A annular volume is assumed to be constant. In reality, the A annulus volume will expand due to ballooning of the production casing and reverse ballooning of the production tubing. The effect of the annular volume expansion is that the APB always will be overpredicted as mentioned earlier. A triangular distribution will therefore be assigned also for the APB model to account for this model uncertainty. The uncertainty is multiplied with the collapse load during the MCS procedure.

For the collapse strength we will begin with the nominal casing parameters given by the *Drilling Data Handbook*. The *ISO/TR 10400* technical report provides bias (conversion factors) for calculating mean values from nominal values as well the covariance (COV) of most input parameters in the API 5C3 collapse equations from nominal parameters. The covariance COV is defined by the *ISO/TR 10400* as the standard deviation divided by the mean. The bias and COV values comes from experimental datasets for different casings. In this case study, we will use the dataset (API 1987) in table F4 for casing data, however for yield stress we use table F3 choosing the (AE04) and (SS22) dataset. The tables are provided by ISO/TR 10400 [12]. The tables are reproduced in Appendix A3 together with the nominal data table from the *Drilling Data Handbook* for convenience.

$$\mu = Nominal\ parameter * bias \tag{83}$$

$$\sigma_{std} = COV * \mu \tag{84}$$

Because we now know the mean μ and standard deviation σ we will use normal distributions for most input parameters in the collapse strength calculation. For some parameters fixed values will be used. In addition, the API collapse model has an uncertainty that will be represented by a normal distribution. The model uncertainty is defined by *"the remaining variability once the effect of variation of the other input parameters has been removed"* [12]. Model uncertainty can therefore be expressed as (actual collapse strength /predicted collapse strength). The normal distribution is therefore given by Mean and COV values from experimental casing dataset (API 1987), see Table F2 in *ISO/TR 10400* [12] or table 30 in Appendix A3. The API model uncertainty is specific to the API model, other model types such as the Tamano collapse model are also assigned uncertainties in table F2. The model uncertainty is multiplied with the collapse strength during the MCS sampling procedure the same way the APB uncertainty is for the load, the uncertainty shifts the strength distribution slightly to the right to fit the mean to the experimental data.

For each time the load and strength are calculated from sample distributions within the MCS procedure, the result is evaluated in the MATLAB code. If the load is larger than the strength, the result is collapse and is stored in a counter, counting each collapse result. When the MCS procedure is complete, the probability of collapse in percent is calculated as follows. N is number of samples or sampling iterations from the MCS.

71

$$P_f = \frac{Counter}{N} \cdot 100 \tag{85}$$

The predicted collapse probability from the QRA need to be below an acceptable collapse probability or target probability P_t. The choice of an acceptable failure probability or target probability relies on the seriousness of a failure. The risk of a failure is defined as consequence times failure probability. So, the target probability will be higher for a failure with small consequence than for one with high consequence, to ensure the risk is similar. We may consider different types of failure events. If the failure event has severe consequences it may be considered a ultimate failure event or blowout event, here the failure is not considered possible to repair. In this case the target probability must be set relatively low. On the other hand, if the failure event has low consequence, it may be considered a repair event, here the failure is considered possible to repair and the target probability can be set relatively higher. In the paper *Casing System Risk Analysis Using Structural Reliability* [30], one of the following generic target probabilities was chosen depending on the consequence of failure, stress check type and load case. The paper also states that 10^{-4} *"is the usual industry standard for the ultimate failure event"*[30]. The table below summarize the selection of target probability as fraction and percent.

Table 13 Target probability selection, modified from [30]

Event type	Target Probability P_t [0-1]	Target probability P_t [%]
Blowout event	10^{-4}	0.01
Repair event	10^{-2}	1

In the paper *A Reliability-Based Approach for Survival Design in Deepwater and High Pressure/High Temperature Wells,* the difference between a service/operating load and a survival load design is explained [38]. A service load has high frequency of occurrence and low uncertainty whilst a survival load has low probability and is of extreme magnitude. Because survival loads are infrequent, the full strength of the casing or tubing may be allowed to be used, it is designed to survive but not necessarily being operable during and after the occurrence of the load. In WSD this may therefore in some instances correspond to applying no design factor at all. In reliability-based design however, the use of a higher target probability for survival loads is used as compared to service loads where the design is made for full operability. However, the

consequence still impacts the choice of target probability. The paper proposes the following target probabilities for survival design of tubulars with high and low consequence of failure, these may coincide with the blowout and repair event previously noted.

Table 14 Target probability selection for survival type loads in tubular design, modified from [38]

Consequence of failure	Target Probability P_t [0-1]
High	$10^{-6} - 10^{-5}$
Low	$10^{-3} - 10^{-2}$

For now, we will consider the worst-case target probability of 10^{-4} from table 13, that is a 0.01% acceptable probability of failure for an anticipated ultimate failure event. We therefore set $P_t = 0.01\%$. We will later discuss the choice of target probability and investigate the effect of increasing it to that of a repair event.

5.4.1   QRA Collapse load calculation

The calculation process for the collapse load will not be demonstrated since it is the same as for WSD, although carried out numeral times for MCS. The input parameter distribution and model uncertainty distribution for the load calculations are given in the table below. The uncertainty in the APB model is based on the previously noted observation *"annular heatup pressures are always overpredicted (by as much as 30%) by fully rigid single-string analysis"* [23]. The uncertainty in the APB model is multiplied with the APB, ΔP for each sampling iteration. Fixed input parameters are the same as in the WSD analysis.

Table 15 Load input parameter distributions (triangle distributions)

Triangle dist.	Min (a)	Mode (c)	Max (b)
T_{wh}	70	80	90
APB-Model Uncertainty	0.70	0.85	1

5.4.2   QRA Collapse strength calculation

The mean input parameter distributions for the API collapse strength calculations are shown in the table below. Other parameters are fixed as in the WSD analysis. The API model uncertainty is multiplied with the predicted collapse strength for each sampling iteration.

Table 16 Strength input parameter distributions (normal distributions)

7inc API 32Ib/ft API 5C3 Model	Nominal	Bias	Mean μ	COV	Standard dev. σ_{std}
L80 σ_y [psi]	80000	1.119	89520	0.0387	3464
C90 σ_y [psi]	90000	1.062	95580	0.0325	3106
T95 σ_y [psi]	95000	1.066	101270	0.0315	3190
P110 σ_y [psi]	110000	1.147	126170	0.0373	4706
OD [inc]	7	1.0058	7.0406	0.00125	0.008801
t [inc]	0.453	1.0058	0.45563	0.0264	0.01203
w [Ibs/ft]	32	N/A	N/A	N/A	N/A
API-Model Uncertainty	N/A	N/A	1.158	0.066	0.07643

*Nominal values taken from Drilling Data Handbook [36], Bias and COV from ISO/TR 10400 [12]

5.4.3   Results of QRA

The MATLAB code for QRA by MCS of production tubing collapse mode generates a schematic of a load and strength distribution. We will now look at the resulting distributions and use different design methodologies for comparing load and strength. The most important difference from the WSD is that the reliability-based design approaches provide a simulated probability of collapse. The probability of collapse will need to be below an acceptable collapse probability, that is the target probability of the design.

The output distributions from the MCS of collapse load and strength is presented below for the considered casing string with the same varying grades used in the WSD analysis. The load and

strength distributions resemble normal distributions and are represented by histograms, a normal distribution is fitted using the distribution fitting tool in MATLAB for each distribution. The tool is also used to generate CDF, and normal probability plots (Normal Quantile-Quantile plot) to compare the histogram data with the normal distribution fit. When the data follows the straight line in the probability plot (see figure 29), this means the data are close to normal since the straight line is that of the normal approximation. The probability axis of the probability plot represents quantiles of the standard normal curve, the data axis represents quantiles from the data. Since the calculation process is identical for each of the gradings, these considerations will only be shown for the L80 tubing as it provides similar results for the same number of MCS.

The MCS results for the QRA from the base case L80 tubing will now be presented. N=1000000 sampling iterations was used for the MCS. The load and strength output data were each divided into bins and presented as histograms using the Distribution Fitting Tool in MATLAB. The Freedman-Diaconis| rule was used to determine the bin width. This ensures a minimal difference between the integral of the histogram and that of the theoretical distribution. The rule states *"Choose the cell width as twice the interquartile range of the data, divided by the cube root of the sample size"* [41]. The interquartile range being the range of collapse load or strength data and the sample size being the number of sampling iterations of the MCS.

The figure below shows the resulting load and strength distributions with fitted normal distributions. The fitted distributions and collapse probability are summarized in the table below. To ensure convergence of the distribution and acceptable variability of the result when performing multiple Monte Carlo Simulations, the simulation was conducted ten times and the mean and standard deviation of the simulated collapse probability was calculated. This consideration will only be done for the base case L80 tubing to establish the number of sampling iterations needed for the MCS.

Table 17 QRA results from MCS of collapse mode on the L80 tubing string

L80 MCS Results: N=1000000	Mean μ	Standard dev. σ
Normal load distribution [psi]	7545	383.3
Normal strength distribution [psi]	9956	869.5
Simulated Collapse Probability P_f [%]	0.4105	0.007624

The standard deviation of the collapse probability can be converted to a $COV = \frac{\sigma}{\mu} = 0.0185725$.

For the other tubing grades, the COV can be used to find the standard deviation of the collapse probability by multiplying by the simulated probability for the selected grade. To account for the variability in the collapse probability we may use the P99.7 (tree standard deviations above the simulated probability), that is using a confidence interval of 99.7% assuming a normal distribution according to the (68-95-99.7). The tree-sigma rule of thumb states that even non-normal distributions has at least an 88.8% confidence interval within tree standard deviations from the mean [42]. For the L80 string this correspond to a collapse probability of 0.4334% to be compared to the target probability.
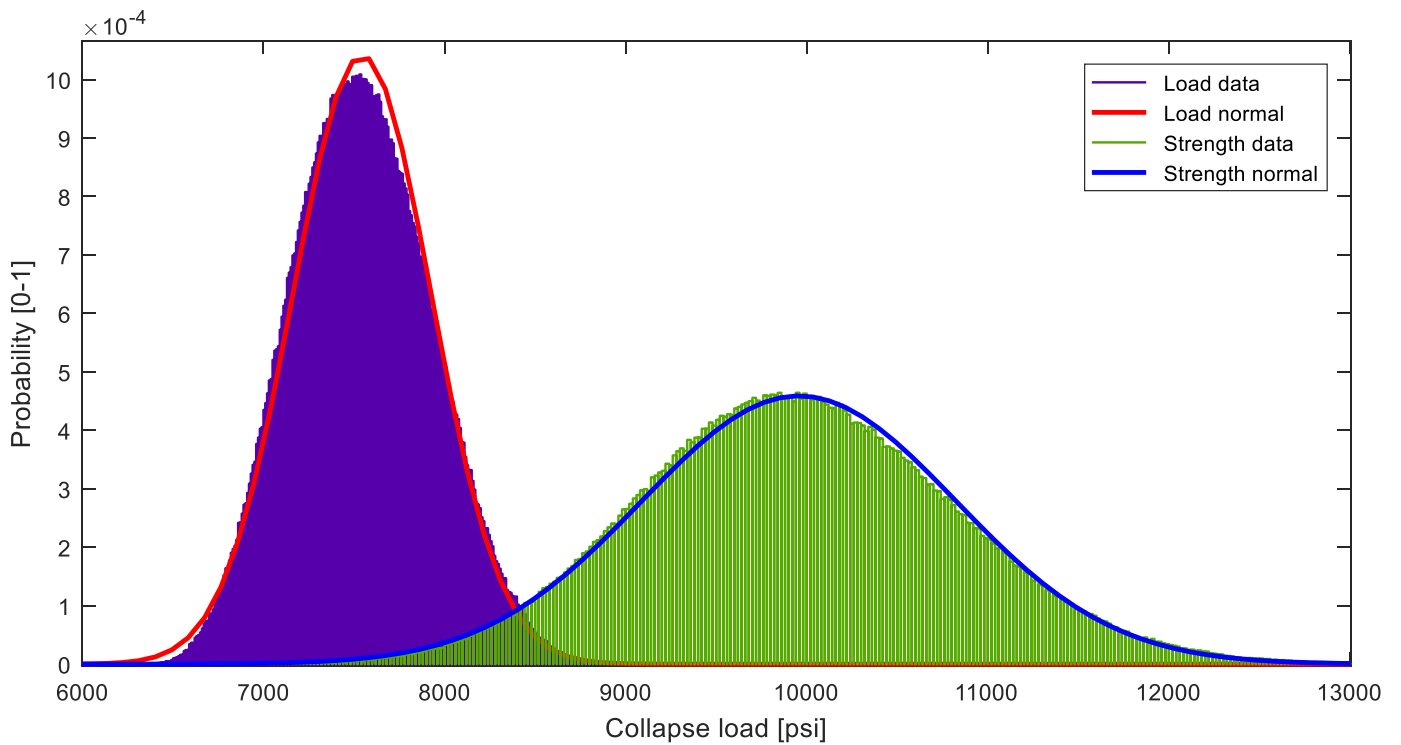
Figure 27 QRA schematics obtained by MCS of collapse mode on an L80 tubing string

The variability in collapse probability is considered acceptable when applying tree standard deviations from the mean, and we will be using N=1000000 sampling iteration also for the other string grades. The resulting collapse probability including tree standard deviations $P_f + 3\sigma = 0.4334\%$ for the L80 tubing are not acceptable as it exceeds the target $P_t = 0.01\%$. This is coherent with the findings from the WSD previously. Similarly as with WSD we will therefore gradually increase the tubing grade until the target probability is fulfilled. The CDF of the load and strength distribution for the L80 tubing is shown below as is the probability plot.
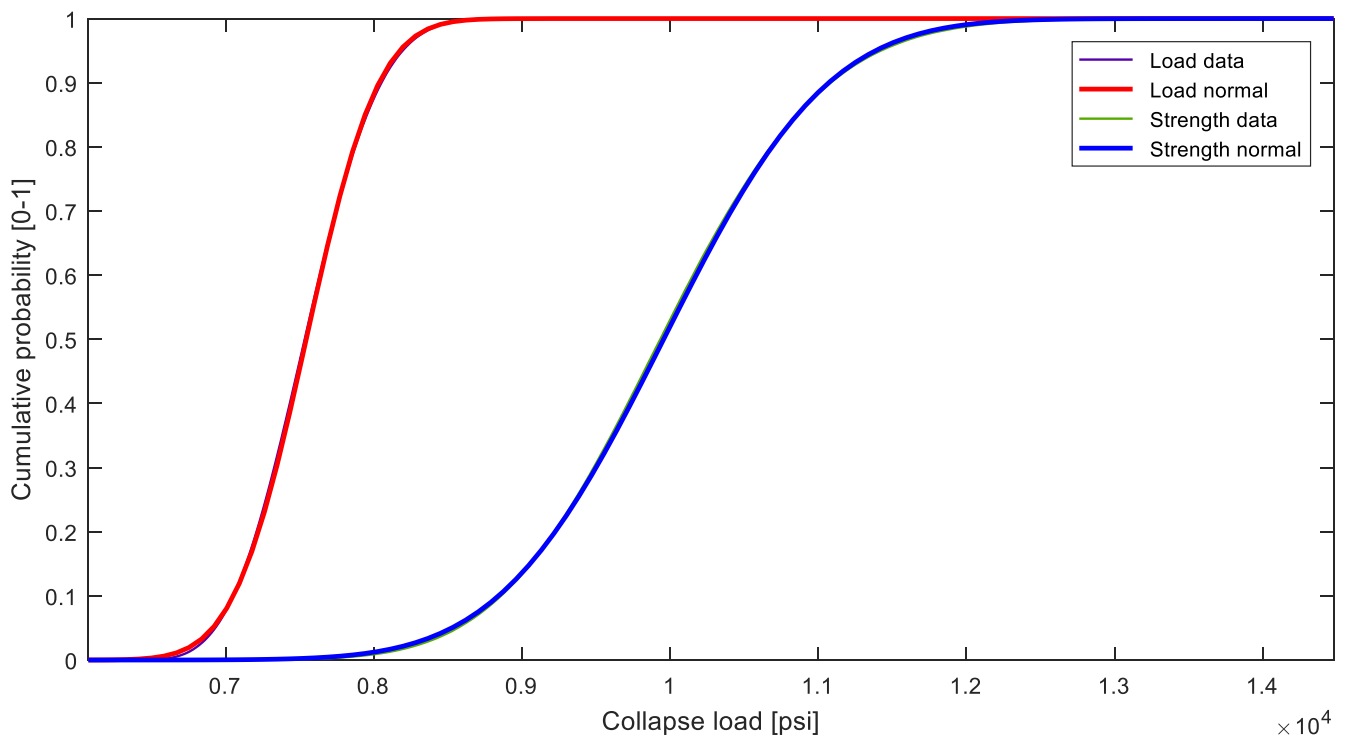
Figure 29 Tubing CDF's from QRA of collapse mode on an L80 tubing
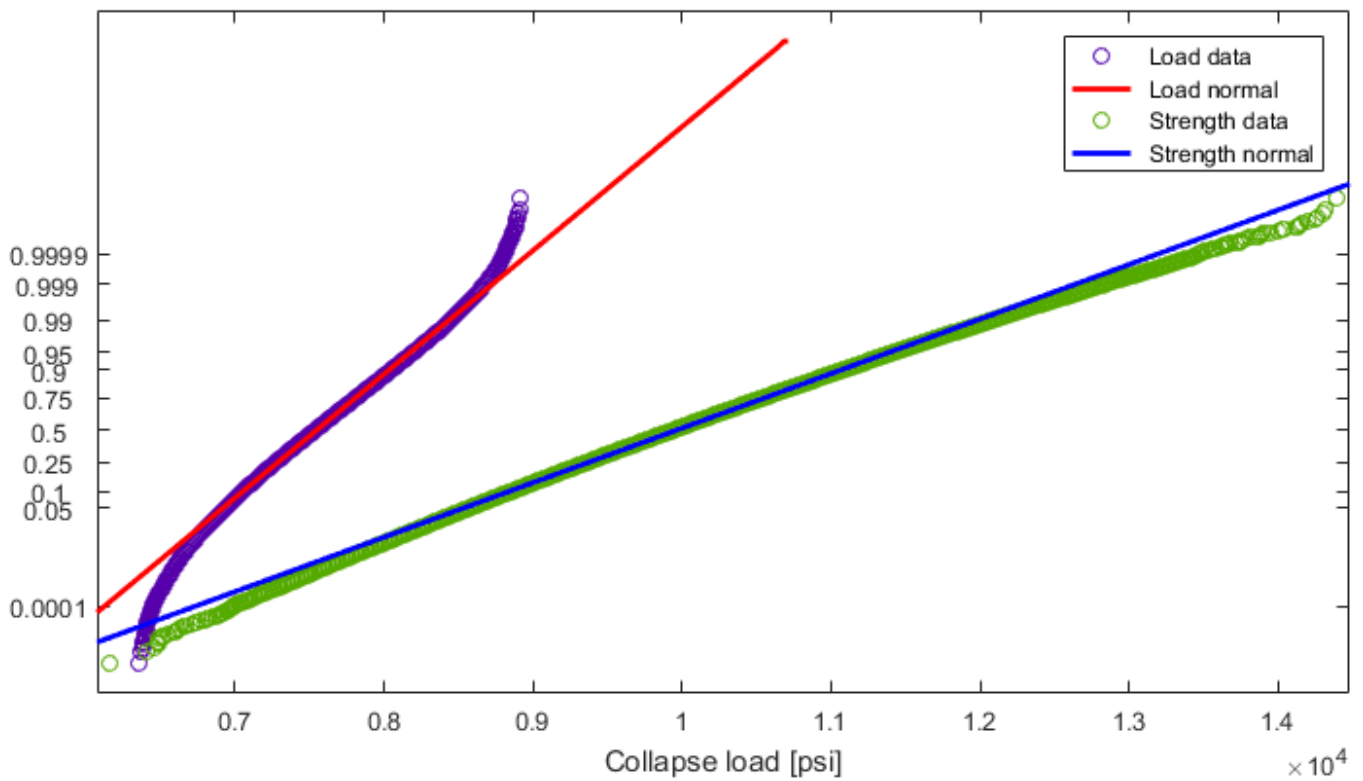
Figure 28 Probability plot for a normal distribution fit to data from the L80 tubing QRA

The CDF's for load and strength are shown for both the simulated data and the fitted normal distribution, the functions overlap greatly. However, the probability plot is used to evaluate how good the normal distribution fits the data. The probability plot shows that the normal distribution fits the data best in the center and gets worse as we move towards the flanks of the distribution. The distribution fit overpredicts the load and strength frequency on the left distribution flank, on the right flank it overpredicts the strength frequency and underpredicts the load frequency. The collapse probability estimate is not affected by the distribution fit, so the accuracy of the fit is not critical for the results. The resemblance of a normal distribution however implies that the simulation has converged, as implied by the Central limit theorem the data will approach a normal distribution as N approaches infinity.

The yield strength will now be increased to the C90, T95 and P110 grades, using similar calculation procedure as described for the L80 string grade to find the minimum tubing grade to obtain the target probability. The results including the L80 grade are listed in the table below for comparison. Note that the standard deviation for the collapse probability of the strings are found from the calculated COV=0.01857 of the L80 grade failure probability. Three standard deviations above the mean are used for comparison with the target probability.

Table 18 MCS results for different grades, collapse probability and ultimate failure event target probability

Tubing Grade	Collapse Load [psi]		Collapse Strength [psi]		P_f [%]	$\sigma(P_f)$ [%]	$P_f + 3\sigma$ [%]	P_t [%] Ult. fail
Normal dist.	μ	σ	μ	σ	N/A	N/A	N/A	N/A
L80	7544.5	383.28	9956.6	869.55	0.4105	0.00762	0.4334	0.01
C90	7545.2	383.37	10465	904.28	0.0854	0.00159	0.0902	0.01
T95	7544.2	383.50	10924	947.30	0.0234	0.000436	0.0247	0.01
P110	7544.7	383.02	12762	1154.1	0.000300	0.00000557	0.000317	0.01

The P110 tubing grade is the first grade that exceed the target probability, this is the same result as for the WSD. The load and strength distributions for all the grades chosen in the above table are presented in the following figure. For the sake of comparison, the load and strength histograms are omitted, only showing the normal distribution fit and simulated data points. The four load simulations with fitted distributions are shown in the same colors as they are indistinguishable.
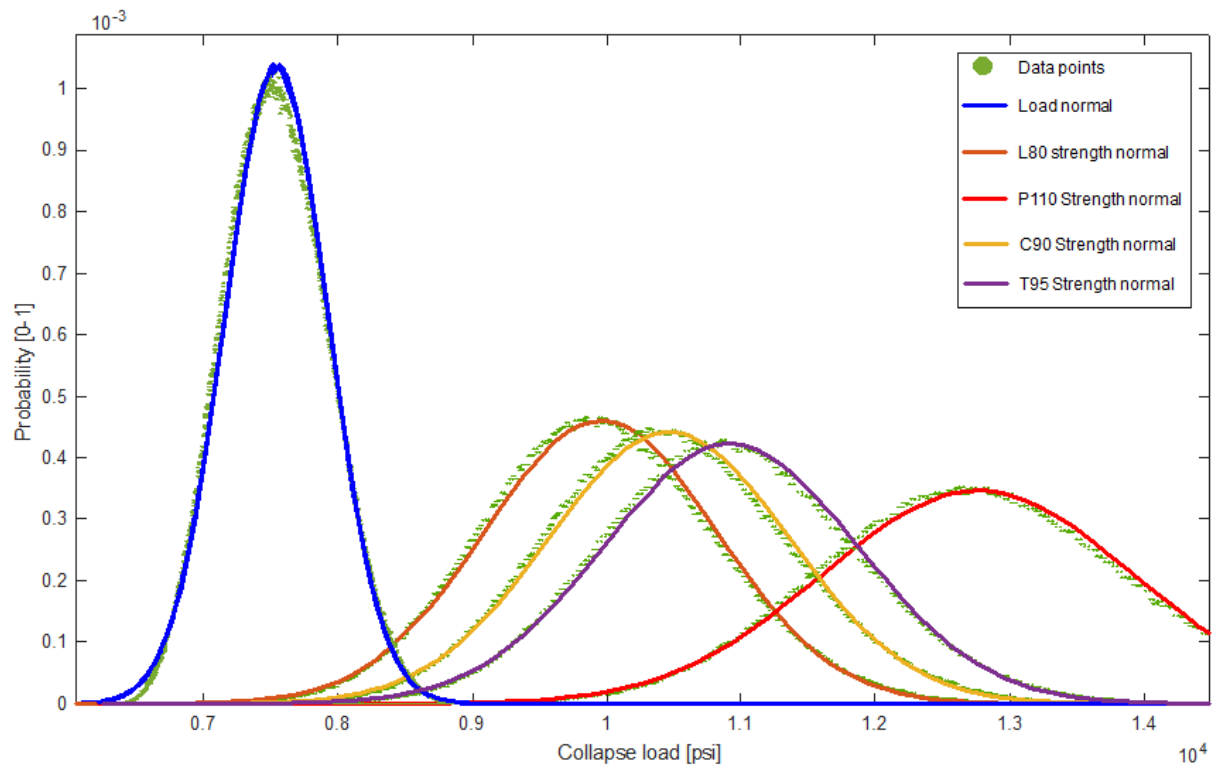
Figure 30 Load and strength distributions for four different tubing grade simulations

5.4.4 Sensitivity analysis of MCS output distributions

The aim of a sensitivity analysis performed on the MCS output is to identify how different input distributions contribute to the mean and spread of the output distributions. The sensitivity analysis can be used to identify faults in the MCS calculation process by identifying input parameters that contributes in an unexpected way. Important knowledge of which inputs contributes mostly to the uncertainty in load and strength allows us to make substantiated decisions on what input parameters we will work on reducing its spread of if possible. This may be achieved my more accurate measurements when creating statistical datasets. Reducing the spread of the input parameters will reduce the spread of the load and strength distributions and in turn reduce the collapse probability.

The strength distribution spread relies on the tubing yield strength, outer diameter and wall thickness. In addition, the API model uncertainty contributes to the strength distribution spread. The load distribution spread only relies on the spread of the predicted wellhead temperature and on the APB uncertainty distribution. In the following figure the result of a sensitivity analysis done on the strength and load distribution of the P110 tubing grade are shown. The sensitivity analysis first conducts a base case with all contributing uncertainties. Later only one of the input variabilities are contributing to the output distribution at a time. The other input distributions are replaced by fixed parameters represented by the input distribution mean. The sensitivity analysis for the MCS of the P110 tubing design are carried out for load and strength individually, as the load calculation impacts the collapse strength. Normal distributions are fitted to the simulated data.

The results for the load distribution is shown in the following figure and corresponding table below. Here the variability is caused by the wellhead temperature and the APB model uncertainty one at a time, while holding all other inputs as fixed parameters. In addition, the base case of the P110 tubing string is shown for comparison. The APB model uncertainty is shown to have greater impact than the wellhead temperature on the variability in collapse load. The figure shows that while only sampling one triangular input distribution, such as the wellhead temperature or APB model uncertainty, the output load distribution from the MCS also becomes a triangular distribution. However, when the two different triangular input distributions are sampled in the MCS procedure, the output distribution approach a normal distribution as the number of sampling iterations increase. This is in accordance with the central limit theorem and implies that the choice of distribution type to represent the input distributions are of lesser importance.

Table 19 Variability contributors to the collapse load distribution

Variability contributor	Mean μ [psi]	Standard deviation σ [psi]
Collapse strength Base Case	7544.73	383.019
Wellhead temperature T_{wh}	7544.38	251.971
APB Model uncertainty [-]	7544.36	289.026
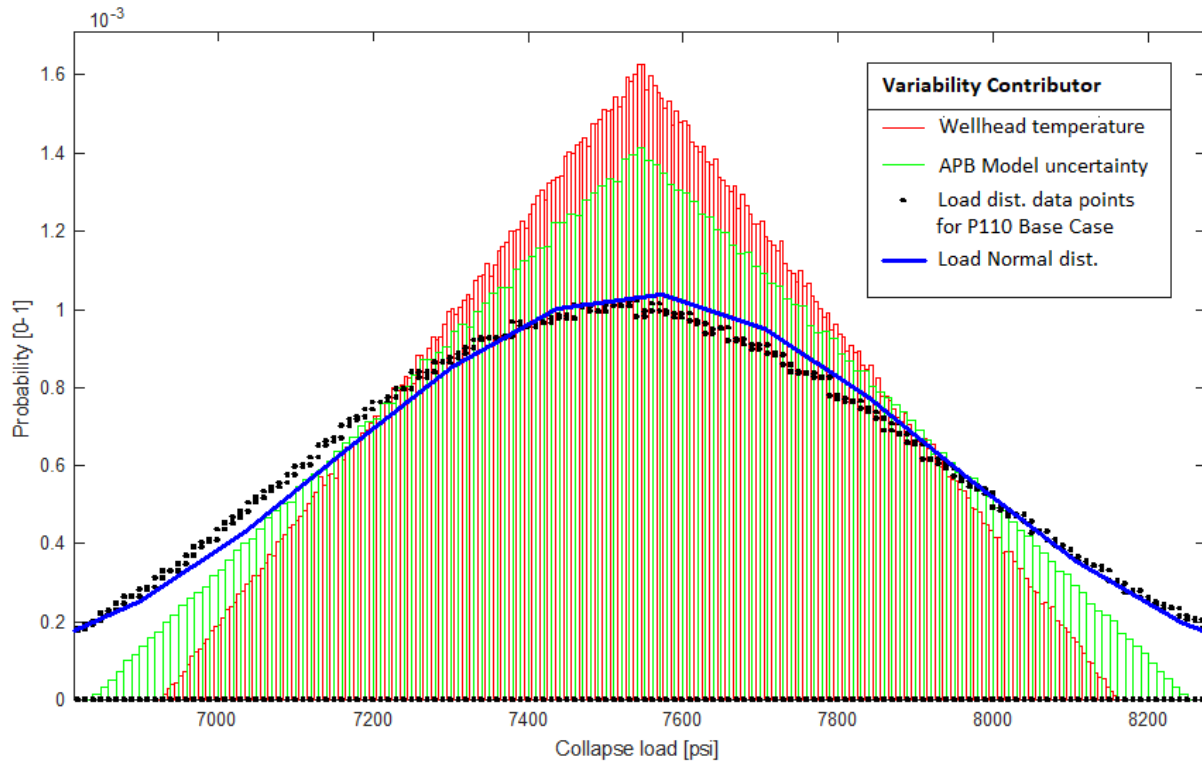
Figure 31 Collapse load sensitivity analysis showing variability due to different contributing parameters

The results for the strength distribution is shown in the following figure and corresponding table below. Here the variability is caused by yield strength, wall thickness, outer diameter and API model uncertainty one at a time, while holding all other inputs as fixed parameters. In addition, the base case of the P110 tubing string is shown for comparison. The API model uncertainty and the wall thickness have the greatest effect on the variability of the collapse strength followed by the yield strength and the outer diameter.

Table 20 Variability contributors to the collapse strength distribution

Variability contributor	Mean μ [psi]	Standard deviation σ [psi]
Collapse load Base Case	12762.4	1154.06
API Model uncertainty	12770.1	843.406
Wall thickness t	12769.9	719.669
Yield strength σ_y	12763.9	321.182
Outer diameter OD	12769.0	34.1034

81
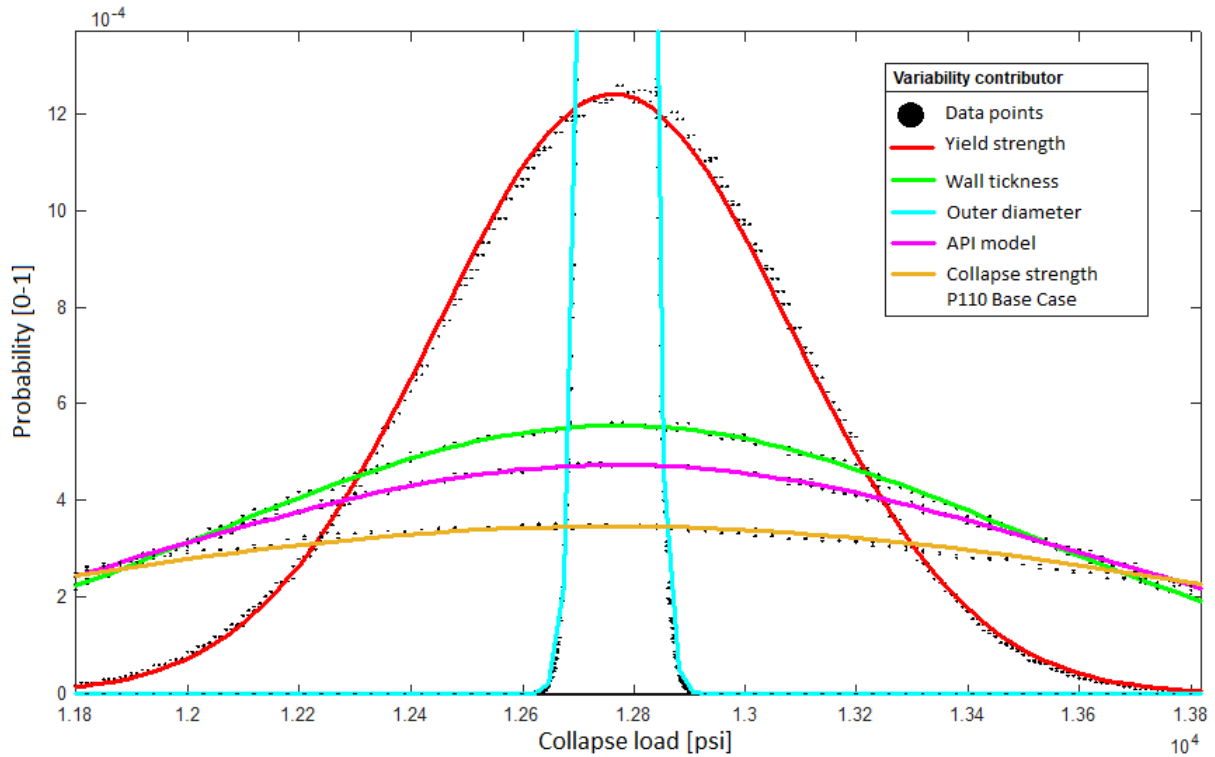
Figure 32 Collapse strength sensitivity analysis showing variability due to different contributing parameters

Another approach to sensitivity analysis is to use a Tornado diagram. We will use it to evaluate how the input parameters for collapse strength impact the output distribution. The goal is to determine which input distribution has the biggest impact on the output. One by one, the yield strength, wall thickness and outer diameter distributions will be replaced by their P5 and P95 percentiles. In this way we will be able to evaluate which input parameter has the greatest impact on the mean of the output distribution, that is the magnitude of the collapse strength. The diagram shows the collapse strength distribution mean, when using the P5, P50 (mean) and P95 of the input distributions, one by one. The case where the input distribution has the greatest impact is placed on top of the diagram, and in decreasing order downward. The relevant percentiles of the input distributions are shown in the table below. The percentiles can be found using the MATLAB function *norminv*.

82

Table 21 Percentiles of input parameters for collapse strength calculation

P110 Tubing	Input parameter distribution percentiles		
Input parameter percentile	P5	P50 (Mean)	P95
Yield strength σ [ksi]	118430	126170	133910
Outer diameter OD [$inch$]	6.6312	7.0406	7.4500
Wall thickness t[$inch$]	0.3339	0.45563	0.5774
API Uncertainty	11383	12769	14155

The output collapse strengths for the tree different cases is calculated next, each using the different percentiles of the corresponding input variable listed in the above table. Note that we do not conduct a MCS to obtain these results, we only calculate the mean of collapse strength by replacing all input distribution by fixed mean values except for the manipulated input variable where the 5th, 50th (mean) and 95th percentile is used. The use of these percentiles in accordance with the (69-95-99.7) rule makes a normal input distribution spread of two standard deviations away from the mean, that is a confidence interval of 95%. The resulting collapse strengths is listed below.

Table 22 Collapse strengths resulting from percentiles of input parameters

P110 Tubing	Collapse strength [psi]		
Input parameter percentile	P5	P50 (mean)	P95
Yield strength σ_y	12227	12769	13283
Outer diameter OD	12825	12769	12713
Wall thickness t	11586	12769	13952
API Uncertainty	11383	12769	14155
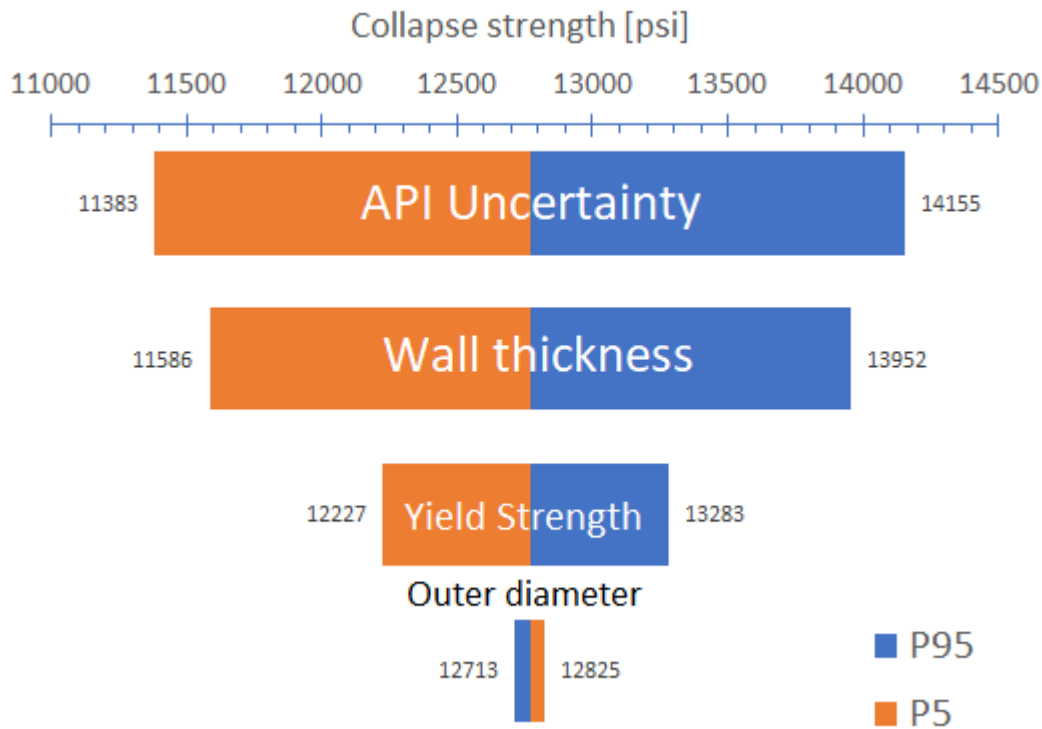
Figure 33 Tornado diagram showing impact of different input distributions on collapse strength spread

From the table and figure above, note that the P50, the mean value of the predicted collapse strength for the different cases deviate slightly from those presented for the P110 quantitative risk analysis. The reason for this is that the mean collapse strength from the quantitative risk assessment is those of the fitted normal distribution of a simulated collapse strength distribution, whilst these are the mean values directly calculated without the process of MCS and distribution fitting. We observe the same results here as in the previous approach for sensitivity analysis. The biggest contributor to the uncertainty in the collapse strength is the API model uncertainty, followed by the tubing wall thickness, yield strength and outer diameter. Note that increasing the outer diameter has the reverse effect compared to the other input parameters, decreasing the collapse strength.

When designing the tubing we increased the yield strength until we reached the minimum of available grades that fulfilled the design target probability, or the design factor in the case of WSD. Other input parameters could also be manipulated. By changing the wall thickness or outer diameter, the collapse strength could be increased. Although the Tornado diagram prepared here only is applicable to evaluate the effect on uncertainty in collapse strength, a

similar approach of a Tornado diagram can be used to evaluate the cost effectiveness of the design. By changing input parameters intentionally to impact the collapse strength, one could use a similar diagram to see which changes in design has the greatest impact on cost. In that case we would not change the percentile used from the input distribution but rather use different combinations of grades, wall thicknesses and outer diameters available on the market to evaluate which of these would meet the target probability, and then range them by cost effectiveness.

The tornado diagram above can be misleading when interpreted in the wrong way. The variability in the different input parameters are not the same, for example the COV of the outer diameter is much smaller compared to that of the wall thickness (COV is comparable as it is standard deviation normalized by mean). This mean that as we in this example don't change the input parameters by the same percentage, the Tornado diagram does not say anything about what parameter has the biggest effect on collapse strength. However, it does say which input distribution has the biggest impact on the variability of the collapse strength as intended. To get an idea about what parameter in isolation has the biggest effect on collapse strength, we need to decrease and increase the input mean by the same percentage one at a time. In the following Tornado diagram and table each input parameter mean was decreased and increased by one percent, one at a time, while holding all other input parameters at its mean value.

Table 23 Collapse strength from changing input parameters one at a time by one percent from its mean value

P110 Tubing	Collapse strength [psi]		
Input parameter using:	Mean Minus 1%	Mean	Mean Plus 1%
Yield strength σ	12682	12769	12855
Outer diameter OD	13044	12769	12499
Wall thickness t	12496	12769	13041
API Uncertainty	12641	12769	12897
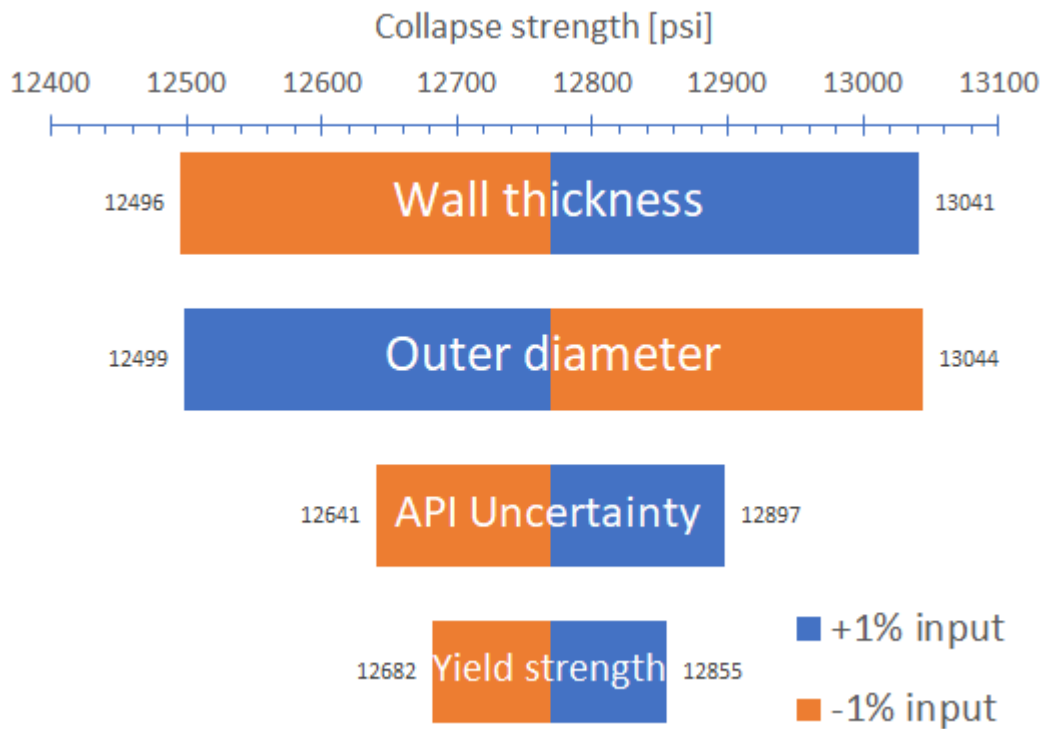
Figure 34 Tornado diagram showing impact of one percent change in input parameters on collapse strength

The Tornado diagram show that wall thickness and outer diameter has the shared largest, but opposite effect on the collapse strength, followed by the API uncertainty and yield strength.

5.4.5   RBD Level 5 vs. RBD Level 4

In section 4.6 we discussed how different design methodologies can be combined. The QRA performed in the case study until now is of RBD Level 5 because both load and strength are represented by probability distributions. We may try to replace the load distribution by a deterministic load calculated by using conservative fixed values for the wellhead temperature and annular pressure buildup, not including the APB uncertainty. This approach corresponds to RBD Level 4. Because we use more conservative values for load, an increased probability of failure is anticipated by using this approach. The same procedure by MCS is used only replacing the appropriate input for load. The wellhead temperature is set at 90 degrees Celsius, the worst case for the wellhead temperature distribution, as that allows for the largest annular heatup and resulting APB. The APB uncertainty is omitted or set to one, as this is the worst case for collapse scenario. All other parameters for load and strength are unchanged. The resulting figure and table below show the results from the QRA, RBD Level 4 approach applied on the P110 tubing design.
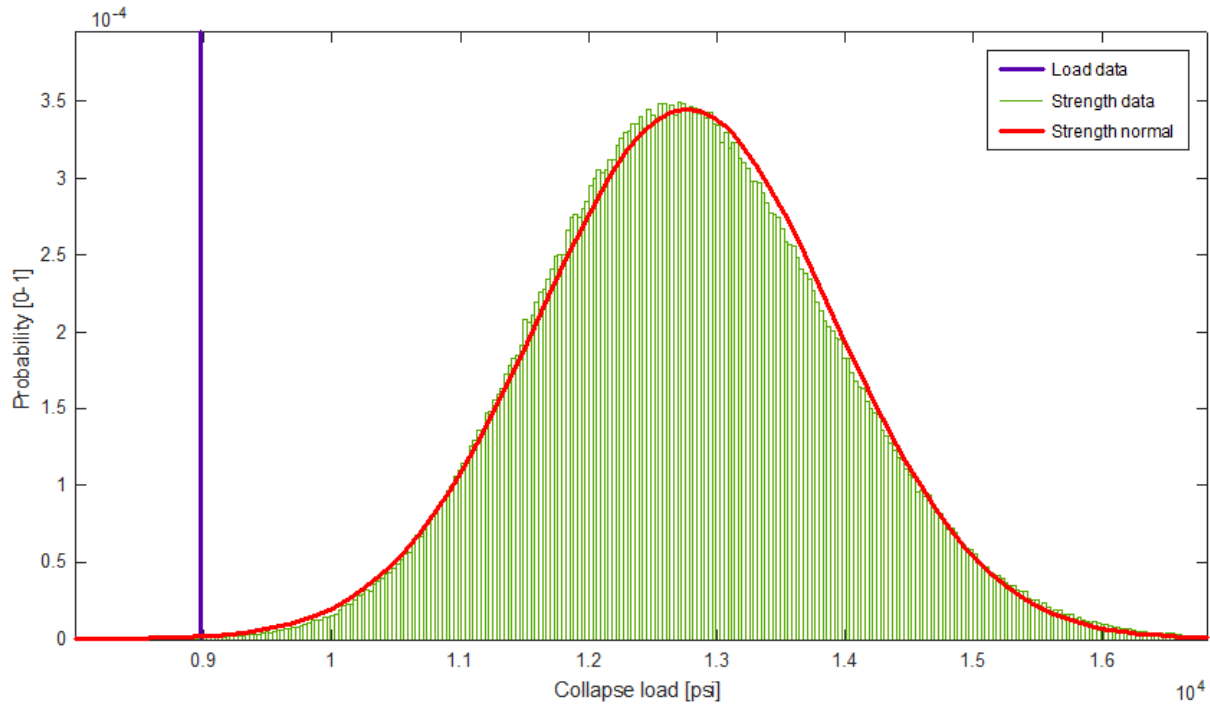
Figure 35 RBD Level 4 applied on the P110 tubing design

Table 24 MCS Comparison of MCS results from RBD Level 4 and 5 for the P110 tubing string

RBD/Grade	Collapse Load		Collapse Strength		P_f [%]	$\sigma(P_f)$ [%]	$P_f + 3\sigma$ [%]	P_t [%]
Normal dist.	μ	σ	μ	σ	N/A	N/A	N/A	N/A
RBD 4 P110	8976.78	0	12765	1156.67	0.0161	0.000299	0.0170	0.01
RBD 5 P110	7544.7	383.02	12762	1154.06	0.000300	0.00000557	0.000317	0.01

The probability of failure for the RBD level 4 case including tree standard deviations of collapse probabilities (using the tree sigma rule) is estimated to 0.0170% and is higher than the target probability of 0.01%. This mean that because of the conservative assumptions done in the load computation in RBD level 4, the P110 tubing design would have been scrapped by using this level of RBD. The tubing grade would have to be increased further by possibly a Q125 grade, or the thickness or diameter would need to be changed. As anticipated the estimated collapse probability is much higher for level 4 than for level 5, in fact the level 4 RBD predict a collapse probability of 53.6 times that of the level 5 RBD when considering the ultimate failure event target probability. Based on these results we can conclude that cost and/or material savings can be made by applying a higher level of RBD.

87

5.4.6 The effect of increasing target probability

In an event where the production tubing of a well collapses, the collapsed tubing might be possible to be patched, otherwise the tubing must be pulled and the well recompleted with new tubing at least for the collapsed section. A tubing collapse only break the primary well barrier, the secondary barrier still separates the well from the external environment by the production packer, the production casing, the production casing hanger and the wellhead. If the tubing can be repaired, the failure event can be viewed as a repair event. Using camera intervention and 3D visualization, an increased number of wells with damaged tubing can be patched [7]. Thereby the consequence of tubing collapse is reduced. With the assumption of a repair failure event we can increase the target probability to the repair event target probability of 10^{-2} from table 13. That is setting the target probability to $P_t = 1\%$. Interestingly our choice of target probability is the same as seen from table 6 when entering low consequence and low cost.

In the table below, the simulated failure probability from different tubing grades are shown as compared to the new target probability. An additional MCS had to be made for a K55 tubing because the L80 tubing now became acceptable for the design. As seen from the table the L80 tubing has the first acceptable tubing grade, that is where the predicted failure probability is below the target probability of the repair event. The predicted probability of collapse for the L80 tubing is 0.4334 %, thereby less than the target probability of 1%. By using a higher target probability, it is now therefore possible to use an L80 tubing instead off a P110 tubing as required both by using the QRA with ultimate failure event and by the WSD. Considerable savings can be made from the change of tubing grade.

Table 25 MCS results for different tubing grades, collapse probability and repair event target probability

Grade	Collapse Load		Collapse Strength		P_f [%]	$\sigma\left(P_f\right)$ [%]	$P_f +$ 3σ [%]	P_t [%] Ult. Fail.	P_t [%] Repair
Normal dist.	μ	σ	μ	σ	N/A	N/A	N/A	N/A	N/A
K55	7545.1	383.06	8306.0	734.99	17.992	0.334	18.994	0.01	1
L80	7544.5	383.28	9956.6	869.55	0.4105	0.00762	0.4334	0.01	1
C90	7545.2	383.37	10465	904.28	0.0854	0.00159	0.0902	0.01	1
T95	7544.2	383.50	10924	947.30	0.0234	0.000436	0.0247	0.01	1
P110	7544.7	383.02	12762	1154.1	0.000300	0.00000557	0.000317	0.01	1

5.5   Comparison of RBD Level 5 with WSD

Using the ultimate failure event, the WSD and RBD level 5 resulted in the same tubing grade to be chosen due to limited available tubing grades (L80, C90, T95, P110). However, this may not always be the case. We want to evaluate how the RBD and WSD compares in relation to the minimum yield strength required. The goal of performing RBD as compared to WSD is to reduce the design cost by decreasing the yield strength of the tubing by quantifying the risk involved. The RBD reduce the chance of overdesigning as well as underdesigning the tubing compared to using conventional WSD. Overdesigning a tubing string results in part of the strength of the tubing not being utilized to withhold the load. By applying RBD, the hope is to be able to use more of the strength of the tubing grades that are available. In the following figure the WSD and QRA for the P110 string is shown. The figure shows that the WSD load limit in fact does not allow for any collapse probability at all as it is to the right of the distribution overlap defining the probability. This indicates that the WSD is more conservative than RBD as anticipated.
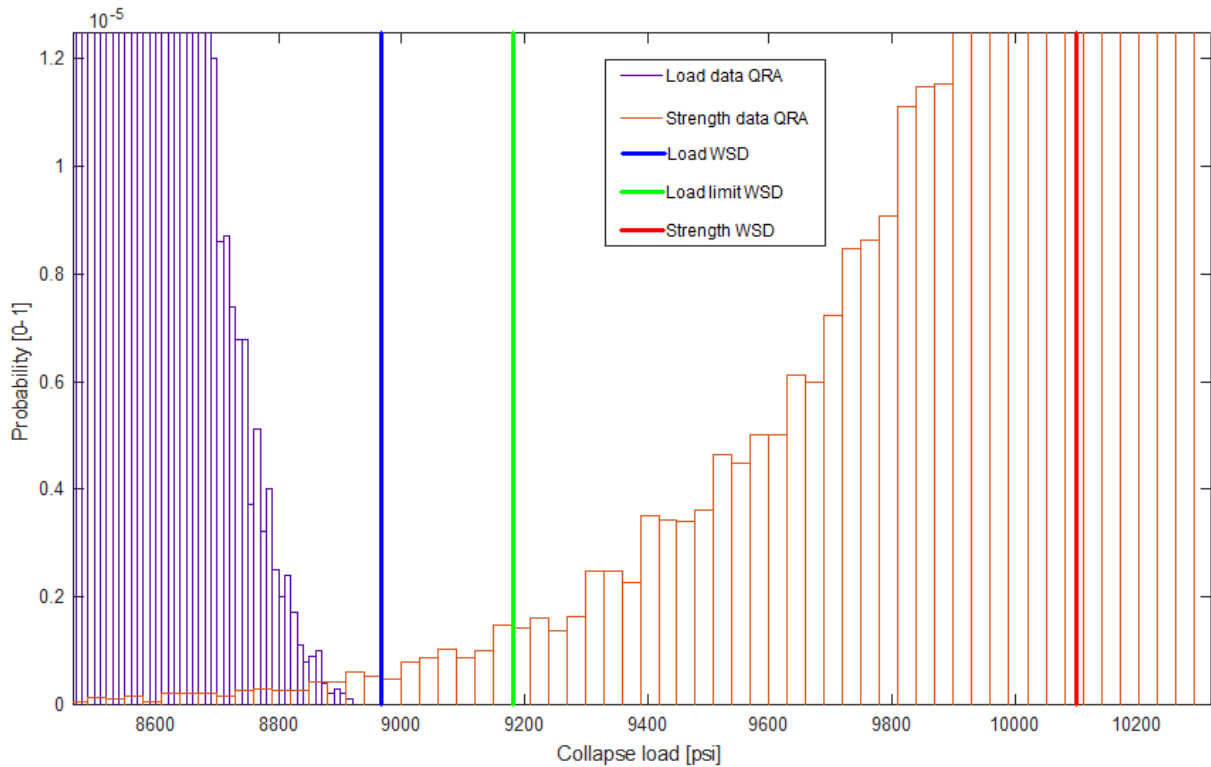
Figure 36 QRA and WDS compared for the P110 tubing grade

To quantify how much more conservative the WSD is compared to the QRA in respect to yield strength, the different tubing grade yield strengths considered up to now will be plotted against the load limit of the WSD and the collapse probability of the QRA for the tubing grades considered.

For the WSD, the minimum required collapse strength $\sigma_{strength} = 8865 psi$ previously calculated (by multiplying design factor DF=1.1 to the load) together with the collapse load limits of the tubing grades (strength divided by DF=1.1) will be plotted against the tubing yield strength. The intersection of an interpolation between different grades with the required collapse strength will give an approximate minimum yield strength required for the WSD, that is if the corresponding tubing grade was available.

$$\sigma_{y,min} = 95 + \left(\frac{110 - 95}{9181 - 8245}\right) \cdot (8965 - 8245) = 106.54 ksi$$
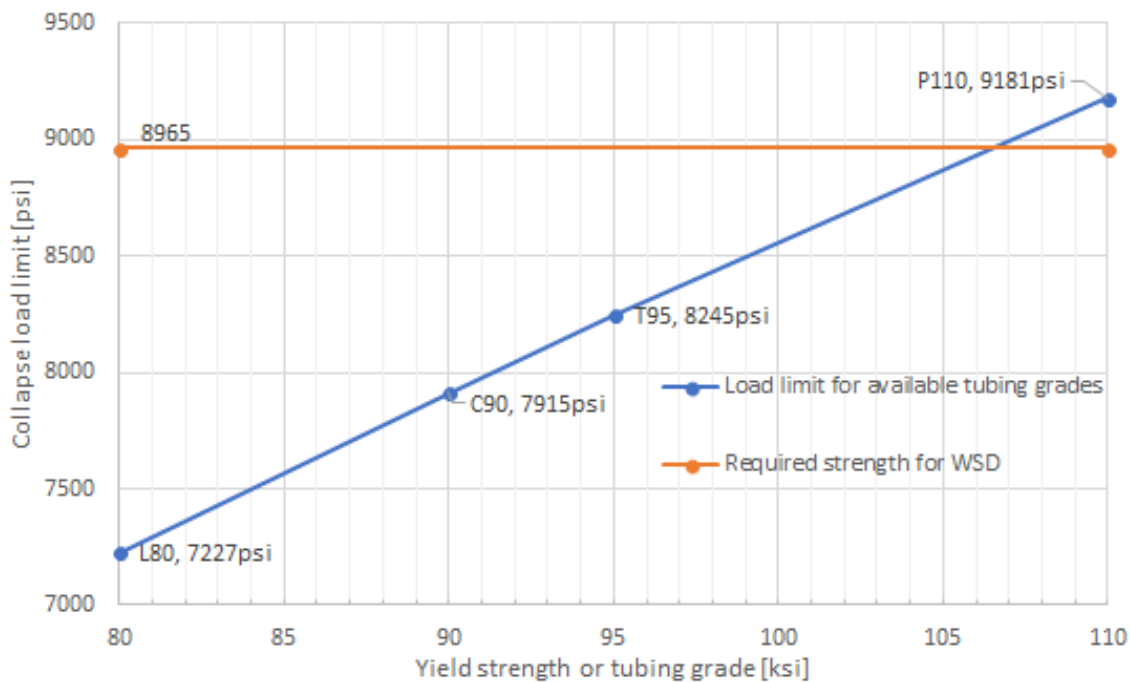
Figure 37 Load limit by WSD vs. Tubing grade

For the QRA considering ultimate failure event, the target probability was $P_t = 0.01\%$ and considering repair event it was $P_t = 1\%$. The collapse probability estimates will be plotted against the tubing yield strength. By using the intersection between the target probability and the interpolated collapse probability estimates on a logarithmic scale, an approximate minimum yield strength can be estimated for the QRA.
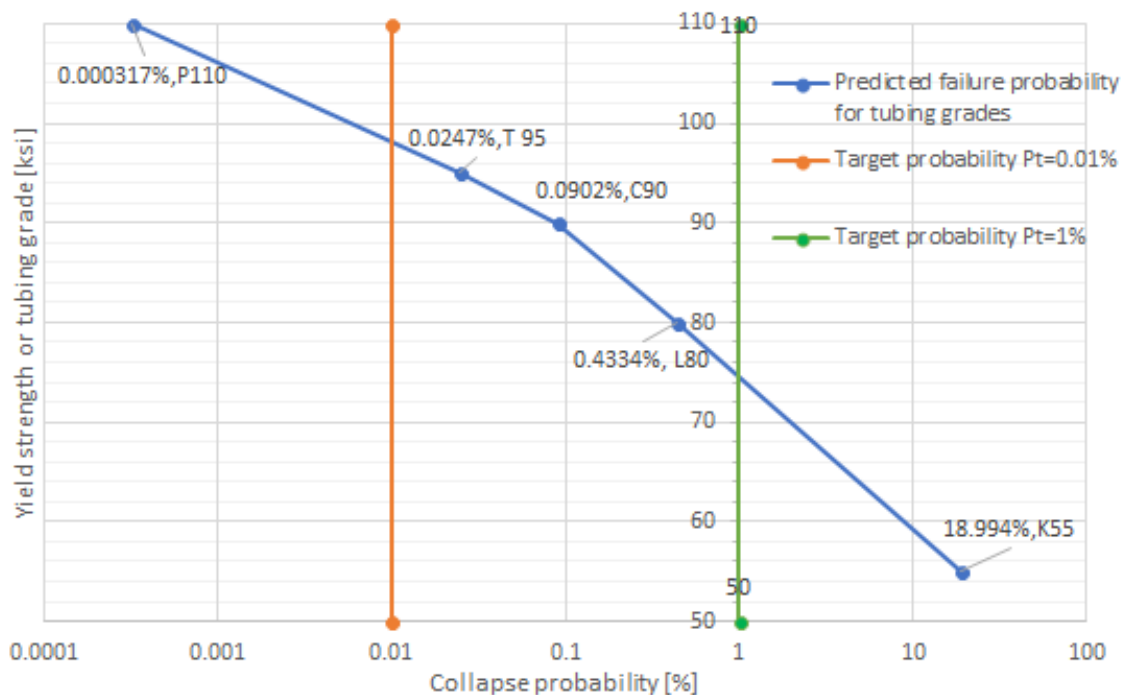
Figure 38 Tubing grade vs. Collapse probability by QRA

91

By using the point-intersection equation the intersection in the above figure for the ultimate failure event target probability $P_t = 0.01\%$ Can be found as following.

$$\sigma_{y,min} = 95 + \frac{110 - 95}{\log(0.000317) - \log(0.02470)} \cdot (\log(0.01) - \log(0.0247)) = 98.114 ksi$$

Similarly the intersection for the repair event target probability $P_t = 1\%$ can be found as following.

$$\sigma_{y,min} = 95 + \frac{80 - 55}{\log(0.4334) - \log(18.994)} \cdot (\log(1) - \log(18.994)) = 74.484 ksi$$

These estimates show that the minimum required yield strength is considerably higher for the WSD compared to the QRA. And that the repair event target probability results in the lowest required yield strength.

For the ultimate failure event, the RBD can reduce the required yield strength of the tubing by as much as $\frac{106.54 - 98.114}{106.54} \cdot 100\% = 7.91\%$ as compared to WSD. One may also say that WSD in this case overpredicts the required yield strength by as much as $\frac{106.54 - 98.114}{98.114} \cdot 100\% = 8.59\%$.

For the repair event, the RBD implementation reduces the required yield strength by as much as $\frac{106.54 - 74.484}{106.54} \cdot 100\% = 30.1\%$ as compared to WSD. One may also say that the WSD in this case overpredicts the required yield strength by as much as $\frac{106.54 - 74.484}{98.114} \cdot 100\% = 32.7\%$.

There are only a limited number of available tubing grades, meaning that the tubing will have to be overdesigned because of the lack of available yield strength. The full benefit of the QRA in RBD will therefore rarely be achieved, as is the case for this case study where the minimum required yield strength was lower for the RBD, although the nearest tubing grade upward was the same as for the WSD, that is the P110 tubing grade when considering the ultimate failure event. The comparison between WSD and RBD with the two different failure events are summarized in the table below.

Table 26 Comparison of required grade and minimum yield strength from WSD and RBD level 5 QRA

7inch, 32Ibs/ft Tubing	Minimum available tubing grade	Minimum required yield strength [psi]	Savings in minimum yield strength compared to WSD	Overpredicted minimum yield strength by WSD compared to RBD
WSD	P110	106.54	N/A	N/A
RBD, $P_t = 0.001\%$ Ultimate failure event	P110	98.114	7.91%	8.59%
RBD, $P_t = 1\%$ Repair event	L80	74.484	30.1%	32.7%

5.6 Assumptions made in case study

Assumptions and simplifications that were made in the case study are summarized in this section. Simplifications were made to simplify load calculation procedures and to direct focus towards the reliability-based design application.

The collapse load, being the differential pressure across the tubing wall are dependent on the external annular and the internal tubular pressure. The external pressure is made up from the hydrostatic annular pressure from the completion fluid and the APB.

The completion fluid gradient is assumed to be constant 1.2sg, the preferred density is often obtained by adding weight material, possibly barite or other substances. On one hand, hydrostatic pressure may over time be reduced due to settling of the weight material. This effect would decrease the collapse load. On the other hand, the increased fraction of clear fluid above the settled barite in the A annulus will lead to a larger temperature increase due to changes in thermophysical properties of the fluid and this will in turn lead to a larger APB, leading to larger collapse load. The compressibility, thermal expansion coefficient and heat conductivity of the completion fluid will change as weight material settles [20]. In addition, the increased pressure will also lead to geometrical changes of the different annuli which will reduce the APB. These considerations should be made when considering wells where the weight material has had time to settle in real-world applications, here more complex modelling will be required.

The case study also relies on a wellhead temperature assumed to have been previously predicted by an engineer with the corresponding uncertainty, however a simple model for a steady state tubing temperature profile solution was presented in section 2.7.1. The APB is dependent on the temperature profile in the tubing, assumed to be linear and the same as that in the A annulus. A more accurate temperature profile could be obtained by discretizing the tubing length and conducting heat loss calculations as in the proposed model. The temperature at the wellhead was assumed to have already been predicted and represented by a triangular distribution. At any point along the wellbore, the temperature decreases logarithmically from the tubing toward the formation [20], an assumption of having the same temperature in the annulus as in the tubing therefore become worse as we move further away from the center of the well. For a more accurate solution, a more complex temperature model is required to describe both the temperature along the tubing and in the radial direction towards the formation. This will involve heat exchange from the tubing towards the formation and will depend on how fluids, steel, cement etc. conduct heat. However, the temperature in the tubing will also depend on conduction, thereby on how fast the fluid is produced toward the surface. These considerations are especially important when considering annuluses further away from the center of the well, such as applications for the B and C annulus.

The internal pressure is made up from the hydrostatic pressure from the production fluid column and the frictional pressure drop along the tubing. The choke is assumed to be fully open yielding no pressure drop, the frictional pressure drop calculation and the hydrostatic pressure assumes a constant oil density along the tubing, in reality the mixture density may decrease upwards as gas may be released when the pressure drops. However, we assume a constant oil density and an oil fraction of one.

In tubular design, connections may pose a bottleneck for the tubing strength, that being burst, collapse or axial strength. Connection limitations along the tubing string was not considered in the case study for simplification.

6   Discussion and Conclusion

6.1   Discussion

In the case study, the *API Bulletin 5C3* collapse equations was used to predict collapse strength both deterministically and statistically from MCS. An attempt was made to show how the *API 5C3* and the *ISO/TR 10400* standards can be used in practice for reliability-based casing design. However, as shown by Adams, A.J. et.al. [17], these equations have an unacceptable spread in collapse probability predictions. The Tamano (1983) equations was shown to be the better choice for reliability-based design, it had the lowest COV and a near unity mean when plotted against actual collapse strength, providing the best fit to actual collapse strength [17]. In the case study we used an uncertainty distribution obtained from the *ISO/TR 10400* standard for the API collapse model, this distribution has a mean above one, such that it shifts the strength distribution to the right (higher) to fit the mean strength to experimental data. Such a distribution can also be obtained from this standard for the Tamano equations, therefore the near unity mean of the Tamano equation is of less importance for our application. However, the low COV of the Tamano collapse strength makes it a more accurate prediction of collapse strength and collapse probability. This is also reflected in the *ISO/TR 10400* standard where the COV of the Tamano model is set lower than that of the API model (using mean input parameters) for most of the datasets (se table 30 in Appendix A3). Fortunately for the API 1987 dataset used in the case study, the API equations (mean) has a slightly lower COV=0.066<0.078 compared to the Tamano (1983) equations, making the API equations the better choice. As the *ISO/TR 10400* also provides a model uncertainty for the Tamano equations, these equations can be used in a similar manner as we did with the API equations. Such an implementation would therefore generally in accordance with Adams, A.J. et.al. contribute to a lower strength distribution spread and collapse probability than with the API equations, and possibly even a lower required yield strength for the tubing.

A number of N=1000000 sampling iterations for MCS was used in the case study, giving a COV of the predicted collapse probability of $COV = 0.0185725$. The higher this number is, the less the spread of the predicted collapse probability becomes. Tree standard deviations above the mean of the predicted probability was used. By using more sampling iteration in the MCS the uncertainty in the prediction would be reduced, giving a slightly lower collapse probability to be compared with the target probability, thereby reducing the required yield strength slightly. When trying to apply N=100000 sampling iterations, the probability prediction COV was

considerably higher. The number of iterations should be adjusted to obtain whatever COV in probability estimates that is considered acceptable.

Choice of appropriate target probability should be based on the cost and consequence of failure considered in reliability-based design approaches. Different proposals and guidelines from literature for selection of target probability were presented in this study. The consequence of failure depends on if the failure event is considered a repair event or an ultimate failure/blowout event, with a higher target probability being acceptable for a repair event. When choosing a guideline for selection of target probability one can consider if the load is a survival load or a service load, as a survival load design only is made for survival, whilst a service load is made for full operability whilst or after the load occurs. The guideline given in table 14 is for survival type loads specifically. However, "*it is not common practice to distinguish between operating and survival loads in tubular design*" [38].

The case study considers a vertical HPHT land well for simplicity. No bleed-off valves at the wellhead is considered for the design, such that the tubing is designed to withstand the full annular pressure after APB in the A annulus. In a real-world application, a land well or an offshore well with dry wellhead will have annular pressure relief valves at the wellhead, such that annular pressure can be monitored and controlled by injection and bleed-off. Even Subsea wells has the requirement of access to the A annulus. The NORSOK D-010 standard states as following.

"For dry wellheads, there shall be access ports to all annuli to facilitate monitoring of annuli pressures and injection/bleed-off of fluids"[1]."For subsea wellheads, there shall be access to the casing by tubing annulus to facilitate monitoring of annulus pressure and injection /bleed-off of fluids" [1].

These requirements of the NORSOK standard implies that such a design made in the case study would not be relevant on the NCS because it would not be permitted and hence the tubing would not have to be designed for a full pressure buildup when pressure relief valves would be implemented in the design. However, in other parts of the world or in older wells, the application may still be relevant, one should in any case allow for APB up to a certain level before the bleed off is made. For a subsea well, the B annulus outside the production casing has no access requirement from the NORSOK standard. The approach made in this case study could therefore be implemented for an APB collapse load on the production and intermediate casing in a subsea well. In addition, one should also consider the burst loads that are occurring.

6.2 Conclusion

This case study attempts to implement reliability-based design on a 7inch 32Lbs/ft production tubing string subjected to APB collapse load, at the same time it is used to compare the outcome to that of a corresponding working stress design analysis. The case study shows that savings in cost or materials can be accomplished by using a higher level of RBD as compared to WSD as well as compared to a lower level of RBD. By applying two different target probability of collapse, the importance of selecting an appropriate target probability was demonstrated. Large savings can be made by increasing the target probability. The reliability-based design approach provides flexibility in choosing a failure target probability that fits the consequences of a failure with the load scenario, making the well design more fit for purpose. In addition, one is able to quantify the risk. On the contrary, the WSD operates with design factors that are the same all over and does not provide insight into how far a certain load actually is from exceeding the strength. WSD is conservative in nature and has as main principle to be on the safe side. It is also simpler to use. However, one should not conclude that reliability-based design is less conservative than WSD for all cases. That depends on the scenario and the chosen acceptance criteria. This study also implements a sensitivity analysis on the collapse load and strength distribution to evaluate what input parameters has the biggest effect on variability of the distributions and therefore also in turn the collapse probability represented by the load and strength distribution overlap.

Interpolation between tubing grades applied in this particular design and base-case imply that RBD level 5 can reduce the required yield strength of the production tubing by as much as 7.9% for a ultimate failure event design and 30.1% for a repair event design, depending on available grades. With the available grades for the selected tubing in this design, the WSD and RBD level 5, with ultimate failure event considered, resulted in the P110 tubing grade being preferred. For the RBD level 5 with repair event considered, the L80 tubing grade was acceptable. Note that the ultimate failure event uses a lower target probability than the repair event because the consequence is higher for ultimate failure than repair. The study also reveals that in our case the RBD level 4 predict a collapse probability of 53.6 times that of the RBD level 5 when considering the ultimate failure event. For ultimate failure event, the P110 tubing grade considered was acceptable when using the RBD level 5 but would not be acceptable by using RBD level 4, although it would be acceptable by using WSD. In our case this leads to the RBD

level 4 being more conservative than the conventional WSD, a Q125 tubing grade would possibly be sufficient for RBD level 4.

Sensitivity analysis show that the uncertainty in the API 5C3 collapse model, the wall thickness, the yield strength and outer diameter has the biggest impact on the spread of the collapse strength distribution in decreasing order. The load distribution spread is a result of uncertainty in the wellhead temperature prediction and the annular pressure buildup model that are represented by triangular distributions. Focus on reducing the uncertainty in the input parameters that has the highest impact on load and strength uncertainty provides an efficient approach to reduce the predicted collapse probability of different designs, such that cost, or material savings can be made.

6.3 Further work on Reliability-Based Design application

This study focuses on the application of reliability-based design on tubular collapse mode. The case study was restricted to a fictitious well with a specific tubing of varied yield strength. The spread of the input distributions determined the spread of the output load and strength distributions and therefore in turn the collapse probability. In the case study, the WSD was shown to be more conservative as compared to RBD level 5. Emphasis was put on the possibility of reducing the required yield strength or tubing grade by applying RBD. The spread of the load distribution was considerably less than that of the strength for this case study. If the spread of the load distribution was higher, then the failure probability would increase for the same yield strength or tubing grade considered. If the load or strength spread was increased, at one point the RBD level 5 would require a higher tubing grade than the WSD as the failure probability would increase, thus WSD would become less conservative in comparison when applying the same design factor. This is where the risk of under-design by applying WSD sets in. Although WSD being generally more conservative, when load and strength is determined deterministically by WSD, both under-design and over-design is possible as the failure probability is not known. The RBD Level 4 was in fact more conservative than the WSD as it did allow for a P110 tubing grade. Casing and tubing failure account for most of the failures associated with wells with well integrity issues. Part of the reason for the high frequency of these failures is the traditional design approach of working stress design. The lack of ability to predict failure probability of the particular design considered poses risk of under-design. A study should be conducted where risk of under-design by WSD is investigated in greater detail.

The *NORSOK D-010* standard does not require access to the B and C annulus in subsea wells, and because the ABP therefore cannot always be bled off from the wellhead, a more rigorous study should be made where APB is considered in the B and C annulus. An advanced temperature model should be implemented where the temperature varies both along the tubing towards the wellhead and radially across the annular spaces and casing towards the formation/cement interface. Additionally, flexibility in the well configuration should be considered contrary to the rigid single string analysis made in our case study. Halal, A.S. and Mitchell. R.F (1994) [23]. developed a complex model for APB considering flexibility in a multiple casing string configuration that could be utilized.

This case study only considers the reliability of the production tubing in an APB collapse mode, to consider the full well integrity reliability, all well barrier elements in the well barriers need to be considered for RBD. As noted earlier, if only one well barrier element fails, the well barrier itself fails. The production tubing considered in the case study in only one of the barrier elements in the primary well barrier. A study should be made where a model for reliability of both the primary and secondary well barrier is developed, considering APB in multiple annuluses.

References

1. Standards Norway, *Well integrity in drilling and well operations*, NORSOK D-010, Rev. 4, 2013, Lysaker, Norway.

2. Bellarby, J., *Well Completion Design*. 2009, Aberdeen, UK: Elsevier.

3. Bratvold, R.B., Beggs, S., *Making Good Decisions*. 2010, Richardson, Texas, USA: Society of Petroleum Engineers.

4. Vignes, B., *Contribution to well integrity and increased focus on well barriers from a life cycle aspect*. 2012, Stavanger, Norway: University of Stavanger.

5. Aadnoy, B.S., *Modern Well Design*. 2010, Leiden, The Netherlands: CRS Press/Balkema.

6. Rahman, S.S., Chillingarian, G.V., *Casing design theory and practice*. 1995, Amsterdam, The Netherlands: Elsevier.

7. Julian, J.Y., Cahalane, T.W., Cismoski, D.A., *Rigless Tubing Repair Using Permanent and Retrievable Patches at Prudhoe Bay.* Paper SPE-104055 presented at the International Oil Conference and Exhibition, Cancun, Mexico, 31 August - 2 September, 2006.

8. Aadnoy, B.S., Cooper,I., Miska, S.Z., Mitchell, R.F., Payne, M.L., *Advanced Drilling and Well Technology*. 2009, Richardson, Texas, USA: Society of Petroleum Engineers.

9. Agonafir, M.B., *Material testing and material properties determination*. 2017, University of Stavanger, Compendium.

10. American Petroleum Institute., *Bulletin on Formulas and Calculations for Casing, Tubing, Drill Pipe, and Line Pipe Properties,* API BULLETIN 5C3, Sixth edition, 1994, Washington, D.C., USA.

11. Agonafir, M.B., *Theoretical bases for tubing design calculations*. 2017, University of Stavanger, Compendium.

12. ISO, *Petroleum and natural gas industries-Equations and calculations for the properties of casing, tubing, drill pipe and line pipe used as casing or tubing*, ISO/TR 10400, First edition, 2007, Geneva, Switzerland.

13. ANSI/API Technical Report 5C3 / ISO 10400, 2007, *Technical Report on Equations and Calculations for Casing, Tubing, and Line Pipe Used as Casing or Tubing; Performance Properties Tables for Casing and Tubing*, Annex M, Addendum. October 2015, API: Washington, DC, USA.

14. Aadnoy, B.S., Looyeh, R., *Petroleum Rock Mechanics: Drilling Operations and Well Design*. 2010, The Boulevard, Langford Lane, Oxford, UK: Elsevier.

15. Aadnoy, B.S., Larsen, K., Berg, P.C., *Analysis of stuck pipe in deviated boreholes.* Journal of Petroleum and Science & Engineering, 2003. 37: p. 195-212.

16. Aasen J.A., O., T.D., Aadnøy B.S, *Revitalized Three-Dimensional Design Method Improves Tubular Design.* Paper SPE-188605-MS presented at the Abu Dhabi International Petroleum Exhibition & Conference, Abu Dhabi, UAE, 13-16 November, 2017.

17. Adams, A.J., Warren, A. V. R., Masson, P.C., *On the Development of Reliability-Based Design Rules for Casing Collapse.* Paper SPE 48331 presented at the SPE Applied Technology Workshop on Risk Based Design of Well Casing and Tubing, The Woodlands, Texas, USA, 7-8 May, 1998.

18. Moe, B., Erpelding, P., *Annular pressure buildup: What it is an what to do with it.* World Oil Deepwater Technology Supplement, 2000. August 2000: p. 21-23.

19. Willhite, G.P., *Over-all Heat Transfer Coefficients in Steam And Hot Water Injection Wells.* Journal of Petroleum Technology, JPT., 1967. 19(5): p. 607-615.

20. Udegbunam, J.E., Sui, D., Moeinikia, F., Lage, A.C.V.M, Fjelde, K.K, Arild, Ø. Rabenjafimanantsoa, H.A, Nygaard, G.H, *A Transient Flow Model for Predicting Pressure Buildup in Closed Annuli.* Paper presented at the 36th International Conference on Ocean, Offshore and Arctic Engineering OMAE2017, Trondheim, Norway, 25-30 June 2017.

21. *Petroleum Engineering Handbook*, ed. R.F. Mitchell. 2006, Richardson, Texas, USA: Society of Petroleum Engineers

22. Alcofra, E.L.M., Lage, A.C.V.M., *Annular Pressure Build-up in Oil Wells* Paper presented at the 15th Brazilian Congress of Thermal Sciences and Engineering, Belem, PA, Brazil, 10-13 November, 2014.

23. Halal, A.S., Michell, R.F., *Casing Design for Trapped Annular Pressure Buildup.* SPE Drilling & Completions, 1994.

24. Agonafir, M.B., *Advanced Drilling Engineering and Technology*. 2017, University of Stavanger, Compendium.

25. Moody, L.F., *Friction Factors for Pipe Flow.* Transactions of The A.S.M.E, 1944. 66(8): p. 671–684.

26. Morley, C.K., Guerin, G. , *Comparison of gravity-driven deformation styles and behavior associated with mobile shales and salt* Tectonics, 1996. 15(6): p. 1154-1170.

27. Willson, S.M., Fossum, A.F, Fredrich, J.T, *Assessment of Salt Loading on Well Casings.* Paper presented at the IADC/SPE Drilling Conference, Dallas,Texas, 26–28 February, 2002.

28. Mitchell, R.F., Miska, S.Z., *Fundamentals of Drilling Engineering*. 2011, Richardson, Texas, USA: Society of Petroleum Engineers.

29. Aadnoy, B.S., Aasen J.A., Pollard M. , *Casing Design – Review of Design Methodology*. 2003, Petil.

30. Adams, A.J., Parfitt, S.H.L., Reeves, T.B., Thorogood, J.L., *Casing System Risk Analysis Using Structural Reliability.* Paper SPE/IADC 25693, presented at the SPE/IACD Drilling Conference, Amsterdam, Netherlands, 23-25 February, 1993.

31. Moore, D.F., Mc.Cabe,G.P., Craig,B.A., *Introduction to the Practice of Statistics*. 2014, New York, USA: W. H. Freeman and Company.

32. Fjelde, K.K., *Monte Carlo Simulations and Applications*. University of Stavanger, Compendium

33. Weisstein, E.W. *Dice*. 2018 [cited 2018, 29 May]; From MathWorld--A Wolfram Web Resource. http://mathworld.wolfram.com/Dice.html

34. Das, B., Samuel, R., *A Model for Well Reliability Analysis throughout the Life of the Well Using Barrier Engineering and Performance.* Paper SPE/IACD-173055-MS presented at the SPE/IADC Drilling Conference and Exhibition held in London, UK, 17-19 March, 2015.

35. Williamson, H.S., Sawaryn, S.J, Morrison, J.W., *Monte Carlo Techniques Applied to Well Forecasting: Some Pitfalls.* Paper SPE 89984 presented at the SPE annual Technical Conference and Exhibition, Houston, Texas, USA, 26-29 September 2006.

36. *Drilling Data Handbook.* 1999, Paris: Èditions Technip.

37. Brand, P.R., Whitney, W.S., Lewis, D.B., *Load and Resistance Factor Design Case Histories.* Paper presented at the 27th Annual OTC, Houston, Texas, USA, 1-4 May, 1995.

38. Suryanarayana, P.V., Lewis, D.B., *A Reliability-Based Approach for Survival Design in Deepwater and High Pressure/High Temperature Wells.* Paper IADC/SPE-178907-MS presented at the IACD/SPE Drilling Conference and Exhibition, Fort Worth, Texas, USA, 1-3 March, 2016.

39. Clinedinst, W.O., *A rational expression for Critical Collapse Pressure of Pipe Under External Pressure.* API Drilling and Production Practice, 1939: p. 383-391.

40. Clinedinst, W.O., *Analysis of collapse test data and development of new collapse resistance formulas.* Report to the API Task Group on Performance Properties, 1977.

41. Freedman, D., *On the histogram as a density estimator: L2 theory.* Probability Theory and Related Fields, 1981. 57(4): p. 453–476.

42. Pukelsheim, F., *The Three Sigma Rule.* American Statistician, 1994. 48: p. 88-91.

Appendix

A1   MATLAB Code for Monte Carlo simulation

Script for WSD collapse load and strength used on tubing with APB in the A annulus

```matlab
%    Collapse model (API 5C3) for Tubing with APB in A annulus
%
%            Script for WSD and plotting of results
%
%This script incorporates WSD of APB collapse load on
%production tubing in a well.

%Author: Erling Bjørndal
%Date: 25.04.2018
clc
clear
%Input parameters
YS0=110000 %psi

OD=7;%inch
ID=6.094
t=0.453;%inch
steelcrossection=9.32; %inch^2
Nweght=32; %Nominal weight Ibs/ft

alfa=3*10^-4;  %Thermal expansivity of packer fluid %Modern well design
p.127 [1/Celsius]
c=3*10^-5;     %Fluid compressibility of packer fluid [1/bar]
packerdensity=1.2; %packer fluid density in sg
packerdepth=5000; %5000m Assuming at entry of reservoir
avdepth=packerdepth/2; %from WH
waterdensity=1.01;% sg
oildensity=0.7; %sg
Q=1600%m^3/day
A=(pi/4)*(ID*0.0254)^2%SQUARE METER
v=(Q/86400)/A %m/s

%WSD Load

%Fixed input parameters we use SI units in calculation
resdepth=5000;  %meter %Planned TD (from WH) of the last section, packer
depth
seawaterdepth=0%500;    %meter

%Input Distributions %If we want it
%rp=trianglerand(rp-0.05,rp,rp+0.05,1);%triangle distribution for res-
pressure

twh=90; %Wellstream temperature at WH (assumed to be known)
seabedtemp=15; % if landwell use 15 as seabedtemp
tgrad=0.03; %geothermal gradient Celsius pr.m
tres=resdepth*tgrad+seabedtemp;%reservoir temperature at crest (assumed to
be known)(0.03*5000m)
tresf=(8/5)*tres+32 %in Fahrenheit
```

```matlab
YS1=YS0-(0.03/100)*YS0*(tresf-70)%73784%80000;%psi derated by 0.03%pr.F from
70F


alfa=3*10^-4;   %Thermal expansivity of packer fluid %Modern well design
p.127 [1/Celsius]
c=3*10^-5;      %Fluid compressibility of packer fluid [1/bar]


avdepth=packerdepth/2; %from WH
waterdensity=1.01;% sg
oildensity=0.7; %sg



%Code for average annular pressure
    T1=seabedtemp;%seabed temperature (at WH)
    T2=tres-tgrad*(resdepth-packerdepth);%formation temperature (at prod.
packer)% Correcting for possible distance between packer and reservoir
    T3=twh;%wellhead temperature
    T4=tres-(resdepth-packerdepth)*((tres-twh)/(resdepth)); %wellflow
temperature at prod packer

    deltat=((T3+T4)/2)-((T1+T2)/2);%TEMPERATURE INCREASE AT AVERAGE ANNULAR
DEPTH

    tgeo=tgrad*avdepth+seabedtemp;
    avt=tgeo+deltat; %average annular temperature after APB

    deltap=(alfa*deltat)/c %APB in bar

    pform=packerdensity*resdepth*0.0981%+seawaterdepth*waterdensity*0.0981;
%Initial hydrostatic pressure in annulus
    apress=(pform+deltap)*14.5037738%convert to psi % annular pressure at
packer depth after APB based on average annular temperature

%Code for tubular pressure at packer
    f=0.0178/4;%Manually read from Moody diagram 0.0178
    pfric=4*f*(resdepth/(ID*0.0254))*oildensity*1000*(v^2/2)*10^-5%bar

ptube=((oildensity*resdepth*0.0981)+pfric)*14.5037738%psi%frictionp+chokep
%Choke assumed open to get minimum pressure ie.chokep=0 ; %convert from bar
to psi;
%Load calculation
    load=apress-ptube %psi



%WSD Strength

%Combined loading equivalent grade
astress=0
YS=(sqrt(1-0.75*((astress+ptube)/YS1)^2)-0.5*(astress+ptube)/YS1)*YS1
%Taking account for inner pressure (no axial stress considered here,
astress=0)

%Code for collapse strength API5C3 IN USC UNITS
    A=2.8762+0.10679*(10)^(-5)*YS+0.2131*(10)^(-10)*YS^2-0.53132*(10)^(-
16)*YS^3
    B=0.026233+0.50609*(10)^(-6)*YS
    C=-465.93+0.030867*YS-0.10483*(10)^(-7)*YS^2+0.36989*(10)^(-13)*YS^3
```

```matlab
    F=(46.95*10^6*((3*B/A)/(2+B/A))^3)/(YS*((3*B/A)/(2+B/A)-B/A)*(1-
(3*B/A)/(2+B/A))^2)
    G=F*B/A
 %If statement for different regions of collapse
    if (OD/t)<((sqrt((A-2)^2+8*(B+(C/YS))+(A-2))/(2*(B+(C/YS)))))
        strength=2*YS*(((OD/t)-1)/((OD/t)^2));
        disp('yield')
    elseif (OD/t)<((YS*(A-F))/(C+YS*(B-G)))
        strength=(YS*((A/(OD/t))-B)-C);
        disp('plastic')
    elseif (OD/t)<(2+(B/A))/(3*(B/A))
        strength=YS*((F/(OD/t))-G);
        disp('transitional')
    else
        strength=((46.95*10^6)/((OD/t)*((OD/t)-1)^2));
        disp('elastic')
    end
strength=strength %without inner pressure correction
%strength=strength0%+(1-2*(t/OD))*ptube %Outdated inner pressure correction

SF=1.1;
margin=strength*(1/1.1);
%Plotting
%     x range              y range
%plotting strength
p1=plot([strength,strength],[1,0],'r','linewidth',2);
hold on  %plotting safety margin for collapse SF=1.1
p2=plot([margin,margin],[1,0],'g','linewidth',2);
hold on%plotting load
p3=plot([load,load],[1,0],'b','linewidth',2);
hold on

axis([0*10^4,2*10^4,0,1])
legend([p1,p2,p3],'Strength','Load limit','Load');
xlabel('Collapse load [psi]')
ylabel('Probability [0-1]')
```

Function for QRA collapse load and strength used on tubing with APB in the A annulus

```
funcion[strength1,load1]=QRATESTP()
%
%    Collapse model (API 5C3) for Tubing with APB in A annulus
%
%
%This function calculates APB collapse load and tubing strength of the
%production tubing in a well.

%Author: Erling Bjørndal
%Date: 25.04.2018
clc
clear
%Input parameters
YS0=110000 %psi
OD0=7;%inch nominal diameter
ID0=6.094%inch nominal inner diameter
t0=0.453;%inch wall thickness
steelcrossection=9.32; %inch^2 steel cross section
Nweght=32; %ibs/ft Nominal weight

resdepth=5000;  %meter %Planned TD (from WH) of the last section, packer
depth
twh=90; %Wellstream temperature at WH (assumed to be already predicted)
seabedtemp=15; % Ambient temperature (4celcuis at seabed or 15celcius on
land)
tgrad=0.03; %Geothermal gradient Celsius pr.m
tres=resdepth*tgrad+seabedtemp;%Reservoir temperature at crest (assumed to
be known)(0.03C/m*5000m+15C)
tresf=(9/5)*tres+32; %in Farenheit

%Mean input parameters
YS1=YS0*1.147;    %Yeald strength of casing in psi (Mean value see table F3
in ISO/TR 10400)
OD=OD0*1.0058;    %Outer diameter in inches (Mean value see table F4 in
ISO/TR 10400)
t=t0*1.0058;     %Average casing wall thickness DDH in inches (Mean value see
table F4 in ISO/TR 10400)
ID=OD-t
tubelength=5000*(1/0.3048); %ft of production tubing (possibly longer than
packerdepth but approximate)
steelcrossection=9.32; %inch^2 Steel cross section

%Temperature deration of yield strength
YS=YS1-(0.03/100)*YS1*(tresf-70)%73784%80000;%psi derated by 0.03% pr.F from
70F

alfa=3*10^-4;  %Thermal expansivity of packer fluid %Modern well design
p.127 [1/Celsius]
c=3*10^-5;      %Fluid compressibility of packer fluid [1/bar]
packerdensity=1.2; %Packer fluid density in sg
packerdepth=5000; %5000m assuming at entry of reservoir
avdepth=packerdepth/2; %from WH, mid depth along tubing string
waterdensity=1.01;% sg
oildensity=0.7; %sg

%Friction loss input
```

```matlab
Q=1600%m^3/day Production rate
A=(pi/4)*(ID*0.0254)^2 %SQUARE METER Inner cross section of tubing
v=(Q/86400)/A %m/s Production velocity in tubing

%Fixed input parameters, we use SI units in calculation
resdepth=5000;  %meter %Planned TD (from WH) of the last section, packer
depth
seawaterdepth=0 %meter

%Input Distributions (load)
twh=trianglerand(70,80,90,1);%90% triangular distribution
apbuncertainty=trianglerand(0.7,0.85,1,1);%1% triangular distribution

%Input Distributions (strength)
%standard deviation of input means variables = COV*MEAN (COV FOUND IN TABLES
IN ISO APENDIX F)
SDYS=(0.0373*YS);
SDOD=(0.00125*OD);
SDt=(0.0264*t);
%Input Distributions (BECAUSE WE KNOW STANDARD DEVIATION WE USE NORMAL
DISTRIBUTON)
YS=normrnd(YS,SDYS);%norminv(0.95,YS,SDYS)%YS%+0.01*YS%
OD=normrnd(OD,SDOD);%OD%+0.01*OD%
t=normrnd(t,SDt);%t%+0.01*t%
ID=OD-t %inch Inner diameter (still random)
APIuncertainty=normrnd(1.158,0.076428);%1.158%norminv(0.95,1.158,0.076428)%1
.158%+0.01*1.158%

%QRA Load

%Code for average annular pressure
    T1=seabedtemp;%seabed temperature or surface ambient temperature (at WH)
    T2=tres-tgrad*(resdepth-packerdepth);%formation temperature (at prod.
packer)%correcting for possible tailpipe length
    T3=twh;%wellhead temperature
    T4=tres-(resdepth-packerdepth)*((tres-twh)/(resdepth)); %wellflow
temperature at prod packer

    deltat=((T3+T4)/2)-((T1+T2)/2);%TEMPERATURE INCREASE AT AVERAGE ANNULAR
DEPTH

    tgeo=tgrad*avdepth+seabedtemp;
    avt=tgeo+deltat; %Average annular temperature after APB

    deltap=(alfa*deltat)/c; %APB in bar
    deltap=deltap*apbuncertainty; %Implement uncertainty in APB model

    pform=packerdensity*resdepth*0.0981%+seawaterdepth*waterdensity*0.0981;
%initial hydrostatic pressure in annulus
    apress=(pform+deltap)*14.5037738%convert to psi % Annular pressure at
packer depth after APB based on average annular temperature

%Code for tubular pressure at packer
    f=0.0178/4;%Manually read from moody diagram 0.0178 Moody friction
factor
    pfric=4*f*(resdepth/(ID*0.0254))*oildensity*1000*(v^2/2)*10^-5%bar
%Frictional pressure drop
```

V

```matlab
    ptube=((oildensity*resdepth*0.0981)+pfric)*14.5037738%psi%+choke
pressure %Choke assumed open to get minimum pressure ie.chokep=0 ; %convert
from bar to psi;
%Load calculation
    load1=apress-ptube %psi




%QRA Strength
astress=0;
YS=(sqrt(1-0.75*((astress+ptube)/YS)^2)-0.5*(astress+ptube)/YS)*YS;
%Multiple load correction, axial and inner pressure

%Code for collapse strength API5C3 IN USC UNITS
    A=2.8762+0.10679*(10)^(-5)*YS+0.2131*(10)^(-10)*YS^2-0.53132*(10)^(-
16)*YS^3
    B=0.026233+0.50609*(10)^(-6)*YS
    C=-465.93+0.030867*YS-0.10483*(10)^(-7)*YS^2+0.36989*(10)^(-13)*YS^3


    F=(46.95*10^6*((3*B/A)/(2+B/A))^3)/(YS*((3*B/A)/(2+B/A)-B/A)*(1-
(3*B/A)/(2+B/A))^2)
    G=F*B/A
 %If statement for different regions of collapse
    if (OD/t)<((sqrt((A-2)^2+8*(B+(C/YS))+(A-2))/(2*(B+(C/YS))))))
        strength=2*YS*(((OD/t)-1)/((OD/t)^2));
        disp('yield')
    elseif (OD/t)<((YS*(A-F))/(C+YS*(B-G)))
        strength=(YS*((A/(OD/t))-B)-C);
        disp('plastic')
    elseif (OD/t)<(2+(B/A))/(3*(B/A))
        strength=YS*((F/(OD/t))-G);
        disp('transitional')
    else
        strength=((46.95*10^6)/((OD/t)*((OD/t)-1)^2));
        disp('elastic')
    end
strength0=strength %With multiple load correction (internal pressure and
axial load)
%strength1=strength+(1-2*(t/OD))*ptube %Outdated internal pressure
correction
strength1=strength0*APIuncertainty %Implement API model uncertainty


end
```

Monte Carlo Simulation script

```
%                    Monte Carlo Simulation
%
%          Script for MCS and plotting of results
%
%This script incorporates MCS in QRA of APB collapse load on
%production tubing in a well. The script calls the function
%QRATESTP for load and strength distribution sampling, calculates
%collapse probability and plots load and strength output distributions
%
%Author: Erling Bjørndal
%Date: 16.04.2018
clc
clear
N=1000000; %Number of MCS (CHANGE UNTIL CONVERTION)

%Defining outputs
load=zeros(1,N);   %Average annular pressure (based on average annular
temperature)
strength=zeros(1,N); %Collapse strength and casing

counter=0; %Variable used to calculate failure probability, count if
(collapseload>collapsestrength)

%MCS LOOP  %Samples input distributions from QRATESTP

for j=1:N  %Monte Carlo loop

   [strength1,load1]=QRATESTP();%Change as required YS in QRATESTP
   strength(1,j)=strength1;
   load(1,j)=load1;


   if(load(1,j)>strength(1,j))
   counter=counter+1; %Used for predicting probability of collapse
   end

end % End of MCS loop

%Mean and std of load
loadmean=mean(load(1,:))
loadstd=std(load(1,:))

%Mean and std of strength
strengthmean=mean(strength(1,:))
strengthstd=std(strength(1,:))

prob=counter/N*100 %PERCENTAGE FOR HAVING LOAD PRESSURE > STRENGTH


% Plot probability density functions
e=min(strength(1,:));
f=max(strength(1,:));
%sbins=(f-e)
sbins=100;
s=[e:1:f];
```

```matlab
[c,d]=hist(strength(1,:),s);

h=min(load(1,:));
f=max(load(1,:));
%lbins=(f-h)
lbins=100;
w=[h:1:f];
[a,b]=hist(load(1,:),w);

%plot(b,a/N,d,c/N);
s=histfit(strength,sbins,'normal')%Fitting histogram for strength
hold on
l=histfit(load,lbins,'normal'); %Fitting histogram for load

hold on
legend('Load','Strength')
xlabel('Pressure (psi)')
ylabel('PDF')

%The Distribution fitting tool can alternatively load the strength and
%load output data and plot PDF and CDF with fitted normal distributions with
corresponding mean and standard deviations.
```

Function for random sampling triangular distributions

```matlab
function f = trianglerand(xstart,mostlik,xstop,N)
% TRIANGLERAND Random numbers from a triangle distribution.
%    R = trianglerand(min,mostlikely,max,N) returns a vector of N draws from a
%    triangular distribution starting at min, maxpoint at mostlikely and endpoint at max.
%
%    Copyright 2003 RF - Rogaland Research
%    Author: Øystein Arild

a = mostlik-xstart;
b = xstop-xstart;

h1 = 2/a;
m1 = h1/a;



A1 = a/b;
p = A1;



f_ = (rand(N,1) < p);
ind1 = find(f_==1);
ind2 = find(f_==0);
N1 = length(ind1);

if (a == b)
  u = rand(N,1);
  f = sqrt(2*m1*u)/m1;
else
  u = rand(N1,1);
  f1 = sqrt(2*m1*u)/m1;

  h2 = 2/(b-a);
  m2 = -h2/(b-a);
  beq=h2;
  u = rand(N-N1,1);
  f2 = a+(-beq+sqrt(beq*beq+2*m2*u))/m2;
  f(ind1) = f1;
  f(ind2) = f2;
  f = f';
end

f = f + xstart;
```

A2 Moody Chart
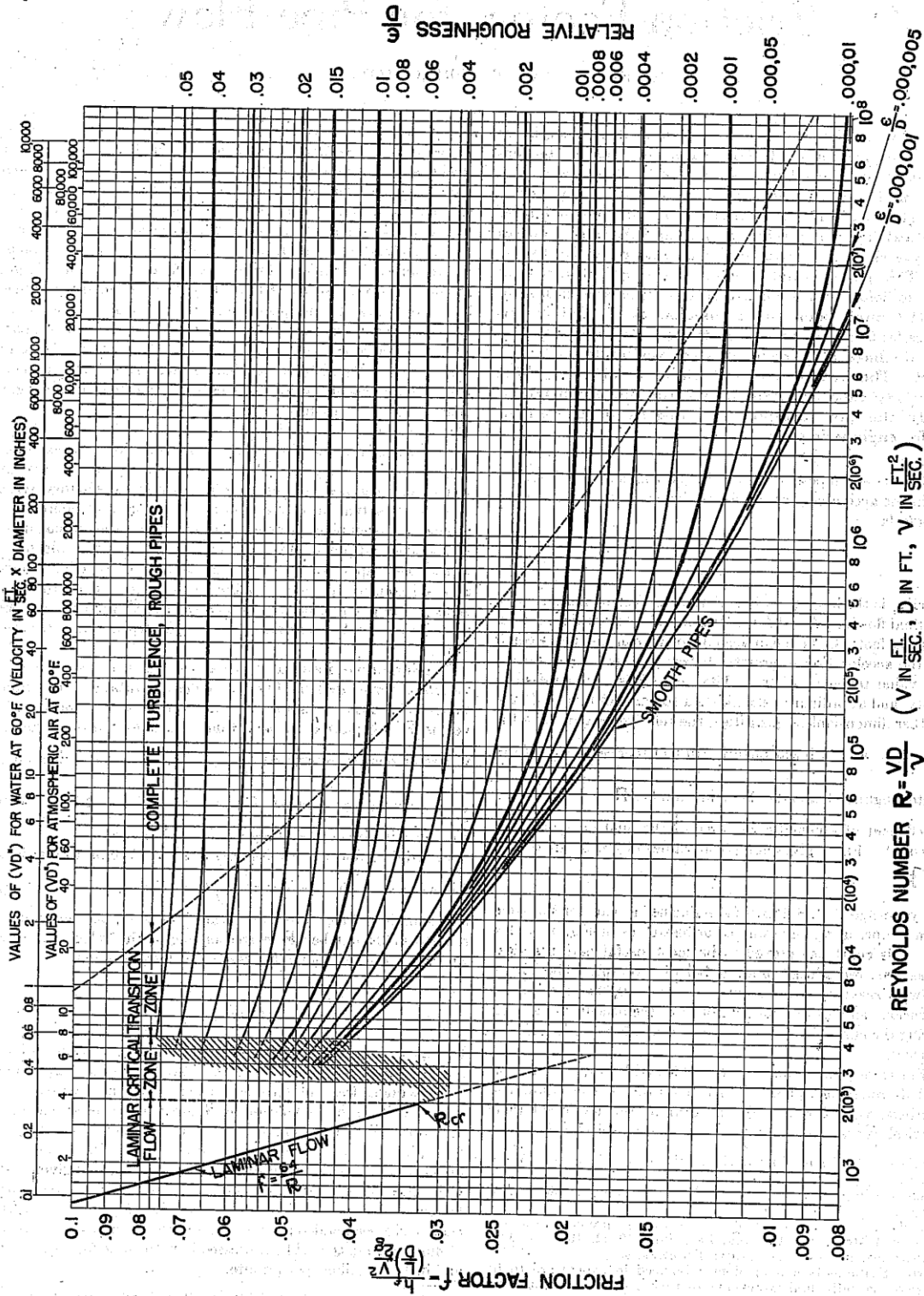
Figure 39 Moody chart taken from [25]

A3 Tubing data tables

Table 27 Tubing data table showing 7inch, 32Ibs/ft tubing/casing, taken from Drilling Data Handbook [36]

Pipe body

			29.00 lb/ft		32.00 lb/ft	
1	Nominal size (OD)	1	7.000 in	177.8 mm	7.000 in	177.8 mm
2	Nominal weight	2	29.00 lb/ft	42.3 daN/m	32.00 lb/ft	46.7 daN/m
3	Wall thickness	3	0.408 in	10.4 mm	0.453 in	11.5 mm
4	Inside diameter	4	6.184 in	157.1 mm	6.094 in	154.8 mm
5	Steel cross-section	5	8.45 in^2	5451 mm^2	9.32 in^2	6011 mm^2
6	Capacity	6	1.56 gal/ft	19.38 l/m	1.52 gal/ft	18.82 l/m
7	Displacement (1)	7	2.00 gal/ft	24.83 l/m	2.00 gal/ft	24.83 l/m

			K55	L80	N80	C90	T95	P110	Q125	K55	L80	N80	C90	T95	P110	Q125
8	Grade	8	K55	L80	N80	C90	T95	P110	Q125	K55	L80	N80	C90	T95	P110	Q125
9	Collapse resistance (MPa)	9	37.3	48.4	48.4	52.3	54.0	58.8	62.8	44.6	59.3	59.3	64.6	67.2	74.3	80.7
10	Internal yield pressure (MPa)	10	38.7	56.3	56.3	63.3	66.8	77.4	87.9	42.9	62.5	62.5	70.3	74.2	85.9	97.6
11	Pipe body yield strength (1000 daN)	11	207	301	301	338	357	413	470	228	332	332	373	394	456	518

Tensile strength (10^3 daN)

			K55	L80	N80	C90	T95	P110	Q125	K55	L80	N80	C90	T95	P110	Q125
12	Buttress Standard	12	295	319	332	342	359	425	465	325	352	366	377	396	468	513
13	Buttress Special Clearance	13	237	237	250	250	262	312	337	237	237	250	250	262	312	337
14	API STC	14	186	238	242	262	277	323	362	209	268	272	295	311	363	407
15	API LTC	15	205	261	266	288	304	354	394	231	294	299	324	342	399	443

Connection efficiency

			29.00 lb/ft	32.00 lb/ft
16	Grant Prideco TCII	16		
17	Grant Prideco STL	17	63.9	67.0
18	Hydril LX	18	76.5	79.5
19	Hydril 563	19	91.8	92.6
20	Hydril 511	20	60.6	
21	Hydril 521	21	73.9	76.1
22	Vallourec & Mannesmann New VAM	22	107.3	97.3
23	Vallourec & Mannesmann VAM ACE	23	104.8	128.1
24	Vallourec & Mannesmann VAM PRO	24	100.0	100.0
25	Vallourec & Mannesmann VAM TOP	25	102.1	102.1
26	Vallourec & Mannesmann FJL	26	61.5	65.1

Connection characteristics

			Make-up torque (daN.m)					OD (mm)	ID (mm)	Drift API (mm)	Make-up torque (daN.m)					OD (mm)	ID (mm)	Drift API (mm)
			K55	LN80	C90/95	P110	Q125				K55	LN80	C90/95	P110	Q125			
27	Buttress Standard	27						194.5		153.9						194.5		151.6
28	Buttress Special Clearance	28						187.3		153.9						187.3		151.6
29	API STC	29																
30	API LTC	30		803	926	1081		194.4		153.9		904	1041	1216		194.5		151.6
31	Grant Prideco TCII	31		1281	1281	1281	1281	193.0	158.2	153.9		1519	1519	1519	1519	194.9	156.2	151.6
32	Grant Prideco STL	32	569	732	732	732	732	177.8	157.2	153.9	637	813	813	813	813	177.8	153.1	151.6
33	Hydril LX	33	786	963	1064	1173	1295	181.1	156.5	153.9	969	1146	1241	1349	1458	181.7	153.3	151.6
34	Hydril 563	34	1139	1139	1139	1139	1139	194.5		153.9	1288	1288	1288	1288	1288	194.5		151.6
35	Hydril 511	35	908	908	908	908	908	177.8	154.8	153.9								
36	Hydril 521	36	1125	1125	1125	1125	1125	187.3	155.2	153.9	1261	1261	1261	1261	1261	189.2	153.7	151.6
37	Vallourec & Mannesmann New VAM	37	1125	1274	1376	1471	1566	195.1		153.9	1227	1376	1471	1566	1668	195.1		151.6
38	Vallourec & Mannesmann VAM ACE	38	1079	1274	1376	1566	1668	194.5		153.9	1274	1519	1668	1864	1959	200.9		151.6
39	Vallourec & Mannesmann VAM PRO	39						195.0		153.9						195.0		151.6
40	Vallourec & Mannesmann VAM TOP	40	1079	1274	1376	1566	1668	194.2		153.9	1274	1519	1668	1864	2007	196.0		151.6
41	Vallourec & Mannesmann FJL	41		864	980	1079	1226	177.8	155.5	153.9		912	1030	1128	1274	177.8	153.3	151.6

(1) The closed-end displacement does not account for couplings. MPa x 145 = psi   daN x 2.25 = lb   daN.m x 7.38 = lb.ft   mm x 0.0394 = in

Table 28 Production quality data for API yield stress taken from ISO/TR 10400 [12]

Table F.3 — Production quality data (API survey only) — API yield stress

Manufact. reference	Quantity	H40	J55	K55	L80	L80 9Cr	L80 13Cr	N80	C90	C95	T95	P110	Q125
AED4	Mean			1,292 NO				1,243 NO				1,147 QT	1,109 QT
	COV			0,0466 CX				0,0483 CX				0,0373 CS	0,0226 CS
	Samples			191 WE				83 WE				133 WE	121 WE
AP00	Mean			1,300 AR	1,087 QT			1,214 QT				1,145 QT	1,120 QT
	COV			0,0333 CX	0,0239 HR			0,0342 HR				0,0257 HR	0,0272 HR
	Samples			220 SS	150 SS			196 SS				220 SS	210 SM
CG37	Mean							1,231 QT				1,117 QT	
	COV							0,0331 CX				0,0463 CX	
	Samples							473 WE				33 WE	
FD00	Mean				1,099 QT			1,205 QT				1,160 QT	
	COV				0,0366 HR			0,0437 HR				0,0354 HR	
	Samples				30 SR			53 SR				46 SR	
FF12	Mean			1,091 AR	1,089 QT							1,087 QT	1,067 QT
	COV			0,0326 HR	0,0398 HR							0,0267 HR	0,0133 HR
	Samples			240 SR	390 SR							300 SR	28 SR
HH02	Mean				1,100 QT			1,233 QT			1,112 QT		1,117 QT
	COV				0,0344 HR			0,0327 HR			0,0235 HR		0,0291 HR
	Samples				166 SR			48 SR			36 SS		298 SR
JP01	Mean		1,198 AR		1,122 QT			1,216 QT					1,101 QT
	COV		0,0491 CX		0,0401 HR			0,0497 HR					0,0322 HR
	Samples		33 SR		185 SR			62 SR					227 SR
RH29	Mean	1,364 AR	1,169 AR										
	COV	0,0417 CX	0,0481 CX										
	Samples	90 WE	684 WE										
SS22	Mean								1,062 QT	1,058 QT	1,066 QT		
	COV								0,0325 HR	0,0176 HR	0,0315 HR		
	Samples								42 SS	63 SS	426 SS		
VT01	Mean		1,199 QT	1,132 AR	1,086 QT			1,187 QT				1,116 QT	
	COV		0,0524 ?	0,0540 ?	0,0472 ?			0,0633 ?				0,0495 ?	
	Samples		21 SR	39 SR	55 SR			33 SR				26 SR	
YF01	Mean	1,603 AR	1,318 AR	1,301 NO	1,098 QT			1,220 QT					
	COV	0,0531 CX	0,0665 CX	0,0621 CX	0,0372 CX			0,0563 CX					
	Samples	98 WE	1 094 WE	28 WE	223 WE			594 WE					
1	Mean						1,126						
	COV						0,0218						
	Samples						65						
2	Mean						1,064						
	COV						0,0262						
	Samples						33						
3	Mean						1,069						
	COV						0,0239						
	Samples						250						
CRS ensemble	Mean [a]	1,35	1,23	1,23	1,10	1,07	1,07	1,21	1,08	1,08	1,08	1,10	1,10
	COV	0,0595	0,0719	0,0719	0,0529	0,0533	0,0533	0,0511	0,0511	0,0500	0,0500	0,0464	0,0432
HRS ensemble	Mean [a]				1,10	1,07	1,07	1,21	1,08	1,08	1,08	1,10	1,10
	COV				0,0422	0,0426	0,0426	0,0405	0,0404	0,0394	0,0394	0,0360	0,0329

XII

Table 29 Quality data for other casing/tubing parameters, taken from ISO/TR 10400 [12]

Table F.4 — Production quality data (all datasets) — Other variables

Dataset	Quantity	Average OD		Average WT		Ovality		Eccentricity		Residual stress [a]		
		SL	EW	SL	EW	SL	EW	SL	EW	Cold str.	Hot str.	Not str.
API 1981	Mean	1,004 8		1,005 4		0,197		5,471		−0,209		0,028 3
	COV	0,001 18		0,019 4		0,613		0,566		0,195		0,377
	Samples	140		140		140		140		84		56
API 1982	Mean	1,007 7	1,009 8	1,009 9	1,001 1	0,525	0,492	8,828	5,114			
	COV	0,001 84	0,002 33	0,030 7	0,028 5	0,558	0,556	0,463	0,605			
	Samples	64	77	64	77	64	77	64	77			
API 1985	Mean					0,298	0,603	7,927	4,534	−0,243		
	COV					0,573	0,395	0,482	0,706	0,278		
	Samples					321	38	321	38	261		
API 1987	Mean	1,005 8		1,005 8		0,345		5,769			−0,123	
	COV	0,001 25		0,026 4		0,588		0,479			0,632	
	Samples	91		91		91		91			75	
Japanese RR 1987	Mean	1,004 8		1,017 6		0,239		5,204				
	COV	0,001 20		0,022 5		0,433		0,291				
	Samples	54		54		54		54				
Mannesmann 1983	Mean	1,001 7		1,035 0		0,424		11,43				
	COV	0,002 76		0,028 9		0,550		0,374				
	Samples	169		169		169		169				
Nippon 1977-87	Mean	1,003 5		0,995 7		0,166		4,883		−0,269		0,019 6
	COV	0,002 06		0,023 1		0,675		0,447		0,288		0,793
	Samples	1 247		1 247		1 247		1 247		235		710
Vallourec 1987-98	Mean	1,005 5		1,011 0		0,198		6,496				
	COV	0,001 49		0,024 0		0,593		0,411				
	Samples	295		304		303		299				
Nippon 1988-2000	Mean	1,003 5		0,999 7		0,184		4,928		−0,239		0,019 2
	COV	0,001 75		0,024 4		0,727		0,428		0,440		0,705
	Samples	583		577		575		578		121		426
Manufacturer AE04	Mean		1,005 8		1,012 5		0,182		3,342			
	COV		0,001 95		0,013 7		0,658		0,501			
	Samples		999		997		997		1 000			
Manufacturer CG37	Mean		1,009 0		1,027 6		0,534		1,857			
	COV		0,002 41		0,013 3		0,425		0,485			
	Samples		62		62		62		62			
Manufacturer DA01	Mean	1,006 5		1,008 2		0,313		1,390				
	COV	0,001 32		0,032 0		0,394		0,556				
	Samples	203		208		201		208				
Manufacturer FD00	Mean	1,007 1		1,006 8		0,241		5,170		−0,211	−0,142	
	COV	0,001 89		0,021 7		0,338		0,317		0,383	0,189	
	Samples	203		132[b]		204		194		84	54	

XIII

Table 30 Collapse model accuracies, taken from ISO/TR 10400 [12]

Table F.2 — Predictive accuracies (Q&T only)

Dataset	Axial force	Position(s) for geometry measurements	Tests	Abbassian and Parfitt 1995-9a Mean	COV	API Bulletin 5C3 (average) Mean	COV	API Bull. 5C3 / Clinedinst 1985 Mean	COV	Haagsma and Schaap 1981 Mean	COV	Jianzeng and Taihe 2001 Mean	COV	Klever-Tamano Mean	COV	Tamano et al. 1983 Mean	COV	Tamano modified 4 Mean	COV
API product																			
Mannesmann 1983	No	Multiple	89	**0,983**	0,069			1,035	**0,049**	0,955	0,067	0,930	0,069	0,956	0,055	0,968	0,064	0,964	0,064
API 1985	No	Not known	106	1,023	0,046	0,978	0,083	1,016	0,048	0,925	0,082	0,973	0,060	0,989	0,044	1,004	0,051	0,996	0,042
Nippon 1977-87	No	Pipe centre	433	0,996	0,072	1,088	0,136	1,054	0,080	0,944	0,100	0,978	0,077	0,982	0,057	1,003	0,069	0,981	0,060
Nippon 1988-2000	No	Pipe centre	85	1,020	0,104	1,026	0,107	1,060	0,097	0,947	0,115	0,994	0,110	1,004	0,093	1,019	0,104	0,996	0,095
Manufacturer FD00	No	Pipe end	129	1,019	**0,077**	1,019	0,085	1,055	0,093	0,956	0,107	0,988	0,095	**1,000**	0,078	1,017	0,087	0,997	0,077
DEA-130	No	Pipe centre	52	1,019	0,066	1,017	0,097	1,065	0,071	0,966	0,083	0,974	0,082	0,993	0,063	**1,006**	0,073	0,987	0,086
API 1981	Yes	Collapse point	96	1,040	0,108	1,037	0,136	1,082	0,099	0,985	0,106	**1,004**	**0,080**	1,030	0,102	1,035	0,085	1,019	0,098
Mannesmann 1983	Yes	Multiple	63	1,030	0,098	1,114	0,168	1,052	**0,082**	1,009	0,084	0,976	0,087	**1,003**	0,084	1,021	0,084	1,016	0,080
Dataset average				1,016	0,080	1,040	0,116	1,050	0,077	0,958	0,093	0,977	0,083	**0,996**	**0,072**	1,009	0,077	**0,994**	0,074
Ensemble average [a]			1 138	1,012	0,080			1,049	0,081	0,952	0,097	0,981	0,083	**0,997**	0,071	1,010	0,077	0,992	0,072
Dataspace average [a]				1,028	0,024					0,875	0,044			0,993	0,011	1,021	0,032	**1,000**	0,015
HC product																			
API 1982	No	Pipe end	141	0,877	0,125	0,961	0,111	**1,013**	0,114	0,949	**0,109**	0,850	0,118	0,944	0,115	0,879	0,118	0,949	0,122
API 1987	No	Pipe end	107	1,093	0,076	1,158	0,086	1,132	**0,054**	**1,054**	0,075	1,073	0,085	1,073	0,065	1,101	0,078	1,069	0,070
Nippon 1977-87	No	Pipe centre	794	1,016	0,052	1,124	0,072	1,135	0,063	1,030	0,073	1,016	0,073	1,005	0,050	1,039	0,063	**1,000**	0,052
Vallourec 1987-98	No	Collapse point	304	1,019	0,054	1,082	0,050	1,135	0,057	1,027	0,064	1,007	0,079	1,009	0,046	1,037	0,068	**1,006**	0,052
Japanese RR 1987	No	Not known	54	1,005	0,056	1,107	0,057	1,077	0,048	0,988	0,065	0,990	0,079	**1,000**	0,053	1,017	0,069	0,988	0,055
Nippon 1988-2000	No	Pipe centre	291	1,012	**0,058**	1,127	0,076	1,124	0,059	1,030	0,063	**1,003**	0,079	0,995	0,059	1,028	0,069	0,992	0,060
Manufacturer FD00	No	Pipe centre	75	0,990	0,058	1,126	0,069	1,034	0,061	0,901	0,063	0,919	0,055	**0,968**	0,054	0,952	0,056	0,946	0,057
DEA-130	No	Pipe end	26	1,019	0,090	1,037	0,087	1,074	**0,062**	0,985	0,088	1,008	0,088	**1,001**	0,072	1,029	0,082	0,997	0,082
API 1981	Yes	Collapse point	56	0,986	0,049	1,218	0,148	1,089	0,059	1,014	**0,048**	0,987	0,062	0,973	0,058	**0,997**	0,052	0,968	0,051
Dataset average				1,010	0,069	1,104	0,082	1,090	0,064	**0,998**	0,072	0,993	0,080	0,996	0,063	1,020	0,073	0,991	0,067
Ensemble average			1 848	1,014	0,068	1,108	0,088	1,115	0,073	1,017	0,080	1,005	0,084	**1,001**	0,064	1,031	0,076	0,996	0,067
Dataspace average				1,028	0,021					1,032	0,048			1,007	0,013	1,039	0,047	**1,007**	0,023

NOTE 1 Of the datasets above, those used for calibration of empirical coefficients were as follows:
- Klever-Tamano: all
- Tamano modified 4: all except manufacturer FD00, Nippon 1988-2000, and DEA-130
- Abbassian and Parfitt 1995-9a: all except Japanese RR 1987, manufacturer FD00, Nippon 1988-2000, and DEA-130
- API Bulletin 5C3/Clinedinst 1985: API 1985.

NOTE 2 Bold type denotes the best fit for each dataset.

[a] Includes one line from Grant Prideco 2000.

XIV